Worcester Polytechnic Institute (WPI)

Multi-scale Surface Metrology of Additive Manufactured Surfaces

A Major Qualifying Project submitted to the Faculty of Worcester Polytechnic Institute in partial fulfillment of the requirements for the degree of Bachelor of Science

By

Adam C. Lemoine, Matthew P. Mancini, Joseluis A. Velez

aclemoine@wpi.edu; mpmancini@wpi.edu; javelez@wpi.edu

Advisor: Professor Christopher A. Brown

Mechanical Engineering Department

Project Number: CAB-1601

Date

April 24th, 2016

Abstract

Additive manufactured surfaces are known to be problematic. Topographic measurements of laser melted surfaces manufactured by additive manufacturing are analyzed in this work. A method for selecting the measurement size and the size of calculation regions for studying surface topographies is discussed[1]. The variance between different locations on a surface tends to be greater when the scale of observation is small. Identifying the scales where individual topographical features become less visible can be useful for selecting necessary scales to study. Additionally, the ability to repeat surface measurements must be established before the influence of manufacturing variables on surface roughness can be properly compared. Measured height data are compared directly, and they are compared using conventional and multi-scale characterization parameters[1]. Also, this work presents a correlation experiment between the linear energy density of the laser used in the laser melting process and conventional and multi-scale parameters, which can support additive manufacturing process design. Recently proposed principles of surface metrology, emphasizing scale, geometric features and measurement fidelity, are examined in light of these results.

[1] This work was presented at the 5th International Conference on Surface Metrology at the Poznan University of Technology, Poznan, Poland, April 4th-7th, 2016

Acknowledgments

The authors would like to thank Matthew Gleason, co-manager of the Surface Metrology Laboratory for his consultation of this work. We would like to thank WPI undergraduates, Daniel Wivagg and Zhijie Wang, for their assistance with data collection. We would like to give additional thanks to Jackie Fanning for her contributions with the axiomatic design decomposition presented in Appendix 7.15. Additionally, we would like to thank Steve Alviti of BelAir Finishing Supply for his consultation, and we would like to thank the graduate students enrolled in ME 5841, Surface Metrology, at WPI for their helpful critiques of this work.

The authors would also like to thank Olympus for the use of the LEXT 4100 scanning laser confocal microscope used to take all surface measurements presented in this work. We would like to thank Digital Surf for the use of MountainsMap Premium®, which was used to perform all conventional analysis and to generate all surface images presented in this work. We would like to thank Surfract, owned by advisor Brown, for the use of Sfrax, which was used to perform all multi-scale analyses. We would also like to thank Dustin Lindley and Stacey Bagg of the NASA Marshall Space Flight Center Advanced Manufacturing Lab for manufacturing the laser melted parts used in this work.

Finally, the authors would like to thank their advisor, Professor Christopher Brown, for his guidance throughout the duration of the project. We would also like to thank Professor Brown for presenting our work on our behalf at the 5th International Conference on Surface Metrology.

Table of Contents

List of Figures

List of Tables

1.0 Introduction

1.1 Objective

The objective of this work is to advance the surface metrology of laser melted surfaces using three different experiments: a homogeneity crossover experiment, a measurement repeatability experiment, and a functional correlation experiment.

1.2 Rationale

The surface topographies of components manufactured through additive manufacturing are known to be problematic. Specific topographical features of surfaces can cause almost 10% of manufactured components to fail (Leach, 2011). Failure of components manufactured using additive manufacturing are estimated to be higher (Grimm et al., 2015). Quality control of the surface roughness is one of the leading inhibitors of mass production using additive manufacturing technology. It is necessary to provide better surface characterizations of additive manufactured surfaces in order to improve process design and quality control.

The repeatability of additive manufactured surfaces must first be established before functional correlations with process variables, and the ability to discriminate, can be adequately established. Additionally, quantifying the variability between surface measurements could provide a better understanding of measurement quality improvement.

The variance of surface topographies can become important when the measurement scale of observation is small. Heterogeneous surface features become visible at smaller measurement scales and are not easily captured at larger measurement scales. Knowing the measurement scale range where the surface transitions from showing heterogeneous features to showing homogenous features can be important in selecting key measurement scales to study.

Discovering correlations between surface topographies and the phenomena that influence the surfaces is a key objective in surface metrology research (Brown, 2014). Discovering a correlation between linear energy densities and additively manufactured surfaces can provide support in manufacturing process design (Brown, 2014).

1.3 State-of-the-art

1.3.1 Homogeneity Crossover

Little work has been done to quantitatively determine the appropriate measurement size and calculation region size needed to successfully discriminate or correlate surface topographies. The majority of works in the literature have determined the appropriate measurement scales by analyzing predictable scales for a particular application, or through a trial and error process. For example, Brown and Siegmann did not know what the fundamental scale of interaction was for adhesion on rough surfaces following the discrete interaction model, and they tested a wide range of scales in order to determine which scale provided the strongest correlation between the surface roughness and adhesive strength (Brown and Siegmann, 2001). Often in surface metrology, fundamental scales of interaction are discovered by chance.

Understanding the measurement scales where heterogeneous surface characteristics become visible can narrow down the range of scales to test. Heterogeneous characteristics, created with different process variables, can increase the probability of discriminating between different surface topographies and also provide stronger correlations with a wider range. Pedreschi et al. attempted to quantify the measurement scale range where heterogeneous surface characteristics of different kinds of chocolate become visible by creating a plot of the coefficient of variation as a function of the measured region size (Pedreschi et al., 2002). The authors used two different characterization parameters in an attempt to make this distinction; the area-scale fractal complexity and the smooth-to-rough crossover. The coefficient of variation (CoV) was calculated by dividing the standard deviation of the two parameters, calculated using specific measurement sizes, by their respective means. Heterogeneous characteristics cause the CoV to increase, because they create larger standard deviations. Plotting the CoV as a function of the measurement size allowed the authors to determine the measurement scales where heterogeneous characteristics became visible on chocolate surfaces (Pedreschi et al., 2002).

1.3.2 Repeatability of Surface Measurements

Little work has been done to quantify the repeatability of surface measurements. However, Annex E in the working draft of ISO 25178-700.3 presents a procedure for quantifying the repeatability of surface measurements (ISO, 2016). This document is a committee working draft that is currently in a state of revision. The annex suggests acquiring a specific number of measurements, and calculating least-square planes of each measurement without averaging the

heights or performing lateral smoothing. An average least square plane can be created, and the average plane can be subtracted from each individual least-square plane. Then the root-mean-square value for each difference can be calculated, and the arithmetic mean of these values would represent the quantitative measurement repeatability (ISO, 2016).

Additionally, Bergstrom et al. compared surface measurements obtained using different measuring systems by plotting the vertical heights of one measurement as a function of the other (Bergstrom et al., 2004). Linear regression analyses were performed between the vertical heights in order to obtain a regression coefficient between the two measurements. Ideally, if two measurements are identical, the regression coefficient, R^2, would be equivalent to 1.0. The overall uncertainty was mapped by plotting the surface fraction represented as a function of the standard deviation, normalized by the root-mean square roughness (Bergstrom et al., 2004).

Similarly, Brown et al. analyzed the reproducibility of replicas using similar repeatability techniques (2003). Difference maps were created between the replicas and original surface measurements by aligning and subtracting one surface from the other. The vertical heights of the replicas and original surfaces were also compared using linear regression. Finally, the fidelity of the replicas were analyzed using multi-scale parameters and statistical F-tests (Brown et al., 2003).

1.3.3 Characterization of Laser Melted Surfaces

The surface topographies of additive manufactured surfaces are problematic, and new, robust correlations need to be established in order to improve additive manufacturing process design and quality control.

Several studies have attempted to characterize surfaces manufactured using traditional machining processes. For example, Vulliez et al. discovered a strong scale-sensitive correlation between the fatigue life of surfaces machined by ball end milling and the mean plus two standard deviations of profile curvature calculated by Heron's method. (2014). Additionally, Berglund et al. found strong scale-sensitive correlations between friction coefficients obtained from bending under tension tests and relative area and complexity (2010). Finally, Hyde et al. discovered strong scale-sensitive correlations between the discharge energy used to manufacture surfaces by micro-EDM and relative area and complexity (2014).

Additionally, several studies have attempted to characterize additive manufactured surfaces. Grimm et al. correlated hybrid parameters, such as Sdr and Sdq, with the inclination angle of surfaces manufactured using laser beam melting. (2015). They also correlated the root-mean square flatness (FLTq), the waviness parameter Wsa, and Sa with the inclination angle of sintered surfaces. The fractal dimension used in the box counting method also correlated well with the inclination angle of the laser melted surfaces (Grimm et al., 2015).

Zeng et al. attempted to characterize surfaces manufactured using fused deposition modeling (2014). They identified a strong correlation between the adjusted layer thickness and the smooth-to-rough crossover calculated using area-scale analysis (Zeng et al., 2014). Brown and Burns also attempted to quantify the influence of outliers on the ability to discriminate surfaces manufactured by laser sintering (2014). There results show that outliers on additive manufactured surface measurements strongly influence the ability to discriminate. Many of these outliers are created around the edges of unsintered particles (Brown and Burns, 2014).

1.4 Approach

In order to analyze the heterogeneous-to-homogeneous crossover of additive manufactured surfaces, the coefficient of variation of conventional and multi-scale parameters were calculated using various regions sizes. Plots similar to those created by (Pedreschi et al., 2002) were constructed by plotting the coefficient of variation as a function of region size.

Additionally, the repeatability of additive manufactured surfaces was analyzed by constructing height comparison plots similar to (Bergstrom et al., 2004) and (Brown et al., 2003). A multi-scale variation experiment was also conducted in order to determine the calculation scales where variation between different additive manufactured surfaces occur.

A correlation study was conducted at various inclination angles using different filter types in order to find potential correlations between conventional and multi-scale parameters and the linear energy density used in the laser melting process.

Finally, the results presented in this work were used to examine the three developing principles on surface metrology (see Appendix 7.17). These principles were first proposed at the Fourth International Conference on Surface Metrology in Hamburg, Germany in 2014, and they were re-presented at the Fifth International Conference on Surface Metrology in Poznan, Poland

in 2016 (Brown, 2016). The three principles state that successful discriminations and correlations in surface metrology require:

1. Characterization of the appropriate geometrical aspects (area, slope, curvature, etc.)
2. Characterization at the appropriate scale
3. Topographic measurements containing the appropriate scales with sufficient fidelity.

The results of the three experiments presented in the objective were examined using these three developing principles, and these assessments are presented in the discussion section.

2.0 Methods

2.1 Analytical Techniques

The following sections discuss two analytical techniques that were applied to laser melted surfaces. The first section presents a method for selecting the appropriate measurement size and the size of calculation regions for studying surface topographies. Additionally, methods for quantifying the degree of repeatability between surface measurements are also presented.

Both methods presented in the following subsections are scale-based analytical techniques, and there are two different kinds of scales used in the calculations. The homogeneity crossover method is sensitive to the measurement scale (the nominal xy area of the measurement). In the following sections, this scale type is termed the "measurement scale". The repeatability section is sensitive to the calculation scale used in multi-scale analysis, such as area-scale analysis. This scale type is termed the "calculation scale".

2.1.1 Homogeneity Crossover

2.1.1.1 Surface Measurements

A 10x10x10 mm cube (Figure 1a) was manufactured on a Concept Laser M2 laser melting machine out of Inconel alloy 718 using powder with particle diameters ranging from 30 to 50 µm. The contour scan speed and contour laser power were 400 mm/s and 100 watts respectively. An Olympus LEXT 4100 scanning laser confocal microscope was used to take a 5x5 stitched measurement on the radial face of the cube (Figure 1b). A 20x objective with a 0.6 numerical aperture, and a field of view of 640 by 640 µm was used. 25 separate measurements were taken and were stitched in a 5x5 array in order to obtain the final stitched measurement. The stitched region size was 2,940 μm^2 with a sampling interval of 0.624 µm. A larger 3D view of the surface, with the conventional parameters tabulated, can be found in Appendix 7.1.

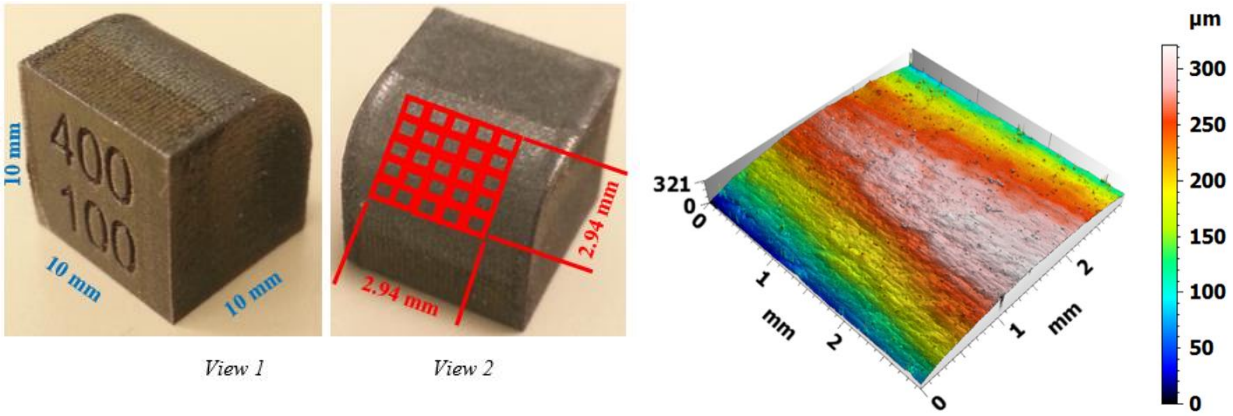

(a) (b)

Figure 1: (a) The location of the stitched measurement taken on the radial face of the laser melted part manufactured using a contour speed of 400 mm/s and a contour power of 100 watts, (b) A rendering of the 5x5 stitched surface (20x objective, 0.6 numerical aperture, stitched region size of 2,940 µm^2, sampling interval of 0.624 µm

2.1.1.2 Tiling Exercises

The stitched surface shown in Figure 1b was broken up into a grid of square sections of a particular size (the measurement scale) using MountainsMap Premium® (Figure 2a). Parameter values were calculated for each individual square. These parameter values were exported into a Microsoft Excel® document, and the coefficients of variation (CoV) of each parameter were calculated (Equation 1). The CoV is calculated by dividing the standard deviation of a particular parameter by the mean calculated using all of the individual sections. This tiling procedure was repeated using multiple measurement scales. Overlapping of the tiles occurred when the size of the square was larger than the region size of a single measurement obtained during the stitching, which was about 588x588 µm (Figure 2b). Plots of the CoV as a function of the measurement scale were generated for the various parameters discussed in the following sections.

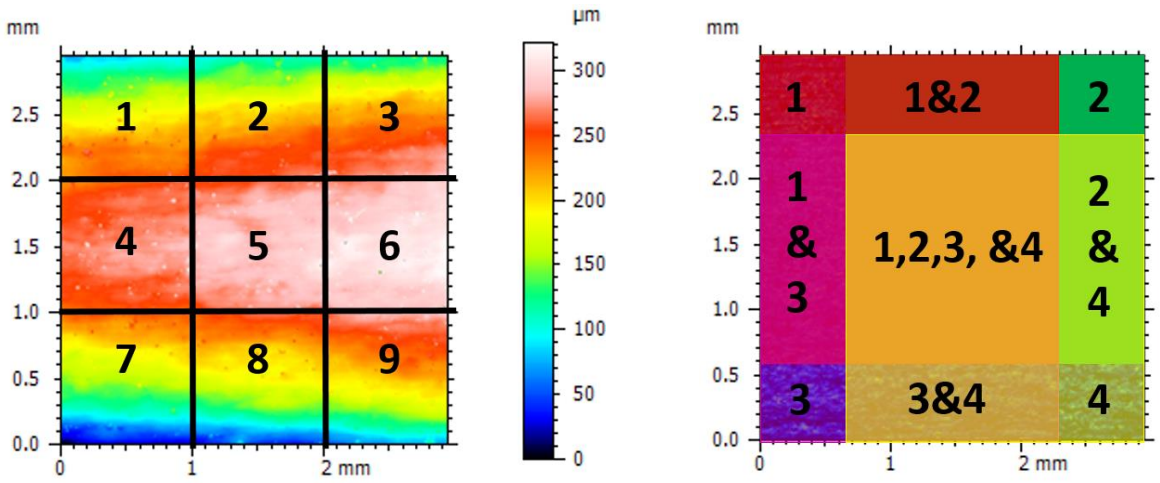

(a) (b)

Figure 2: (a) An example of non-overlapping tiling on the measurement in Figure 1b, (b) An example of overlapping tiling on the measurement in Figure 1b

$$CoV = \frac{\sigma}{\mu} = \frac{\sqrt{\frac{\sum_{i=1}^{n}(P_i-\mu)^2}{n-1}}}{\frac{1}{n}\sum_{i=1}^{n} P_i}$$

Where P is a specific parameter of a specific section

Equation 1: The calculation of the coefficient of variation (CoV)

2.1.1.3 Homogeneity Crossover of Conventional Height Parameters

Conventional parameters were calculated for each individual section and for each measurement scale. The CoV for each parameter was obtained at each measurement scale, and plots of the CoV as a function of the measurement scale were generated in order to observe any potential heterogeneous-to-homogenous crossovers. CoV versus measurement scale curves that showed a clear transition from a high CoV to a low CoV, with clear plateaus on the heterogeneous and homogenous ends, were considered to have a homogeneity crossover.

2.1.1.4 Homogeneity Crossover of Multi-Scale Parameters

Three multi-scale parameters were used in the homogeneity crossover analysis. Area-scale analyses were performed on each individual square section and at each measurement scale using Sfrax (Surfract, 2007). The CoV of the maximum relative area and complexity were obtained and plotted as a function of the measurement scale. Additionally, the CoV of the smooth-to-rough crossover (SRC) was calculated within Sfrax and plotted as a function of the measurement scale. The SRC in area scale analysis is the calculation scale at which the relative

area approaches one (ASME B46.1, 2009). An example of locating the SRC on a relative area plot is shown in Figure 3. A 10% crossover threshold of the maximum relative area was applied for each section calculated at each measurement scale within Sfrax (ASME B46.1, 2009).

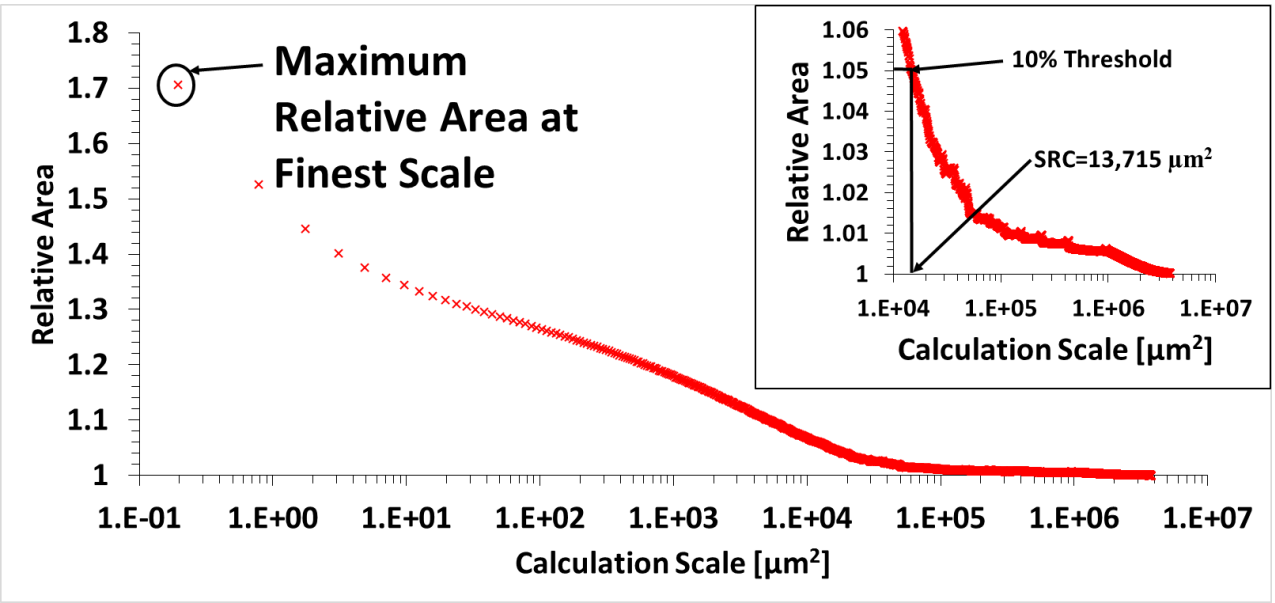

Figure 3: An example of locating the maximum relative area and the smooth-to-rough crossover (SRC) on a relative area vs. scale plot calculated from a single 2,750 µm^2 section from the stitched measurement in Figure 1b

2.1.2 Repeatability

2.1.2.1 Repeatability between Multiple Measurements

A specimen laser melted using a contour laser power of 100 watts and a contour scan speed of 400 mm/s was placed on a 45° v-block, and a set of 10 repetitive surface measurements were taken on the radial face at a single location without changing any measurement parameters. An Olympus LEXT 4100 scanning laser confocal microscope with a 20x objective (numerical aperture of 0.6 and a sampling interval of 0.625µm) was used to take the surface measurements. These repetitive measurements were taken in succession without altering or dismantling the measurement setup.

Both sets of measurements were leveled, and the form was removed, using MountainsMap Premium®. The spatial and vertical height data from each measurement was exported into a Microsoft Excel® file, and several height vs. height plots were constructed in order to compare the repeatability of the vertical heights between each measurement. A single height vs. height plot was constructed by plotting the height data of one surface as a function of

the height data of an alternate measurement. The MATLAB script presented in Appendix 7.4 was used to construct these height vs. height plots. If the vertical height data between two measurements was identical, the resulting plot would contain a linear line with a regression coefficient of 1.0. Several plots were created, and linear regression analyses were performed between each height comparison. A matrix of regression coefficients was constructed in order to analyze the repeatability between the 10 measurements. This procedure was repeated using measurements that had outliers removed using an outlier filter within MountainsMap®. Therefore, two resulting matrices were constructed, and these matrices are presented in Appendix 7.6.

2.1.2.2 Repeatability between Multiple Locations of a Single Specimen

The specimen shown in Figure 4 was laser melted out of Inconel 718 using powder with particle diameters ranging from 30 to 50 µm. The contour laser power was 100 watts and the contour scan speed was 400 mm/s. The specimen was placed on a 45° v block, and surface measurements were taken at six different locations on the radial face (Figure 4). A 20x objective with a 0.6 numerical aperture and a 0.625µm sampling interval was used. A total of 6 measurements were taken (see Appendix 7.8).

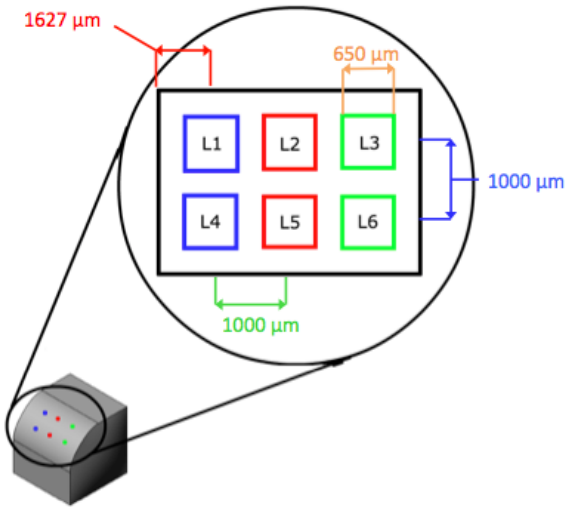

Figure 4: The size and location of the six measurements taken on the radial face of laser melted specimen with a contour speed of 400 mm/s and contour power of 100 watts

All six measurements were leveled using the subtraction method, and outliers were removed using the outlier filter within MountainsMap. Area-scale analyses were performed on both the unfiltered and filtered surfaces in order to observe the influence of the filtering on the multi-scale results. Area-scale analysis calculates the relative area of a surface by tiling the surface with virtual triangles of a specific area (the calculation scale). The number of triangles needed to tile the surface is multiplied by the tile area, and then divided by the projected area of the surface in order to get the relative area at a specific calculation scale (Equation 2). (Leach, 2013). As the calculation scale decreases, the relative area of a surface increases, because smaller tiles are likely to include surface topographic features that would increase the relative area.

$$Rel\ A_i = N_i \left(\frac{scale\ (i)}{nominal\ area\ (i)} \right)$$

Equation 2: The calculation of the relative area at a particular scale (leach, 2013)

An F-test was conducted in order to test the ability to discriminate between the unfiltered and filtered surfaces. An F-Test is used to identify the fundamental calculation scale where two groups of surfaces can be discriminated. The mean square ratio is plotted as a function of calculation scale. The confidence level of the F-Test runs parallel to the x-axis, and determines the calculation scale at which surfaces can be discriminated. A 99% confidence level was used. Mean square ratios that lie above the 99% confidence level therefore have a 99% discrimination confidence.

Finally, the coefficient of variation (CoV) of the relative area at each calculation scale between the 6 locations was calculated. The CoV was calculated by dividing the standard deviation of the relative areas at a particular calculation scale by the mean. A curve of the CoV as a function of calculation scale was constructed in order to obtain the calculation scales at which variation between the different locations appear. This procedure was repeated using the filtered surfaces obtained at the different locations, and the CoV plots were compared.

2.1.2.3 Repeatability between Multiple Specimens at the Same Location

Four different specimens were laser melted out of Inconel 718 using powder with particle diameters ranging from 30 to 50 µm. A contour laser power of 100 watts, and a contour scan speed of 400 mm/s was used. The specimens were each placed on a 45° v block, and surface measurements were taken using an Olympus LEXT 4100 scanning laser confocal microscope. A 20x objective with a 0.6 numerical aperture and a 0.625µm sampling interval was used. Nine individual measurements were taken on each part and stitched into 3x3 grids to create stitched measurements with a final region size of about 1,790 μm^2.

All four stitched measurements were leveled using the subtraction method within MountainsMap premium, and outliers were removed using the outlier filter within MountainsMap. Area-scale analyses were performed on both the unfiltered and filtered surfaces in order to observe the influence of the filtering on the multi-scale results, similar to Section 2.1.2.2. The CoV of the relative area at each calculation scale between each part was calculated for the unfiltered and filtered data, and plots of the CoV as a function of the calculation scale were created and compared.

2.2 Process Analysis: Correlation of Relative Area and Linear Energy Density

A correlation experiment between the linear energy density (LED) and conventional and multi-scale parameters was conducted. This experiment was performed at various inclination angles (Figure 5a). Four different laser melted specimens were manufactured using different combinations of contour scan speed and contour laser power (Table 1); resulting in four different linear energy densities (Figure 5b). Measurements were taken using and Olympus LEXT 4100 scanning confocal microscope at various inclination angles. A 50x objective (numerical aperture of 0.95), with a region size of 256 µm2 and a sampling interval of 0.25 µm, was used. A total of 20 measurements were taken (see Appendix 7.9).

Combination #	Contour Laser Power (Watts)	Contour Speed (mm/s)	LED (J/mm)
1	100	1600	0.0625
2	180	1600	0.1125
3	100	400	0.25
4	180	400	0.45

Table 1: The different combinations of contour scan speeds and contour laser powers of the laser melted parts analyzed in the correlation experiment

$$Linear\ Energy\ Density = \frac{Laser\ Power}{Scan\ Speed}$$

Equation 3: The calculation of the linear energy density

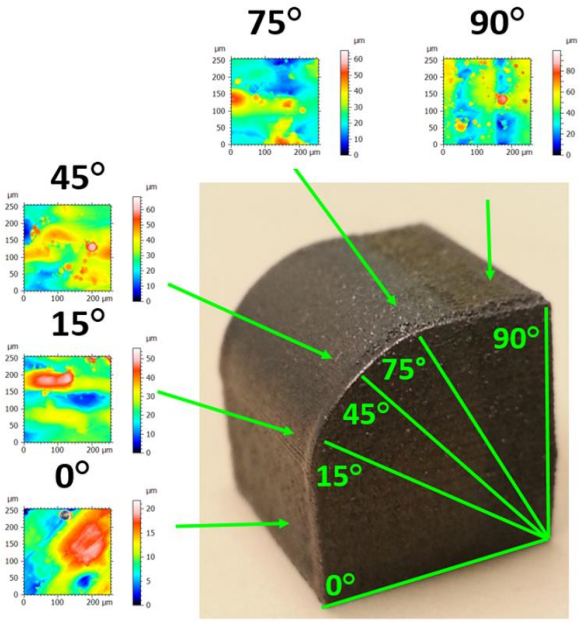

Figure 5: (a) The surface measurement orientations with inclination angles taken on all of the specimens presented in Table 1

Two different outlier filters were used to remove outliers from the measurements. An outlier filter within MountainsMap® was used. Isolated outliers and outliers around edges were removed, and non-measured points were filled in. Additionally, a modal-based filter was used (Le Goïc et al., 2012). Three different mode numbers were used (125, 250, and 500), with a confidence interval of 0.001.

Conventional height parameters were calculated for each surface measurement. Linear regression analyses were performed between each conventional parameter and the linear energy densities. The regression coefficients R^2 were obtained and tabulated.

Area-scale analysis was performed on each unfiltered and filtered surface. Scale-based linear regression analyses between the relative area and the linear energy density were conducted for each inclination angle and for each filter method. The scales where the strongest regression coefficients occurred, and at which inclination angle and using which filter type, were identified.

3.0 Results

3.1 Analytical Techniques

3.1.1 Homogeneity Crossover

In the following sections, various plots of the coefficient of variation as a function of the measurement scale for both conventional and multi-scale parameters are discussed.

3.1.1.1 Homogeneity Crossover of Conventional Height Parameters

The arithmetic mean height (Sa) and the root-mean-square height (Sq) show a clear heterogeneous to homogenous crossover (Figure 6a). This homogeneity crossover occurs within a measurement scale range of 411 and 3,063 mm^2. At scales smaller than 411 mm^2, the coefficient of variation was between about 0.45 and 0.52 for Sq, and between about 0.51 and 0.55 for Sa. The larger CoVs at these fine measurement scales are caused by heterogeneous surface characteristics that cannot be characterized by the coefficient of variation at larger measurement scales. Similarly, the coefficient of variation at measurement scales greater than 3,063 mm^2 were between 0.075 and 0.168 for Sq and between 0.049 and 0.187 for Sa. The unique features that were visible at the smaller measurement scales are not as visible at the larger measurement scales. A similar result occurred with the 2nd and 3rd statistical moments, skewness and kurtosis (Ssk and Sku respectively), as shown in Figure 6b. The homogeneity crossover for the two statistical moments occurred between about 345 and 3,063 mm^2. These homogeneity crossover results are summarized in Table 2.

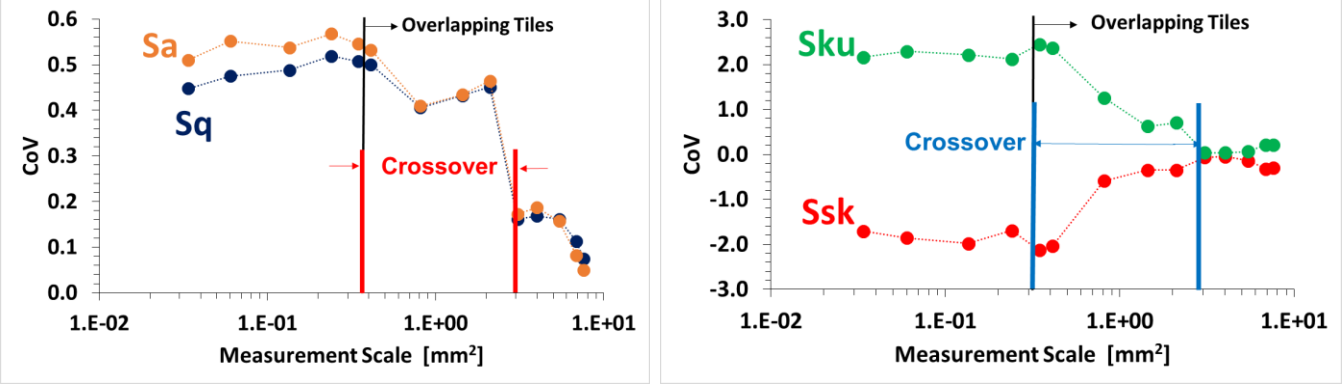

(a) (b)

Figure 6: (a) The plots of the homogeneity crossovers vs. measurement scale: height parameters with visible homogeneity crossover calculated at each measurement scale using the stitched measurement in Figure 1. (b) The 2nd and 3rd statistical moments with visible homogeneity crossovers calculated at each measurement scale using the stitched measurement in Figure 1

Additionally, several conventional parameters did not show a clear heterogeneous-to-homogeneous crossover (Figure 7). These parameters include the maximum peak height (Sp), maximum pit height (Sv), and the maximum height St (Figure 7a). Sz also did not show a clear homogeneity crossover. The results of St and Sz were identical, and Sz was not reported in this work. The hybrid parameters, developed interfacial area (Sdr) and the root-mean square slope (Sdq) also did not show a clear heterogeneous-to-homogeneous crossover (Figure 7b). The CoVs of these parameters decreased gradually as the measurement scale increased. These results are summarized in Table 2.

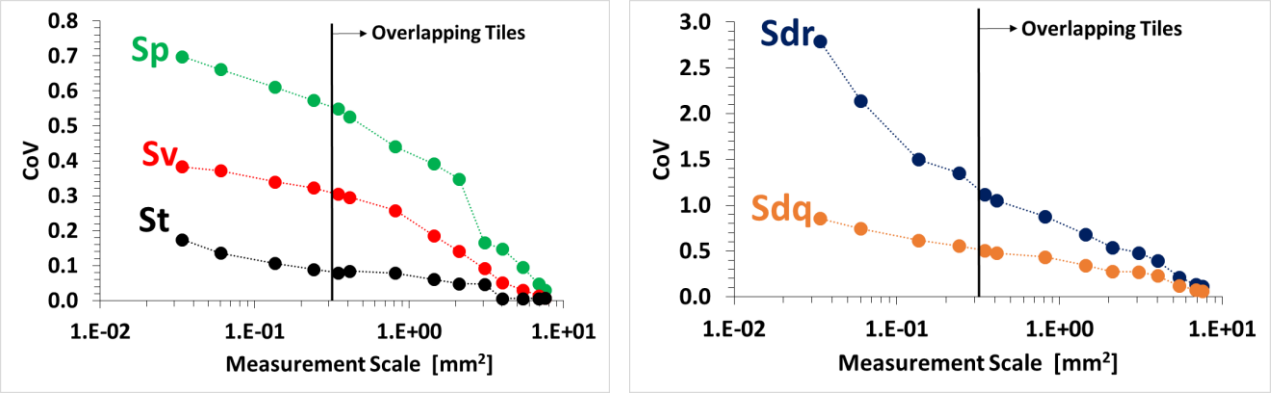

(a) (b)

Figure 7: (a) The plots of the homogeneity crossover vs. measurement scale: height parameters with decreasing CoV calculated at each measurement scale using the stitched measurement in Figure 1. (b) The hybrid parameters with decreasing CoV calculated at each measurement scale using the stitched measurement in Figure 1

Parameter	Parameter Type	Standard	Homogeneity crossover	Measurement Scale Range [mm^2]
Sa	1st Statistical Moment	ISO 25178	Yes	411-3,063
Sq	1st Statistical Moment	ISO 25178	Yes	411-3,063
Ssk	2nd Statistical Moment	ISO 25178	Yes	345-3,063
Sku	3rd Statistical Moment	ISO 25178	Yes	345-3,063
Sp	1st Statistical Moment	ISO 25178	No	
Sv	1st Statistical Moment	ISO 25178	No	
St	1st Statistical Moment	ASME B46.1	No	
Sdr	Hybrid Parameter	EUR 15178N	No	
Sdq	Hybrid Parameter	EUR 15178N	No	

Table 2: The conventional parameter homogeneity crossover results summary. Parameters that exhibited a homogeneity crossover are highlighted in green, and the parameters that did not are highlighted in orange

A cross correlation matrix between all of the conventional parameters was constructed in order to quantify their similarities. Sz was not included in the cross correlation matrix, because the results were exactly the same as St. A linear regression analysis was performed between each parameter calculated at all of the measurement scales. The regression coefficients for each regression analysis were calculated, and the correlation matrix was populated appropriately (Table 3). The strongest cross correlation occurred between Sa and Sq (R^2=0.993). Figure 8 shows the cross correlation plot between Sa and Sq. The calculated values of these two parameters increased as the measurement scale increased. Therefore, it is clear that differences between Sa and Sq do not begin to appear until the measurement scale becomes small, and this is

supported by the CoV curves presented Figure 6a. At the small measurement scales, the CoVs of Sa are larger than the CoVs of Sq. This indicates that Sa has to have either larger standard deviations or smaller means, resulting in the larger coefficients of variation. It is clear in Figure 8 that the off diagonal points where differences occur have smaller values of Sa compared to Sq. This indicates that Sa must have a smaller mean. A strong correlation between skewness and kurtosis and between Sdr and Sdq was also found (R^2 = 0.893 and 0.859 respectively). These plots can be found in Appendix 7.3. The strong cross correlations are highlighted in green in Table 3.

Furthermore, the hybrid parameters Sdr and Sdq are calculated at the finest scales equivalent to the sampling interval of the measurement. Therefore, they are not expected to correlate well with other conventional parameters. The maximum heights Sz, obtained from the ISO standard and St, obtained from the ASME B46 standard did not correlate well with the maximum peak height, Sp. It is possible that specific topographical features influence the calculation of one parameter and not the other. It is also possible that small outliers could also be influencing the calculations and therefore the cross correlations. Additionally, the statistical moments did not correlate well with the parameters that are calculated using single height points, such as Sv and St. These parameters are not expected to correlate well, because their calculation methods are different. Finally, some of the parameters that are calculated as averages, such as Sq and Sa did not correlate well with parameters that are calculated using single height points, such as Sv. These weak correlations are highlighted in orange in Table 3.

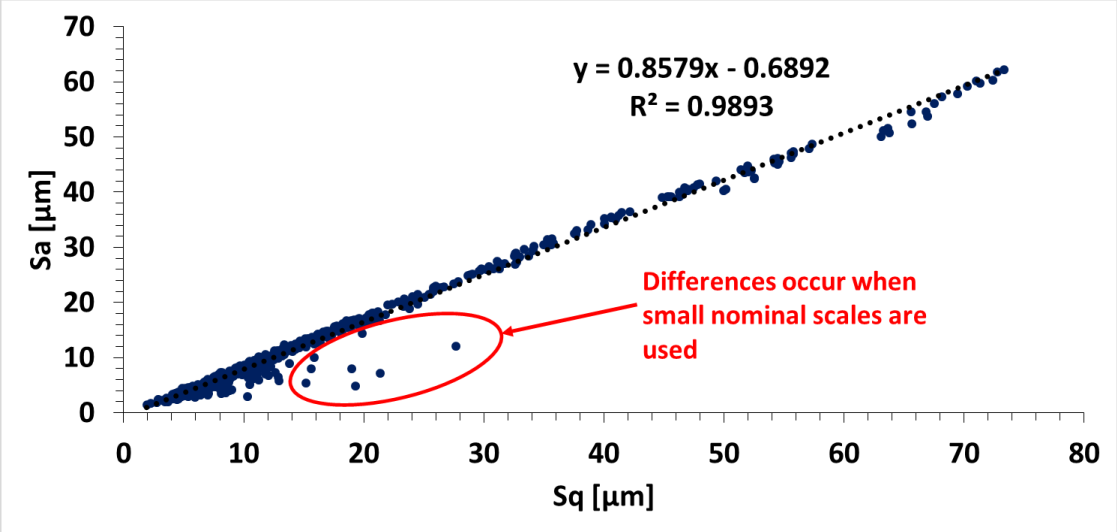

Figure 8: The cross correlation between Sa and Sq at all measurement scales used in the homogeneity crossover analysis of the measurement in Figure 1b

R^2	Sa	Sq	Ssk	Sku	Sp	Sv	St	Sdr	Sdq
Sa	1.00	0.99	0.12	0.10	0.32	0.01	0.21	0.00	0.00
Sq		1.00	0.08	0.08	0.28	0.00	0.26	0.00	0.00
Ssk			1.00	0.84	0.24	0.36	0.11	0.13	0.24
Sku				1.00	0.16	0.21	0.05	0.03	0.07
Sp					1.00	0.50	0.00	0.02	0.03
Sv						1.00	0.44	0.17	0.33
St							1.00	0.17	0.41
Sdr								1.00	0.81
Sdq									1.00

Table 3: The correlation coefficients R^2 between the various conventional parameters

3.1.1.2 Homogeneity Crossover of Multi-Scale Parameters

Three multi-scale parameters were used in the homogeneity crossover analysis; the maximum relative area, which is calculated at the finest scale calculated in the area scale analysis, the maximum complexity, and the smooth-to-rough crossover.

Figure 9a shows an example of where the maximum relative areas occur on a plot of relative area as a function of calculation scale. Area-scale analyses were conducted on each individual tile used to cover the stitched surface. The size of the tiles was very large for the results in Figure 9a. Therefore, the coefficient of variation of the maximum relative area was small. Figure 9b shows a second example of a plot of relative area as a function of scale. The

size of the tiles was smaller; causing the coefficient of variation of the maximum relative area to increase.

Figure 10 shows a plot of the coefficients of variation of the maximum relative area and maximum complexity as a function of the measurement scale. It is clear that the CoVs of the maximum relative area and maximum complexity did not show a distinct heterogeneous-to-homogenous crossover. The CoVs steadily decreased as the measurement scale increased.

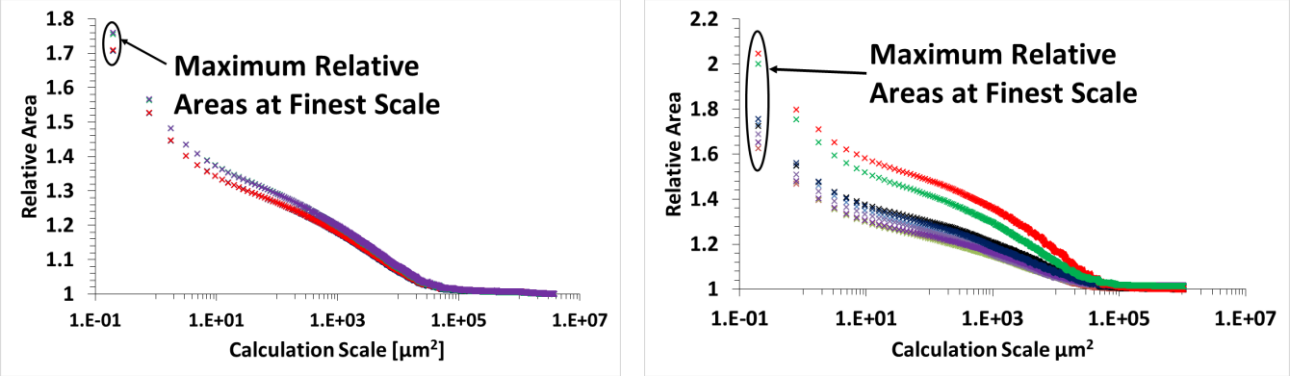

(a) (b)

Figure 9: (a) Relative area vs. scale plot for tiled sections of size 2,450 x 2,450 µm^2. (b) Relative area vs. scale plot for tiled sections of size 1,450 x 1,450 µm^2

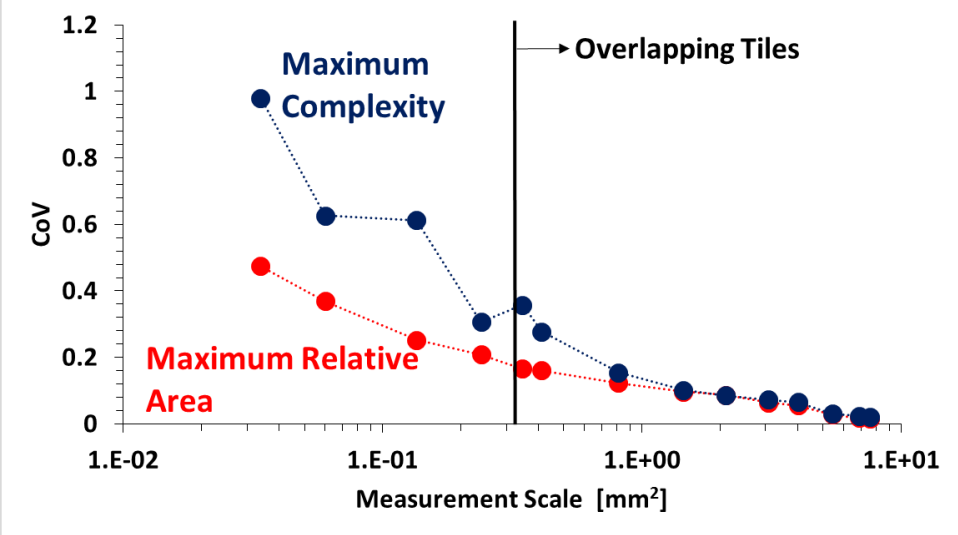

Figure 10: The homogeneity crossover vs. measurement scale of the maximum relative area and complexity calculated at each measurement scale using the stitched measurement in Figure 1

The developed area ratio Sdr and the maximum relative area are calculated at the finest scale. Figure 11 shows a cross correlation between Sdr and the maximum relative area. The regression coefficient, R^2, was calculated to be 0.88. Therefore, there was a strong cross correlation between Sdr and the maximum relative area.

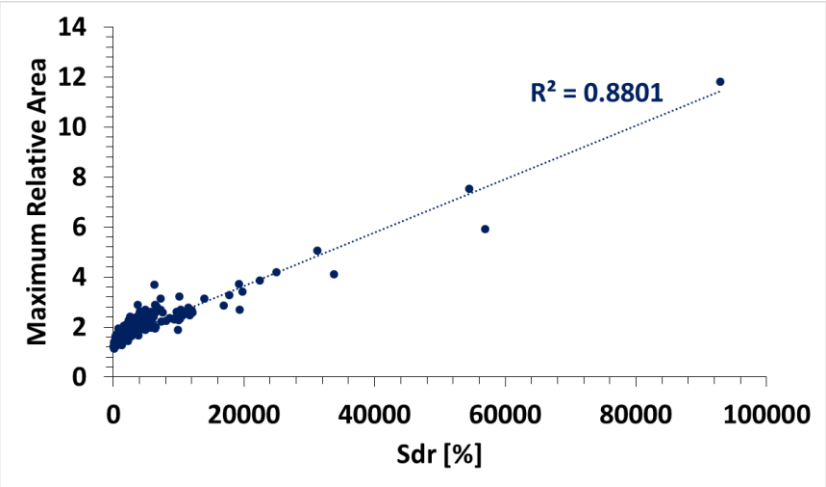

Figure 11: The cross correlation between Sdr and the maximum relative area calculated at all measurement scales used in the homogeneity crossover analysis from the measurement in Figure 1b

Finally, the smooth-to-rough crossovers (SRC) were obtained from the area-scale analyses using a 10% threshold value. Figure 12 shows a plot of the average relative areas for each measurement scale. It is clear that as the measurement scale decreased, the smooth-to-rough crossover also decreased. The surfaces appear to be less "smooth" at the smaller measurement scales, and the relative areas have a smaller tendency to approach one.

Figure 13 shows a plot of the coefficients of variation of the smooth-to-rough crossovers as a function of the measurement scale. The CoVs steadily increase to a maximum of 1.29 at a scale of 490 x 490 μm^2, and then steadily decrease as the measurement scale increases. Therefore, a clear heterogeneous-to-homogeneous crossover could not be identified using the SRC.

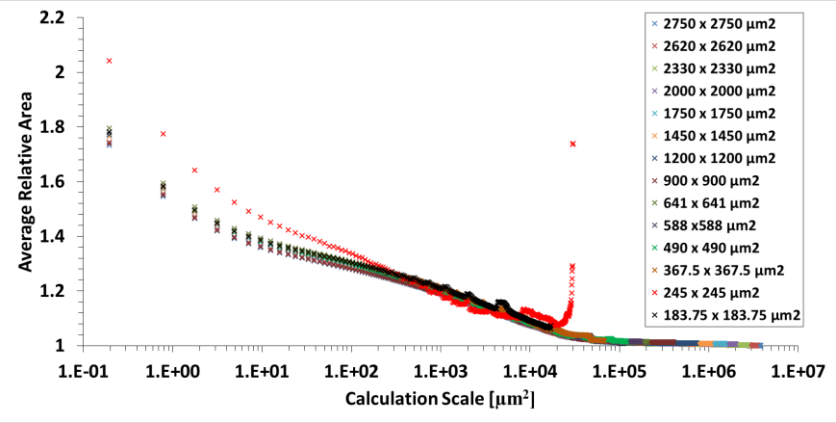

Figure 12: A plot of the average relative area per measurement scale used in the homogeneity crossover analysis

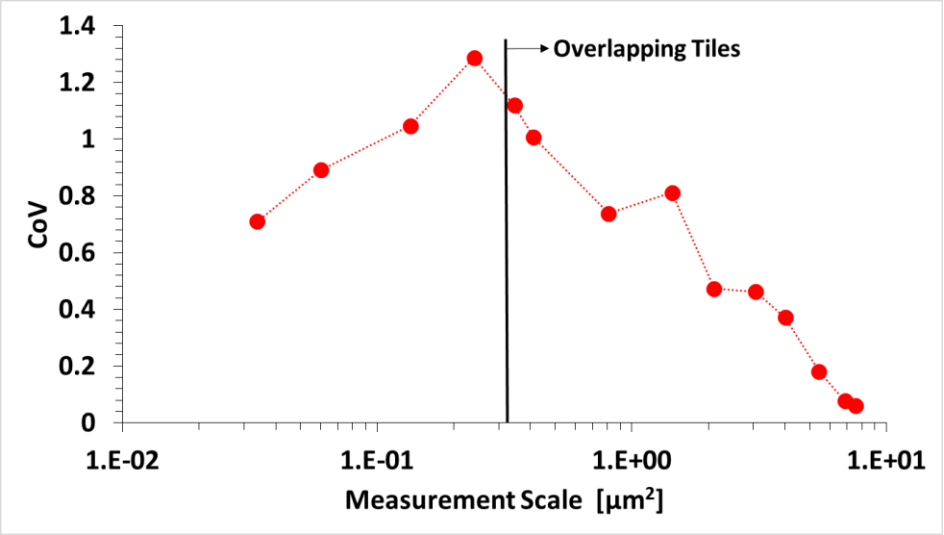

Figure 13: The homogeneity crossover vs. measurement scale: smooth-to-rough crossovers calculated at each measurement scale using the stitched measurement in Figure 1

3.1.2 Repeatability

3.1.2.1 Repeatability between Multiple Measurements

The repeatability of multiple measurements experiment was performed on a set of unfiltered surfaces and on a set of filtered surfaces. Ten measurements were taken at the same location on the radial face of a laser melted part manufactured using a contour speed of 400 mm/s and a contour power of 100 watts (Figure 14). It is clear that the majority of the outliers were below the apparent plane of the surface, and that outliers greatly influence some conventional parameters of the laser melted surfaces (Figure 15). For example, the maximum peak height, maximum height, skewness, kurtosis, developed interfacial area, and root-mean-square slope all showed large differences between the unfiltered and filtered surfaces, because

their calculations are greatly influenced by the presence of outliers. Additionally, the Sdr values were also reduced. The developed interfacial area is calculated at the finest scale. Therefore, it is clear that the outlier filter removed fine-scale features from the surface because the Sdr values were greatly reduced when the outliers were removed.

Figure 14: The approximate location of the surface measurements used in the measurement-to-measurement repeatability experiment

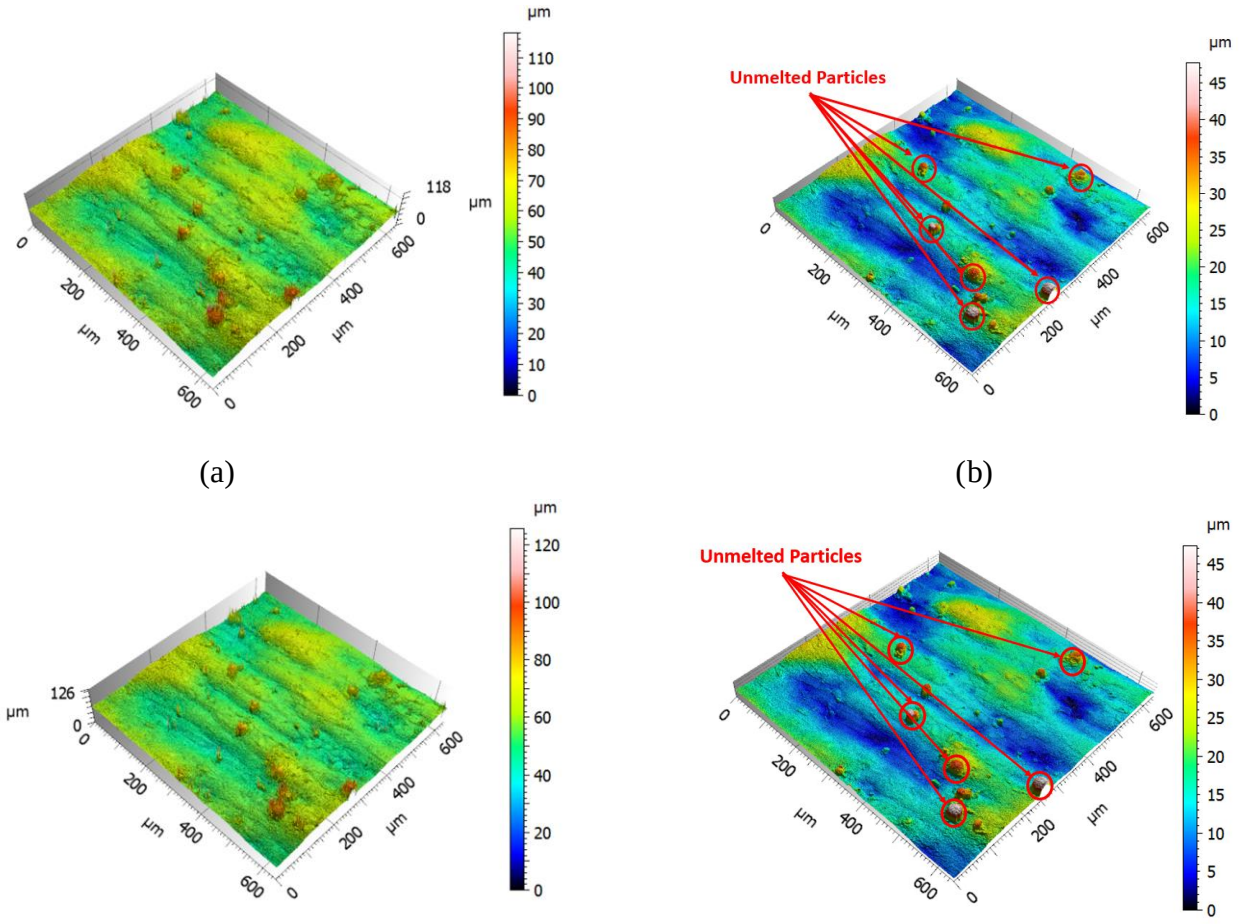

(a) (b)

(c) (d)

Figure 15: The surface measurements taken from laser melted specimen manufactured using a contour speed of 400 mm/s and a contour power of 100 watts: (a) unfiltered measurement 1, (b) filtered measurement 1, (c) unfiltered measurement 2, and (d) filtered measurement 2

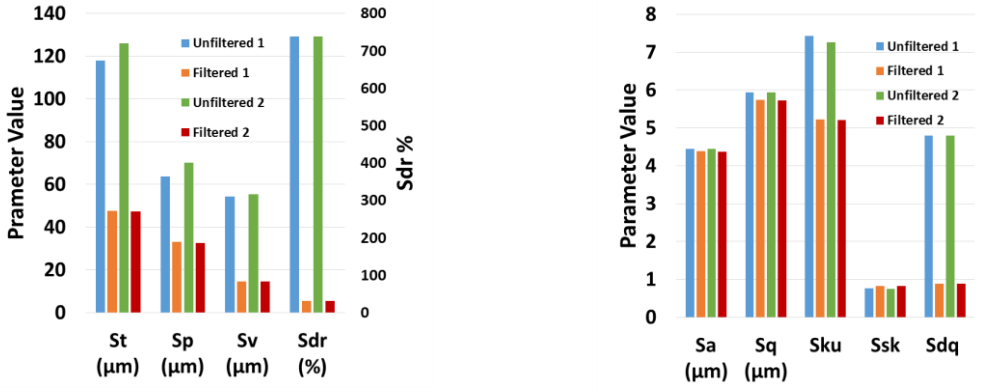

(a) (b)

Figure 16: The conventional parameters of the surfaces presented in Figure 15

Height vs. height plots were created (Figure 17), and several matrices were created illustrating the regression coefficients, R^2, obtained from the height to height comparisons. These matrices can be found in Appendix 7.6. One matrix shows the regression coefficients obtained from the unfiltered surfaces, and the second matrix shows the coefficients from the filtered surfaces. It is clear that outliers greatly influence the repeatability of vertical height data on the additive surfaces (Figure 17a). The regression coefficient was only 0.85, and many of the data points were off of the linear trend-line. After the additive surfaces were filtered, the regression coefficient increased to 0.99, and more data points were closer to the linear trend-line. The average unfiltered regression coefficient obtained from the linear regression analyses was 0.85, with a standard deviation of 0.006. The average filtered regression coefficient obtained from the linear regression analyses was 0.99, with a standard deviation of 0.002.

It is also clear that it is difficult to repeat vertical heights of additive manufactured surfaces. Height plots of areal calibration surfaces used to calibrate optical microscopes were constructed (Figure 17b), and it is clear that outliers on these surfaces to not affect the repeatability of the height data. The regression coefficients for both the unfiltered and filtered surfaces were about 0.999, and were therefore repeatable. Surface measurements of the calibration surfaces are shown in Appendix 7.7.

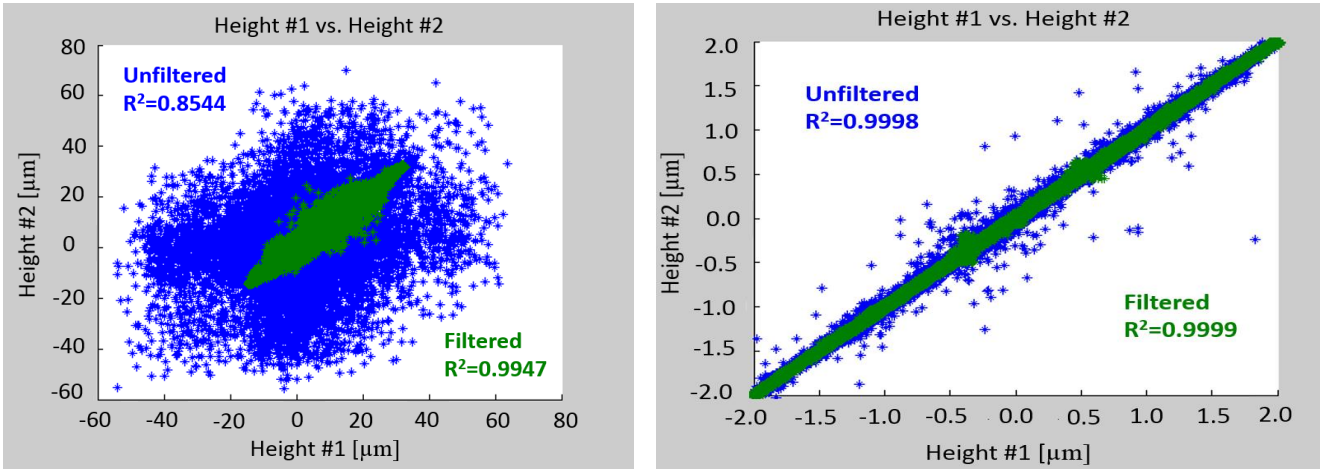

(a) (b)

Figure 17: (a) A height vs. height plot from additive surfaces presented in Figure 15. (b) A height vs. height plot from national physical laboratory calibration surfaces

3.1.2.2 Repeatability between Multiple Locations of a Single Specimen

Outliers were removed from the leveled surfaces using an outlier filter within mountains. Area-scale analyses were performed on both sets of surfaces, and the unfiltered results were compared with the filtered results (Figure 18a). At the larger calculation scales, the relative area of both the unfiltered and filtered surfaces approach one. However, as the calculation scale decreases, the relative area begins to vary. The relative areas for the unfiltered data are relatively higher than the filtered data, and the spread of relative areas is larger for the unfiltered data when compared to the filtered data.

Both sets of data were also compared using an F-Test (Figure 18b). There is a 99% confidence that the unfiltered and filtered surface data can be discriminated at calculation scales below 60 μm^2.

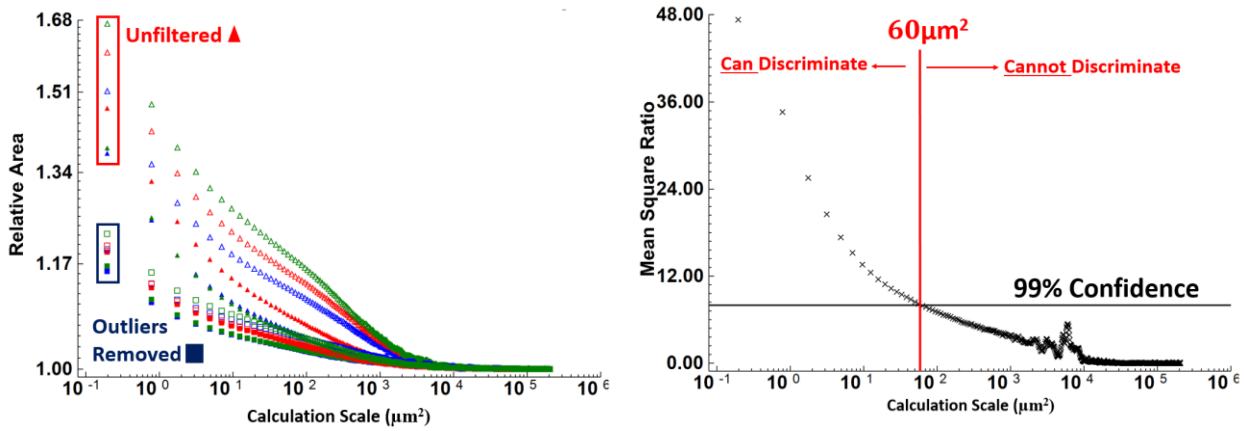

(a) (b)

Figure 18: (a) An area-scale analysis plot of unfiltered and filtered surfaces presented in Figure 4. (b) An F-Test between unfiltered vs. filtered surfaces

Finally, the coefficient of variation (CoV) of each relative area at each individual calculation scale was calculated, and a plot of the coefficient of variation as a function of the calculation scale was constructed (Figure 19). Two curves of the CoV were created; one for the unfiltered surfaces and one for the filtered surfaces. The CoVs for the unfiltered data are much higher than the CoVs for the filtered data. The figure shows a zoomed y-axis CoV plot for the filtered data, giving a better visualization of the changes in CoV as the calculation scale changes, as well as the aliasing that appears between 1,000 and 10,000 μm^2. Removing the outliers causes a decrease in variation at the different locations of the specimen, thus increasing the degree of repeatability. Variance between the unfiltered surfaces begin to occur at a calculation scale of about $4.5x10^3$ μm^2, and variance between the filtered surfaces does not begin to occur until about 5 μm^2.

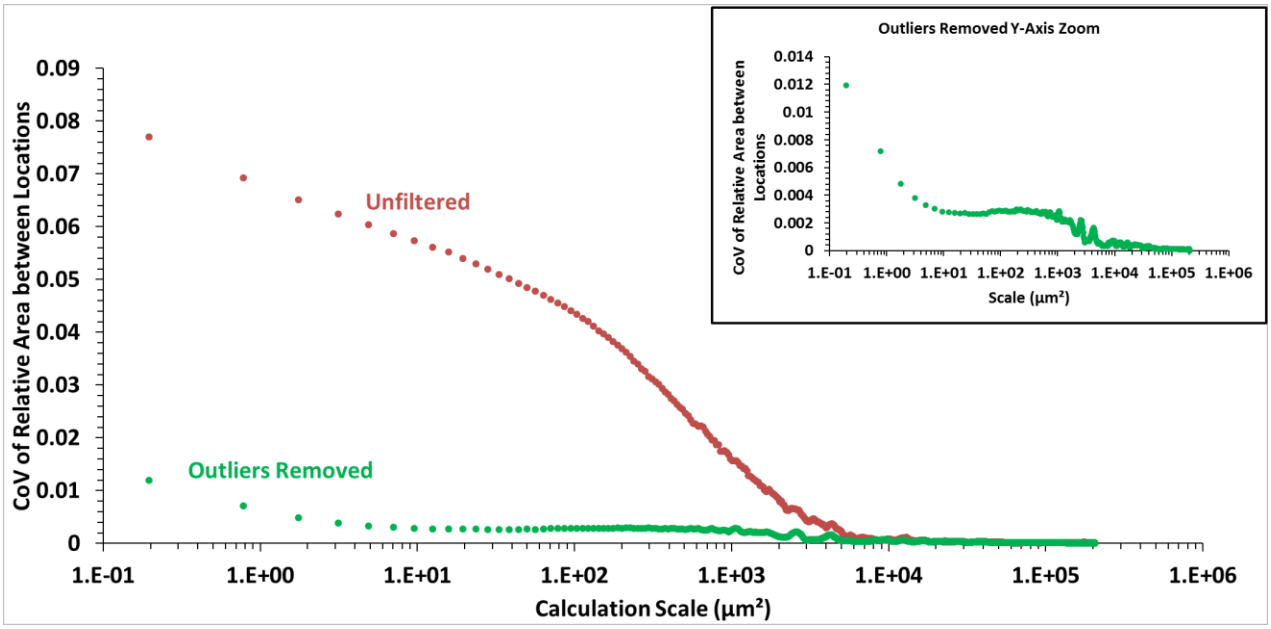

Figure 19: Plots of the CoV of relative areas presented in Figure 18 as a function of scale: unfiltered and filtered surfaces

3.1.2.3 Repeatability between Multiple Specimens at the Same Location

The same procedure used in the location-to-location repeatability experiment was used in the part-to-part repeatability experiment. Measurements were taken at similar locations on four different parts manufactured using the same contour scan speed and contour laser power (Figure 20b).

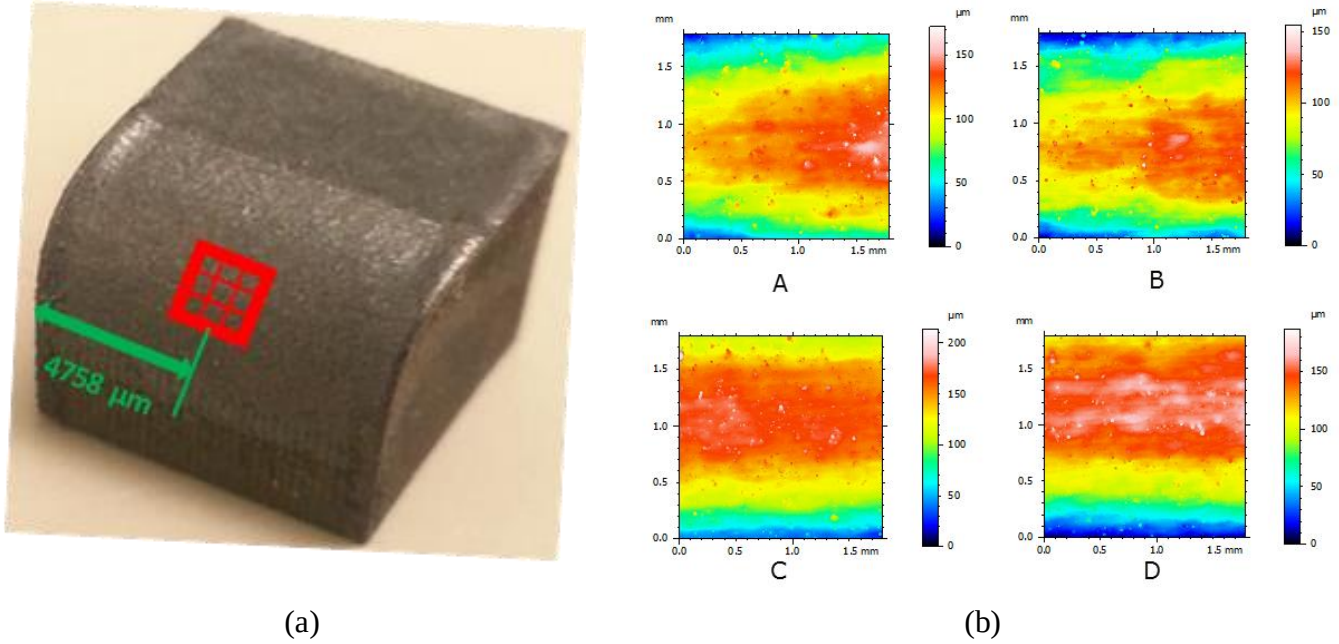

(a) (b)

Figure 20: (a) The location of 3x3 stitched measurement. (b) The four 3x3 stitch measurements on each of the four parts. The measurements were taken on the radial face of the four different parts laser melted using a contour speed of 400 mm/s and a contour power of 100 watts

The four surfaces were leveled, the form was removed, and the outliers were removed using the outlier filter in MountainsMap. Both sets of unfiltered and filtered surfaces were split into quarter sections, and area scale analyses were conducted on each individual section (Figure 21a). An F-test was performed between the filtered and unfiltered surfaces, and a 99% confidence level was used to determine the calculation scale where the surfaces could be discriminated (Figure 21b). This calculation scale was determined to be about 1.8×10^4 µm^2. The CoVs between the four unfiltered and filtered surfaces were calculated as a function of the calculation scale in order to determine the calculation scales where variances can be detected between the surfaces (Figure 22). Variance between the unfiltered surfaces begin to occur at a

calculation scale of about $3x10^4$ μm^2, and variance between the filtered surfaces does not begin to occur until about $1x10^3$ μm^2.

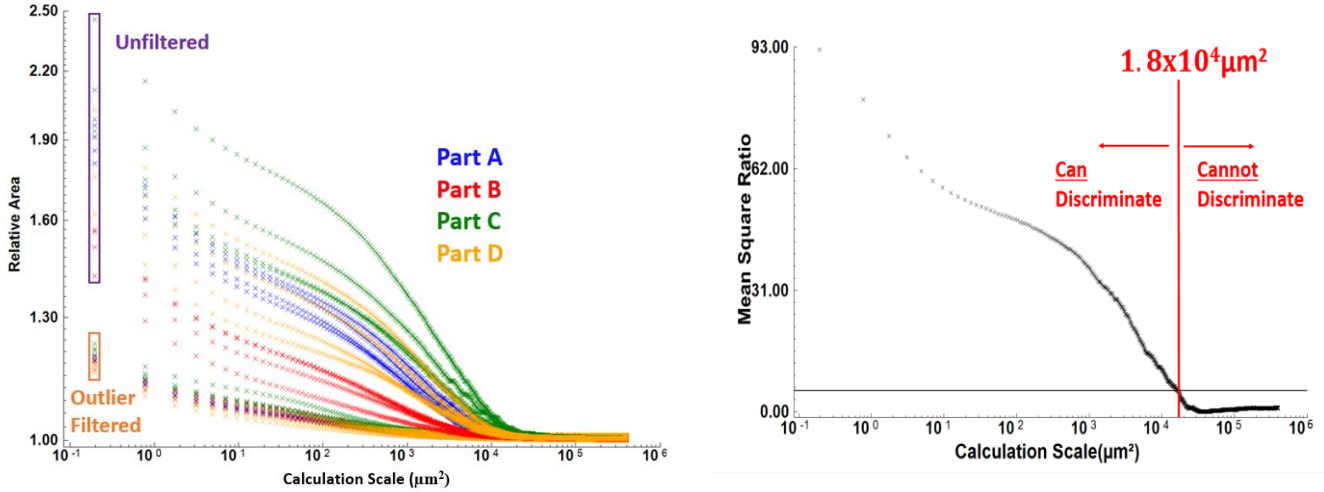

(a) (b)

Figure 21: (a) A relative area vs. calculations scale plot of the unfiltered and filtered surfaces shown in Figure 20, (b) An F-Test between the unfiltered vs. filtered surfaces

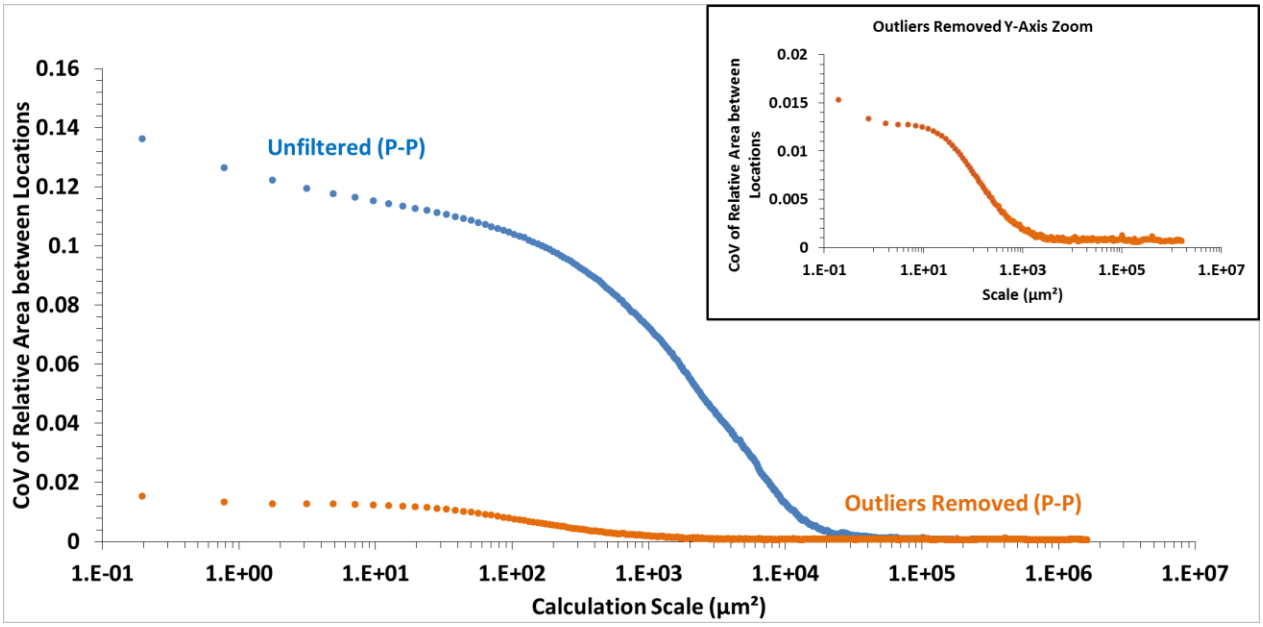

Figure 22: A plot CoVs of the relative area of the unfiltered and filtered surfaces in Figure 21 vs. the calculation scale

3.2 Process Analysis: Functional Correlations

The following sections discuss the calculated correlations between the linear energy density (LED) and both conventional and multi-scale parameters. Linear regression analyses were conducted using surfaces from multiple inclination angles, and using both unfiltered and filtered surfaces. The strongest correlations that were calculated are summarized in Table 4.

Parameter	Inclination Angle [°]	R^2	Equation	Scale [μm^2]	Filter Type
Relative Area	90	0.999	y = -0.6302x + 1.2902	2,964.50	Unfiltered
Sku	90	0.996	y = -3.0564x + 3.449		Unfiltered
Sv	90	0.9799	y = -64.391x + 43.107		Mountains
Sku	90	0.9732	y = -2.2556x + 3.1213		Mountains
Sv	90	0.9577	y = -74.214x + 48.935		Unfiltered
Complexity	0	0.9566	y = -91.558x + 88.464	0.03125	Unfiltered
Sv	90	0.9497	y = -74.214x + 48.935		Modal: 125
Sa	75	0.9208	y = -10.1x + 6.9873		Modal: 500
St	90	0.9134	y = -178.09x + 121.94		Unfiltered
Sa	75	0.9105	y = -10.048x + 6.9545		Modal: 125
Sa	75	0.91	y = -10.048x + 6.9545		Modal: 250
Sv	90	0.898	y = -68.626x + 45.357		Modal: 500
St	90	0.890	y = -129.51x + 98.697		Mountains
St	90	0.888	y = -216.65x + 128.98		Modal:125
Relative Area	0	0.8803	y = -0.1006x + 1.0733	3.78	Mountains
Sdq	90	0.876	y = -85.102x + 46.612		Modal:125
Sp	90	0.871	y = -103.87x + 73.005		Unfiltered
Sv	75	0.871	y = -40.971x + 30.13		Unfiltered
Sv	90	0.857	y = -72.606x + 47.808		Modal: 250

Table 4: Correlations with regression coefficients above 0.85 between linear energy density and conventional and multi-scale parameters ranked by regression coefficient strength. Correlations at 90°, 75°, and 0° are highlighted in green, blue, and orange respectively

3.2.1 Correlations between Conventional Parameters

Conventional parameters were calculated for each unfiltered and filtered measurement. The maximum pit height (Sv), maximum height (St), maximum peak height (Sp), and the kurtosis (Sku) all had regression coefficients larger than 0.85, and these correlations were calculated using the unfiltered surfaces at an inclination angle of 90° (Figure 23a). Additionally, Sku, Sv, and St correlated well using the surfaces that were filtered using the mountains outlier filter, and these correlations occurred at an inclination angle of 90° (Figure 23b).

Sv, St, and Sdq correlated well using the surfaces that were modal filtered using 125 modes at an inclination able of 90° (Figure 23c), and Sv correlated well using the surfaces that were modal filtered using 250 and 500 modes at an inclination angle of 90° (Figure 23d).

Additionally, a strong correlation occurred between Sv and the linear energy density using the unfiltered surfaces at an inclination angle of 75° (Figure 23e). Strong correlations also occurred at an inclination angle of 75° between the arithmetic mean height (Sa) and LED using the modal filter with all three mode types (Figure 23f). The tabulated results of the regression coefficients for inclination angles inclination angles are reported in the Appendix 7.10.

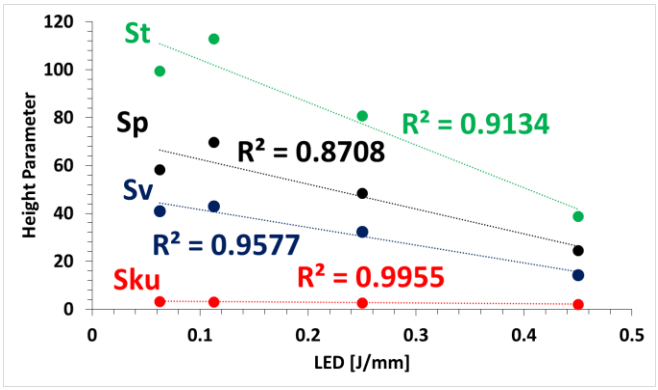

(a)

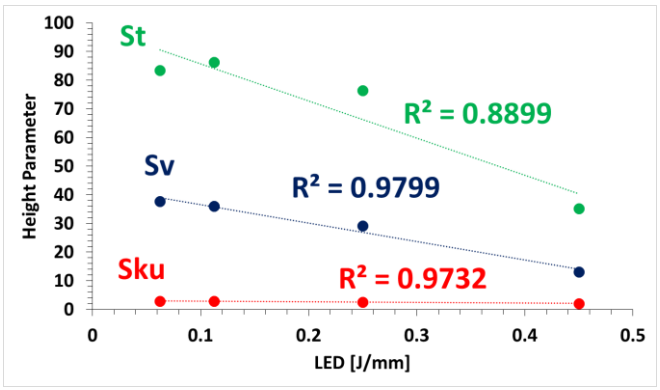

(b)

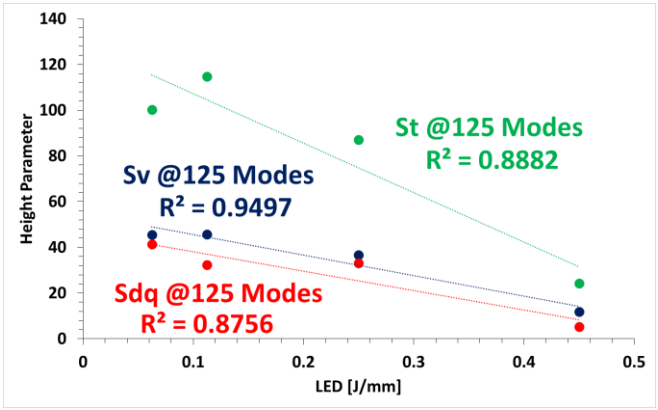

(c)

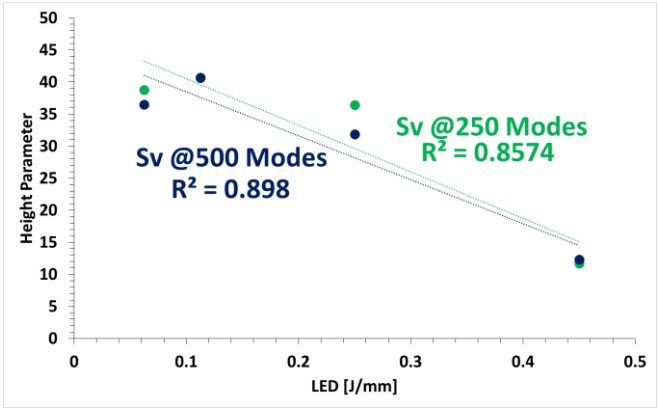

(d)

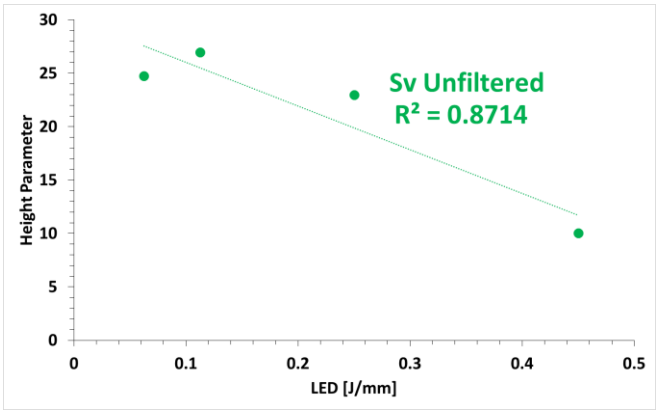

(e)

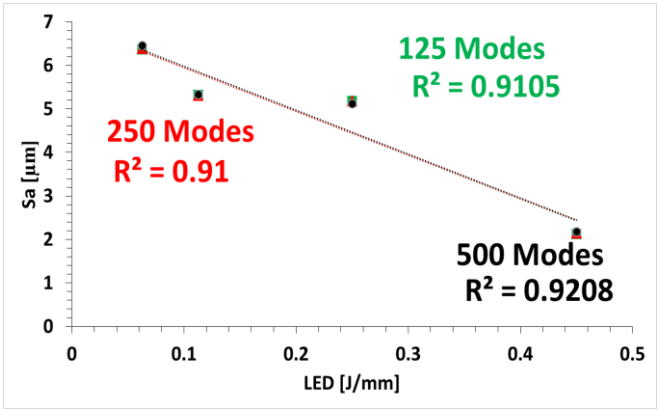

(f)

Figure 23: (a) The correlations between the height parameters and LED at 90° unfiltered, (b) filtered in mountains at 90°, (c) filtered using the modal filter with 125 modes, (d) Sv filtered using the modal filter at 90°, (e) Sv unfiltered at 75°, and (f) Sa filtered using the modal filter at 75°

Furthermore, the root-mean-square gradient (Sdq) relates the inclinations of a surface. The relative area of a surface at the finest scale is similar to the developed area ratio (Sdr) (Berglund et al., 2010). Therefore, the Sdq and Sdr should correlate well. Figure 24shows the correlation between Sdr and Sdq, and it is clear that they are strongly correlated.

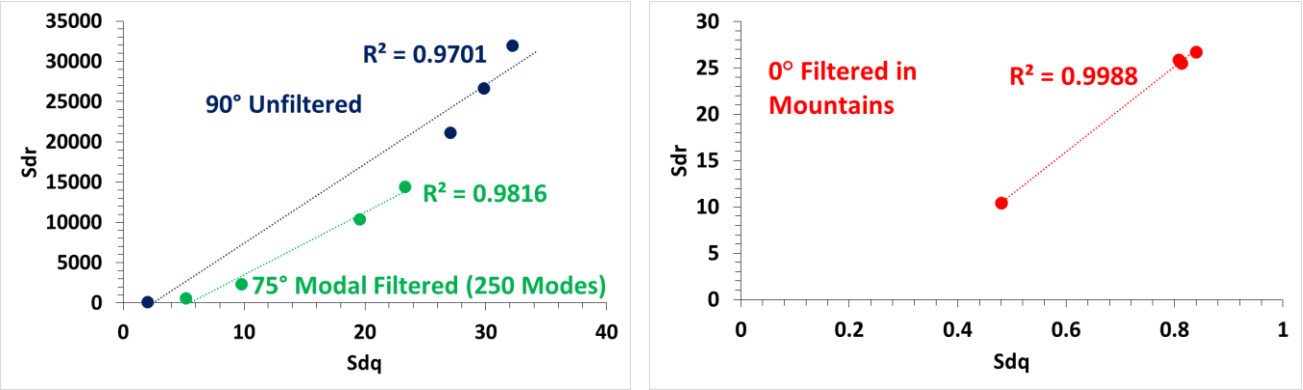

(a) (b)

Figure 24: The cross correlations between Sdr and Sdq

3.2.2 Correlations between Multi-Scale Parameters

Several multi-scale correlation experiments were performed using both the unfiltered and filtered surfaces. The first correlation experiment was conducted using relative area as a function of scale, and the second experiment was conducted using complexity as a function of scale.

3.2.2.1 Correlations between Relative Area and Linear Energy Density

Area-scale analyses were performed on all unfiltered and filtered surfaces, and plots of relative area as a function of the calculation scale were constructed (Figure 25a). These plots can be found in Appendix 7.11. 7.11 Additional Relative Area Plots at Different Inclination Angles

Regression analyses were performed between relative area as a function of scale and linear energy densities. The analyses were calculated at various inclination angles and for both the unfiltered and filtered surfaces. The surface files discussed in this section were not leveled. Plots of the regression coefficients as a function of the calculation scale for various inclination angles and filter types are presented in the Appendix 7.12. Correlations above 0.9 occurred at inclination angles of both 0 and 90° respectively for the unfiltered surfaces (Figure 25b). At an inclination angle of 0°, the correlation coefficients exceeded 0.95 within a calculation scale range of 12,168 and 12,800 μm^2. However, these strong correlations occur above the smooth-to-rough

crossover value calculated in the area-scale analyses. At calculation scales above the smooth-to-rough crossover, the surface appears relatively smooth, and the relative area approaches one. Therefore, it is expected that strong correlations will occur at these larger calculation scales, and these strong correlations are not useful. At an inclination angle of 90°, the correlation coefficients exceeded 0.95 within a calculation scale range of 1,906.53 and 3,528 μm^2. The R^2 curve steadily increased to this relative maximum (Figure 25b). The maximum regression coefficient that occurred at 90° is presented in Figure 27b. The strong correlation at this large calculation scale is useful, because it lies below the smooth-to-rough crossover, and the regression coefficient curve approaches a relative maximum with a periodic trend in the curve. Therefore, there is a strong chance that topographical features at this calculation scale are influencing the relative areas, thus providing justification of the strong correlation.

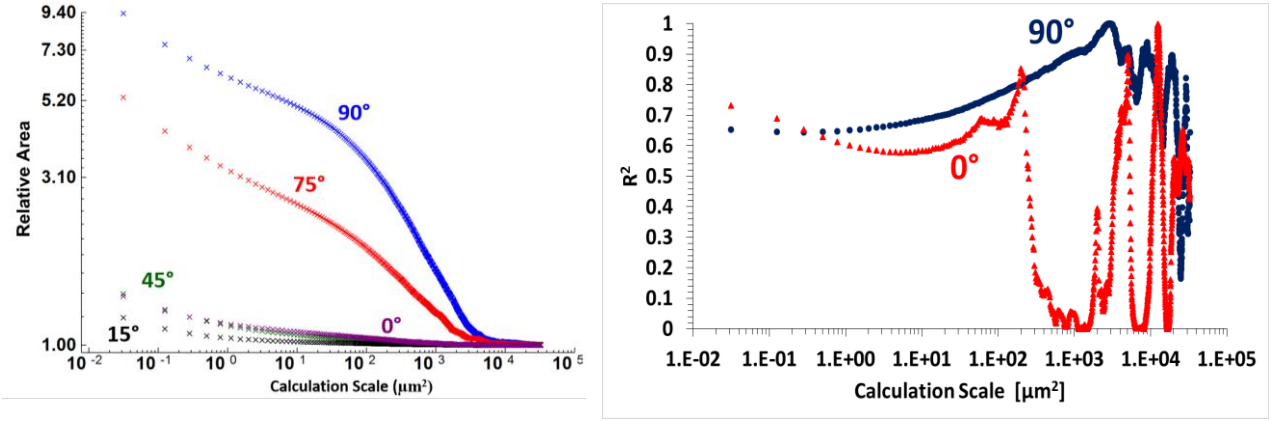

(a) (b)

Figure 25: (a) A plot of the relative area as a function of the calculation scale for the unfiltered surfaces of a single part melted with a contour speed of 400 mm/s and contour power of 100 watts at various inclination angles. (b) The plot of the regression coefficients r^2 for correlations between relative area and LED as a function of the calculation scale using the unfiltered surfaces at 0° and 90°

Filtering the surfaces within mountains reduced the strength of the correlations at 90° (Figure 26a). The strongest correlation was reduced from 0.993 to 0.894. Additionally, the strength of the correlation at 0° increased at the finer calculation scales, and the R^2 curve steadily increased to a relative maximum (Figure 26b). The regression coefficients at these fine calculation scales were larger than 0.8 between a range of 0.281 μm^2 and 26.3 μm^2.

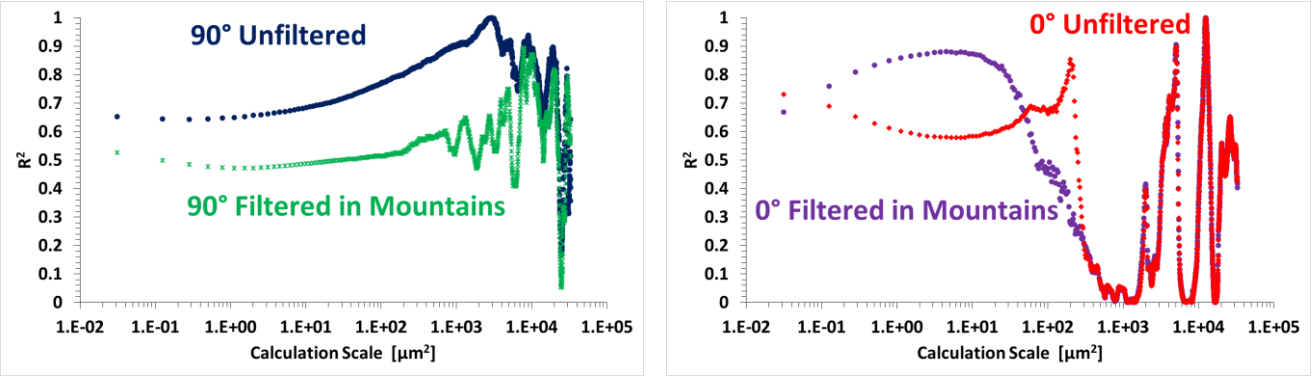

(a) (b)

Figure 26: (a) A plot of the correlation coefficients R^2 for correlations between relative area and LED at 90°. (b) A plot of the correlation coefficients R^2 for correlations between relative area and LED at 0°

Finally, the strength of the correlation at an inclination angle of 75° also increased at the larger calculation scales when the surfaces were filtered using the MountainsMap outlier filter and the modal filter (Figure 27a). The maximum regression coefficients at these large calculation scales were 0.9917, 0.9997, and 0.9992 for 125, 250, and 500 modes respectively (Figure 27a). Similarly, these correlations are not useful, because they were calculated at calculation scales above the smooth-to-rough crossover.

Figure 27b shows the strongest correlations that were calculated using the relative area at specific calculation scales. The strongest calculated correlation occurred at an inclination angle of 90° using the unfiltered surfaces.

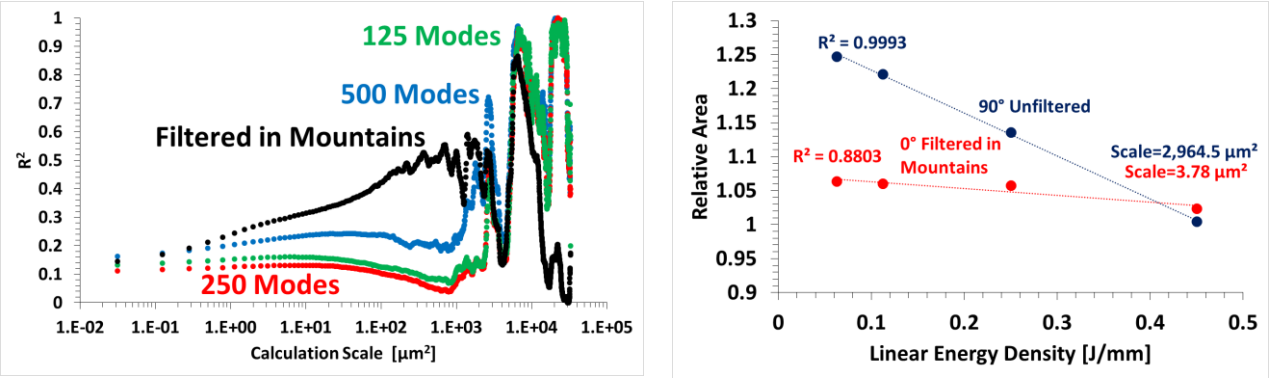

(a) (b)

Figure 27: (a) A plot of the correlation coefficients R^2 for correlations between relative area and LED at 75°. (b) Correlations at specific scales between the relative area and the LED

The relative area at the finest scale and the developed area ratio are similar (Berglund et al., 2010). Therefore, there should be a strong correlation between Sdr and the relative area calculated at the finest calculation scale. Figure 28 shows examples of these cross correlations, and it is clear that the relative area at the finest calculation scale and Sdr correlate well.

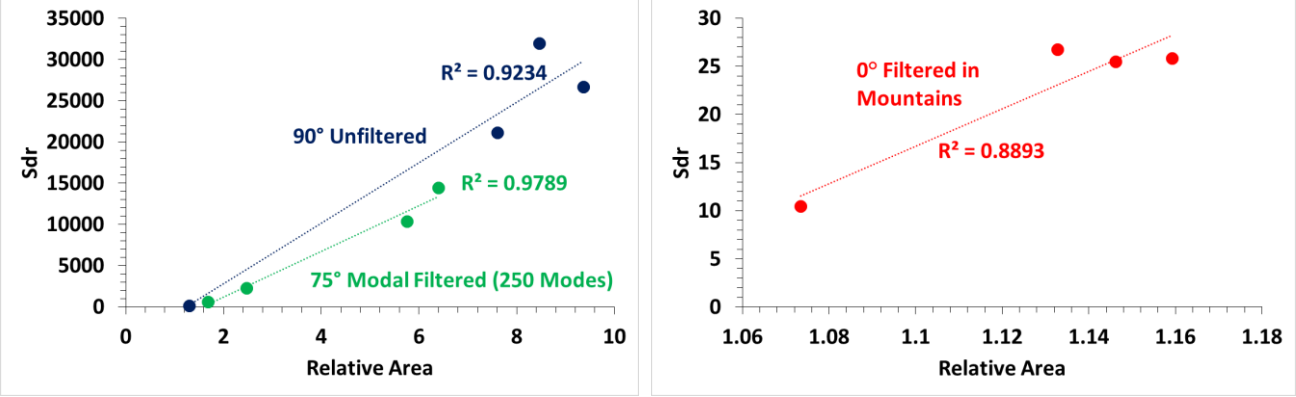

Figure 28: The cross correlations between the relative area at the finest scale and Sdr

3.2.2.2 Correlations between Complexity and Linear Energy Density

Plots of complexity as a function of the calculation scale were constructed (Figure 29a). These plots can be found in Appendix 7.13. Regression analyses were performed between complexity as a function of scale and linear energy density at various inclination angles. Plots of the regression coefficient, R^2, as a function of scale for each inclination angle, and for each filter type, can be found in Appendix 7.14. 7.13 Additional Complexity Plots at Different Inclination Angles

A relative maximum regression coefficient of 0.999 occurred at an inclination angle of 90° at a calculation scale range of 9,146 and 9,488 μm^2 for the unfiltered surfaces (Figure 29b). However, this strong correlation is not useful, because it was calculated at a calculation scale that was above the smooth-to-rough crossover.

Additionally, strong regression coefficients occurred at an inclination angle of 0° at the finer calculation scales. Coefficients exceeding 0.95 occur at calculation scales of 0.03125 and 0.125 μm^2 for the unfiltered surfaces (Figure 29b). Figure 29b. illustrates correlations that occur at inclination angles of 0 and 90° at specific calculation scales. Strong correlations are not clearly visible at inclination angles of 15, 45, or 75°

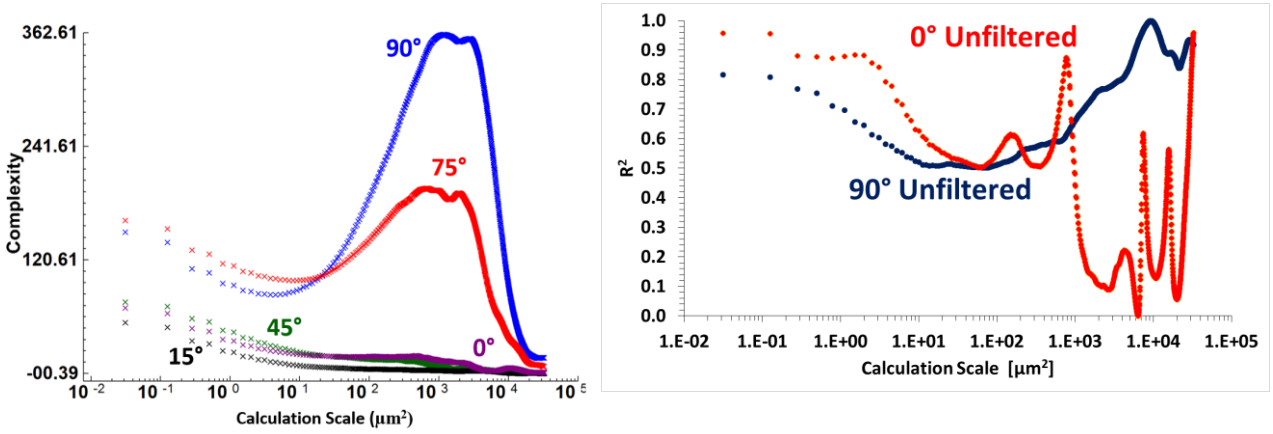

(a) (b)

Figure 29: (a) A plot of the complexity as a function of scale for the unfiltered surfaces of a single part melted with a contour speed of 400 mm/s and contour power of 100 watts at various inclination angles, (b) A plot of the correlation coefficients R^2 for correlations between complexity and LED at 0° and 90°

Filtering the surfaces using the MountainsMap outlier filter caused the large-scale correlation at 90° to weaken (Figure 30a), and it caused the fine-scale correlations at 0° to also weaken (Figure 30b). At the 90° inclination angle, the maximum regression coefficient was reduced from 0.999 to 0.947. At the 0° inclination angle, the maximum regression coefficient was reduced to 0.305 at the same calculation scale after the surfaces were filtered.

Additionally, two relative maximum correlation coefficients occurred at 75°, and these correlation coefficients occurred at calculation scales of about 5,000 and 19,000 μm^2 respectively when the MountainsMap outlier filter was used. (Figure 30c). Again, these correlations were not useful, because they were calculated at calculation scales above the smooth-to-rough crossover. Figure 31 shows the strongest correlation that used complexity. The strongest correlation occurred at an inclination angle of 90° using the unfiltered surfaces. The regression coefficient was 0.9566.

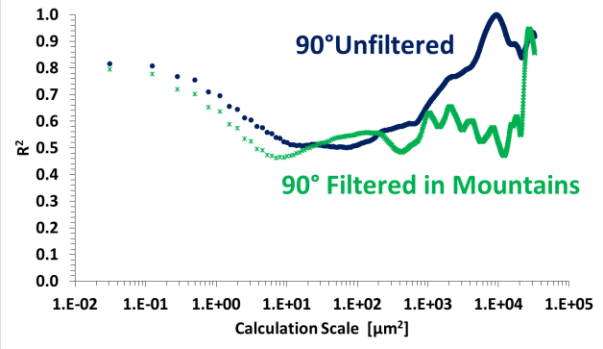

(a)

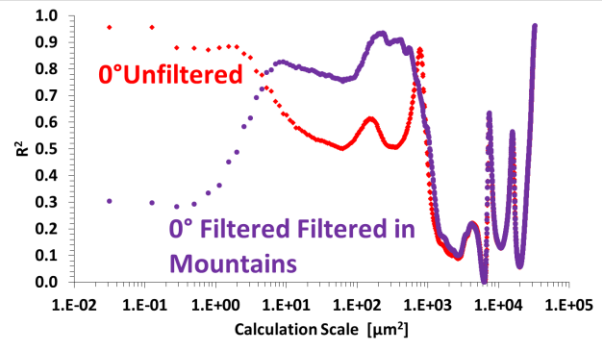

(b)

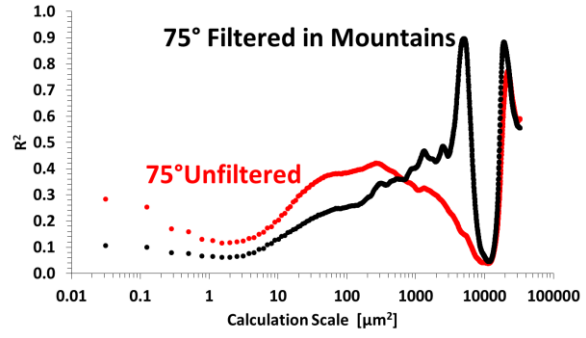

(c)

Figure 30: Plots of the correlation coefficients R^2 for correlations between complexity and LED at 90° (a), at 0° (b), and at 75° (c)

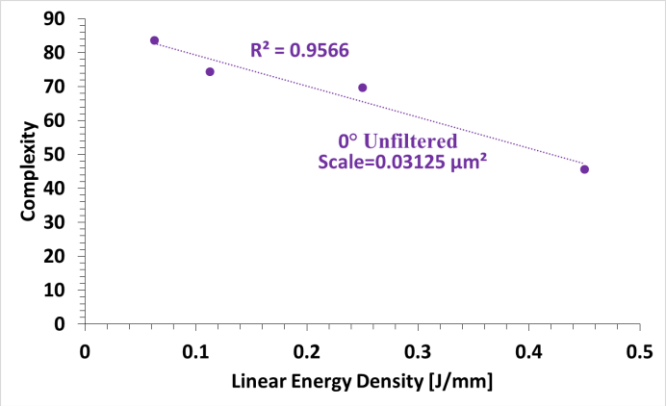

Figure 31: The strongest regression coefficient between complexity and linear energy density obtained at a fine scale

4.0 Discussion

4.1 Homogeneity Crossover

It is clear that the arithmetic mean height, Sa, root-mean-square height, Sq, skewness, Ssk, and Kurtosis, Sku, showed heterogeneous-to-homogeneous crossovers. Their curves of the coefficient of variation as a function of measurement scale showed a clear transition from larger CoVs to lower CoVs, and their curves appeared to level out on either side of the transition. However, the remaining conventional parameters did not exhibit this behavior. Their curves of CoV as a function of measurement scale gradually decreased as the measurement scale increased. Similarly, the CoV curves of the maximum relative area and complexity also gradually decreased as the measurement scale increased. Finally, the curve of the smooth-to-rough crossover increased to a relative maximum, and then gradually decreased as the measurement scale increased.

Both Sa and Sq are calculated using averages of height data over the spatial region (Equation 4), and Sku and Ssk both use Sq in their respective calculations (Equation 5). The remaining height parameters (Sp, Sv, and St) all use single height points in their calculations (ISO/DIS 25178-2). For example, Sp is the maximum peak height. Therefore, only a single height point is used to calculate Sp. Sv is the maximum pit height, and St is the maximum height (ISO/DIS 25178-2). One hypothesis is that the CoV curves of Sa, Sq, Ssk, and Sku show stronger crossover regions because more height data over the spatial region is used in their respective calculations.

$$S_a = \iint_a |Z(x,y)| dxdy$$

(a)

$$S_q = \sqrt{\iint_a (Z(x,y))^2 dxdy}$$

(b)

Equation 4: (a) The arithmetic mean height equation, (b) and the root-mean-square height equation (Michigan Metrology, 2014)

$$Ssk = \frac{1}{{S_q}^3} \iint_a (Z(x,y))^3 dxdy$$

(a)

$$Sku = \frac{1}{{S_q}^4} \iint_a (Z(x,y))^4 dxdy$$

(b)

Equation 5: (a) The skewness equation, (b) and the kurtosis equation (Michigan Metrology, 2014)

However, the hybrid parameters Sdr (Developed interfacial area) and Sdq (Root-mean-square slope) both use spatial data in their calculations (EUR 15178N, 1993), and the maximum relative area and complexity use spatial data in their calculations (Leach, 2013). Their curves of CoV did not show a clear crossover. One hypothesis is that the CoV curves for these parameters would begin to level off if more measurement scales were tested. It is recommended that the coefficients of variation at measurement scales below 0.0338 mm^2 and at measurement scales larger than 7.5625 mm^2 be calculated in order to test this hypothesis.

It was also determined that the homogeneity crossover region on the CoV curves began when the square tiles at the larger measurement scales began to overlap (Figure 2). Therefore, some unique topographical features could have been shared between the tiles, and could have influenced the decrease in the coefficients of variation at the larger measurement scales. Furthermore, the individual tiles at all measurement scales were not outlier filtered or leveled, because there were no outliers visible on the stitched surface, and the surface appeared leveled (Figure 1). Therefore, there is a possibility that the presence of small outliers on the stitched surface could have influenced the CoV calculations. It is recommended that the procedure presented in section 2.1.1 be repeated using measurements that have been outlier filtered.

The strong cross correlation between skewness and kurtosis was expected, because skewness illustrates the degree of symmetry of heights about a mean plane, and kurtosis illustrates unusual peaks or valleys (Michigan Metrology, 2014). The 2nd and 3rd statistical moments share a strong relationship. Similarly, the developed interfacial are and root-mean

square slope were expected to have a strong cross correlation, because the developed area can be influenced by the slope (Berglund et al., 2010). Finally, a strong cross correlation between the root-mean-square height and the arithmetic mean height occurred, and differences were clearly visible at finer measurement scales. This observation was supported by the coefficient of variation plots presented in the results section.

Finally, this study served as an excellent case study for three developing principles of surface metrology. All three of these principles influenced the homogeneity crossover experiment presented in this work. For example, certain parameters that characterize the geometry of the surface in specific ways proved useful in characterizing the homogeneity crossover, while other parameters did not. It is also clear that there is a necessary range of measurement scales needed to characterize the homogeneity crossover. A smaller range was needed in order to visualize the homogeneity crossover using Sa, Sq, Ssk, and Sku, and it is possible that the range of tested measurement scales was too small in order to properly characterize the homogeneity crossover using Sdr, Sdq, and the multi-scale parameters. Finally, the size of the stitched measurement also provided enough testable measurement scales needed to characterize the homogeneity crossover using Sa, Sq, Ssk, and Sku. However, in order to test the hypothesis that larger measurement scales may be needed for Sdr, Sdq and the multi-scale parameters, a larger stitched measurement may be needed. Additionally, the fidelity of the measurement may need to be improved through outlier filtering and leveling. It is clear that a larger range of measurement scales need to be analyzed in order to see if other parameters can be used to characterize the heterogeneous-to-homogeneous crossover presented in this work.

4.2 Repeatability

It is clear that there is a low degree of repeatability of vertical height data between multiple measurements of the laser melted surfaces when compared to the repeatability of the areal calibration surfaces. It is also clear that outliers in the surface measurements greatly impact the repeatability of vertical height data between multiple measurements taken at a single location. The linear regression coefficients between the unfiltered surfaces did not surpass 0.86, while the regression coefficient from the NPL surfaces was 0.9998. When the outliers were removed, the regression coefficients increased, reaching about 0.99. However, the regression coefficients of the filtered surfaces were still not as strong as the filtered NPL coefficient of 0.9999. Additive manufactured surfaces are naturally chaotic with distinct surface characteristics

that are very different from surfaces that are manufactured using traditional processes. Therefore, it is difficult to repeat the vertical height data of additive manufactured surfaces multiple times.

However, this work presents alternative ways of characterizing the repeatability of additive manufactured surfaces. The relative area as a function of the calculation scale was used as a repeatability parameter to test the ability to repeat surface measurements between multiple locations on the same part and between multiple parts at the same location. It is clear that differences in the relative area occur as the calculation scale decreases (Figure 18a and Figure 21b). Plotting the coefficients of variation of the relative area as a function of the calculation scale also served as a means of visualizing the degree of repeatability (Figure 19 and Figure 22). It is also clear that outliers in the surface measurements also influence the variance of the relative area at these calculation scales. Variance between the unfiltered surfaces, visible through the CoV curves, begins at larger calculation scales, and variance between the filtered surfaces begins at much finer calculation scales. This observation occurred between different locations on the same part, and it occurred between different parts at relatively the same location.

One of the developing principles in surface metrology states that measurements of high fidelity are required in order to successful discriminate and correlate. The repeatability studies in this work support this developing principle. Surface measurements must have a high degree of repeatability in order for any discrimination or correlation experiment in surface metrology to be valuable. This work showed that outliers influence the ability to repeat surface measurements of additive manufactured parts. Therefore, it can be concluded that outlier removal is a necessity in discrimination and correlation experiments using additive manufactured surfaces. Outliers affect the overall fidelity of these surface measurements. However, it is also clear that the degree of repeatability is influenced by the geometrical parameter used to quantify it. Simply using the vertical height data to quantify the degree of repeatability is not sufficient. Using the relative area as a means of quantifying the repeatability proved to be more robust. The CoVs for both location-to-location and part-to-part repeatability fell within a range of 0 to about 0.14 at the finest calculation scales, which is relatively low. Therefore, the degree of repeatability between additive manufactured surfaces can be considered relative high when it is quantified using relative area. A second developing principle of surface metrology states that the proper geometrical parameter must be used in order to successful discriminate or correlate. Therefore, if

a particular correlation or discrimination experiment successfully used relative area as a characterization parameter, and the CoV curves calculated using multiple measurements are relatively low, the results of the study become more valid.

4.3 Correlation with Linear Energy Density

It is clear that the orientation of the build and the method of filtering greatly impacts the correlation strength between conventional and multi-scale parameters and the linear energy density of the laser. For example, strong correlations using conventional parameters occurred at an inclination angle of 90° and at 75° (Figure 23). Additionally, the method of outlier filtering also influenced the strength of these conventional correlations. Many correlation strengths of some conventional parameters were weakened after filtering the surfaces (such as Sv and St at 90°) while others were improved after filtering (such as Sa at 75°) (Figure 23). Similarly, the correlation strengths using relative area were improved at an inclination angle of 0° when the surfaces were filtered, while the strengths at a 90° inclination angle were weakened after the surfaces were filtered (Figure 26). Similar observations were seen using complexity. When the surfaces were filtered at a 0° inclination angle, the fine-scale correlations using complexity were greatly weakened, while the large-scale correlations were improved (Figure 30b). The filter method and inclination angle are both factors that influence the correlation strength of the linear energy density with surface parameters.

It is also clear that certain multi-scale correlation strengths are more useful than others. For example, at very large scales, many surfaces will have the same relative area, and they will typically approach one (Figure 25a). Therefore, the chance that strong correlations will occur at large scales increases. Examples of this phenomena are visible on the unfiltered 0° R^2 curve where the relative maximums occur (Figure 25b). More reliable correlations occur when the R^2 curves approach a relative maximum, but also follow a predictable trend. An example of this phenomena is visible on the unfiltered 90° R^2 curve (Figure 25b). However, correlations that occur above the smooth-to-rough crossover calculated in the area-scale analyses are not useful, because the relative areas approach one at larger calculation scales, and strong correlation coefficients are expected. It is also typical that strong correlations on the R^2 curve do not follow a trend at these calculation scales. Furthermore, strong correlations that occur at finer calculation scales are more useful than correlations that occur at larger ones, because more topographical features of the surface are characterized at the smaller calculation scales. This work showed that

the complexity provided the strongest correlations with the linear energy density at the finest calculation scales (Figure 29b). Additionally, strong correlations occurred using several conventional parameters that are not sensitive to the calculation or measurement scale. The first developing principle states that the appropriate measurement and calculation scales must be analyzed in order to properly discriminate or correlate. These strong correlations using conventional parameters provided an example where strong correlations were calculated when the first developing principle was not maintained.

Furthermore, the confidence of the correlations could be improved with a stronger understanding of the scan pattern used during the build. The confidence of the correlations could be improved if the degree of repeatability was better established, as discussed in Section 4.1. Finally, this correlation study served as an excellent case study for the developing principles. Strong correlations were obtained in this study using surface measurements that contained the necessary measurement scales needed to discover these correlations, and several conventional parameters and multi-scale parameters provided the necessary geometrical characterization. It is also possible that undiscovered correlations exist at measurement scales that were not captured in the surface measurements presented in this work, and it is possible that other geometrical parameters could be suitable to make the correlations. It is recommended that wider measurement scale ranges be tested using additional geometrical parameters that were not presented in this work.

5.0 Conclusions

The following conclusions can be drawn from this work:

1. The height parameters: root-mean-square height and arithmetic mean height exhibit a heterogeneous-to-homogenous crossover behavior (between about 0.411 $mm^2$and 3.0625 mm^2) when their coefficients of variation, calculated at each measurement scale, are plotted as a function of the measurement scale. The coefficients of variation CoVs at the fine measurement scales below 0.411 mm^2 begin to plateau, and the coefficients of variation at the large measurement scales above 3.0625 mm^2 also begin to plateau.
2. The statistical moments: Skewness and Kurtosis exhibit heterogeneous-to-homogenous crossover behavior (between about 0.345 $mm^2$and 3.0625 mm^2). The coefficients of variation at the fine measurement scales below 0.345 mm^2 begin to plateau, and the coefficients of variation at the large measurement scales above 3.0625 mm^2 also begin to plateau.
3. The heterogeneous-to-homogenous crossover behavior occurs when the tiling begins to overlap at measurement scales larger than 0.345 mm^2.
4. Strong cross correlation regression coefficients were calculated between skewness and kurtosis, arithmetic mean height and root-mean-square height, the maximum heights, and the root-mean-square slope and the developed interfacial area.
5. The presence of outliers was quantified and visualized when plots of the vertical height data between surface measurements were constructed, but these plots cannot be used as a repeatability quantifier for laser melted surfaces.
6. Plots of the coefficient of variation of the relative area between surface measurements as a function of the calculation scale provided a scale-based quantification of the degree of repeatability. These plots also showed that scale limits of repeatability exist.
7. The strongest correlations with the linear energy density occurred at an inclination angle of 90° using relative area at a calculation scale of 2,964.50 μm^2, Sku, Sv, Sp, Sdq, and St. Additionally, the relative area and complexity provided strong correlations at fine calculation scales at a 0° inclination angle, and Sv correlated well at a 75° inclination angle. The strength of the calculated correlations is influenced by the inclination angle and by the method of outlier filtering.

8. The three experiments presented in this work provided critiques of the developing principles of surface metrology. The ability to characterize the homogeneity crossover depends on the size of the measurement scales. Measurement fidelity strongly influences the degree of repeatability between surface measurements of laser melted parts. The multi-scale correlations between the linear energy density and the relative area and complexity are clearly scale dependent, and the relative area and complexity of the surface as a function of the calculation scale were appropriate geometrical parameters. However, strong correlations occurred using conventional parameters that are not scale dependent, which does not abide by the first principle.

6.0 References

1. ASME B46.1 2009. Surface Texture (Surface Roughness, Waviness, and Lay), ASME, New York 2009.
2. BERGLUND, J., BROWN, C. A., ROSÉN, B.-G. & BAY, N. 2010. Milled die steel surface roughness correlation with steel sheet friction. *CIRP Annals-Manufacturing Technology,* 59**,** 577-580.
3. BERGSTROM, T. S., HAMEL, R. A., KUMMAILIL, J., GRAY, A. R. & BROWN, C. A. Comparison of surface texture measurement systems. XIth International Colloquium on Surfaces, 2004 Chemnitz, Germany.
4. BROWN, C. 2014. Functional Correlation. *In:* LAPERRIÈRE, L. & REINHART, G. (eds.) *CIRP Encyclopedia of Production Engineering.* Springer Berlin Heidelberg.
5. BROWN, C. Fundamentals of Multi-scale Analysis, Characterization, Discrimination and Correlation in Surface Metrology. 5th International Conference on Surface Metrology, 2016 Poznan, Poland.
6. BROWN, C. & BURNS, C. 2014. Form and Outlier Removal By Modal Filtering of Confocal Measurements of Laser-Sintered Additive-Manufactured Surfaces. *29th Annual Meeting of the American Society for Precision Engineering.* Boston, Massachusetts.
7. BROWN, C. A., HAMEL, R., KUMMAILIL, J., O'CONNELL, M. & BERGSTROM, T. S. Analyzing the Accuracy of Surface Measurement Systems and Replicas. 9th International Conference on the Metrology and Properties of Engineering Surfaces, 2003 Halmstead, Sweeden.
8. BROWN, C. A. & SIEGMANN, S. 2001. Fundamental scales of adhesion and area–scale fractal analysis. *International Journal of Machine Tools and Manufacture,* 41**,** 1927-1933.
9. EUR 15178N 1993. "The development of methods for the characterisation of roughness in three dimensions", Stout, Sullivan, Dong, Mainsah, Luo, Mathia, Zahouani, Commision of the European Communities, EUR 15178 EN.
10. GHANEKAR, A., CRAWFORD, R. & WATSON, D. Optimization of SLS process parameters using D-optimality. Proceedings of the 14th International Solid Freeform Fabrication Symposium, 2003. 348-362.

11. GRIMM, T., WIORA, G. & WITT, G. 2015. Characterization of typical surface effects in additive manufacturing with confocal microscopy. *Surface Topography: Metrology and Properties,* 3**,** 014001.
12. GU, D. & SHEN, Y. 2009. Balling phenomena in direct laser sintering of stainless steel powder: Metallurgical mechanisms and control methods. *Materials & Design,* 30**,** 2903-2910.
13. GU, K. K., LIN, Q., WANG, W. J., WANG, H. Y., GUO, J., LIU, Q. Y. & ZHU, M. H. 2015. Analysis on the effects of rotational speed of grinding stone on removal behavior of rail material. *Wear,* 342–343**,** 52-59.
14. HASHMI, M. S. J. 2014. *Comprehensive Materials Processing,* Waltham, MA, Elsevier
15. HYDE, J., CADET, L., MONTGOMERY, J. & BROWN, C. 2014. Multi-scale areal topographic analysis of surfaces created by micro-EDM and functional correlations with discharge energy. *Surface Topography: Metrology and Properties,* 2**,** 045001.
16. ISO 2016. ISO 25178-700-draft-presentation Poznan. *Annex E Repeatability and Reproducibility.*
17. ISO/DIS 25178-2 Geometrical Product Specifications (GPS)- Surface Texture: Areal-Part 2: Terms, Definitions and Surface Texture Parameters.
18. KALPAKJIAN, S. & SCHMID, S. 2014. *Manufacturing Engineering and Technology,* Saddle River, New Jersey, Pearson Prentice Hall.
19. KRUTH, J.-P., LEVY, G., SCHINDEL, R., CRAEGHS, T. & YASA, E. Consolidation of polymer powders by selective laser sintering. Proceedings of the 3rd International Conference on Polymers and Moulds Innovations, 2008. 15-30.
20. LE GOÏC, G., BROWN, C., FAVRELIERE, H., SAMPER, S. & FORMOSA, F. 2012. Outlier filtering: a new method for improving the quality of surface measurements. *Measurement Science and Technology,* 24**,** 015001.
21. LEACH, R. 2011. *Optical Measurement of Surface Topography,* Berlin, Germany, Springer Berlin-Heidelberg.
22. LEACH, R. 2013. *Characterisation of areal surface texture,* Verlag Berlin Heidelberg, Springer.

23. MICHIGAN METROLOGY, L. 2014. *3D S Parameters-Height (Amplitude) Parameters* [Online]. Available: http://www.michmet.com/3d_s_height_parameters.htm [Accessed April 17 2016].
24. MUMTAZ, K. & HOPKINSON, N. 2009. Top surface and side roughness of Inconel 625 parts processed using selective laser melting. *Rapid Prototyping Journal,* 15**,** 96-103.
25. PEDRESCHI, F., AGUILERA, J. M. & BROWN, C. A. 2002. Characterization of the surface properties of chocolate using scale-sensitive fractal analysis. *International Journal of Food Properties,* 5**,** 523-535.
26. SUH, N. P. 1990. *The Principles of Design,* New York, Oxford University Press.
27. SURFRACT. 2007. *Surfract Surface Metrology and Fractal Analysis* [Online]. Available: http://www.surfract.com/ [Accessed March 27 2016].
28. VULLIEZ, M., GLEASON, M. A., SOUTO-LEBEL, A., QUINSAT, Y., LARTIGUE, C., KORDELL, S. P., LEMOINE, A. C. & BROWN, C. A. 2014. Multi-scale curvature analysis and correlations with the fatigue limit on steel surfaces after milling. *Procedia CIRP,* 13**,** 308-313.
29. ZENG, Y., WANG, K., MELLOW, B. C., WANG, J. & BROWN, C. A. Multi-scale Evaluations of the Roughness of Surfaces Make By Additive Manufacturing. American Society of Precision Engineering 2014 Spring Topical Meeting: DImensional Accuracy and Surface Finish in Additive Manufacturing, 2014 Raleigh, North Carolina.

7.0 Appendices

7.1 Surface Measurement Used in the Heterogeneous-to-Homogenous Crossover Analysis

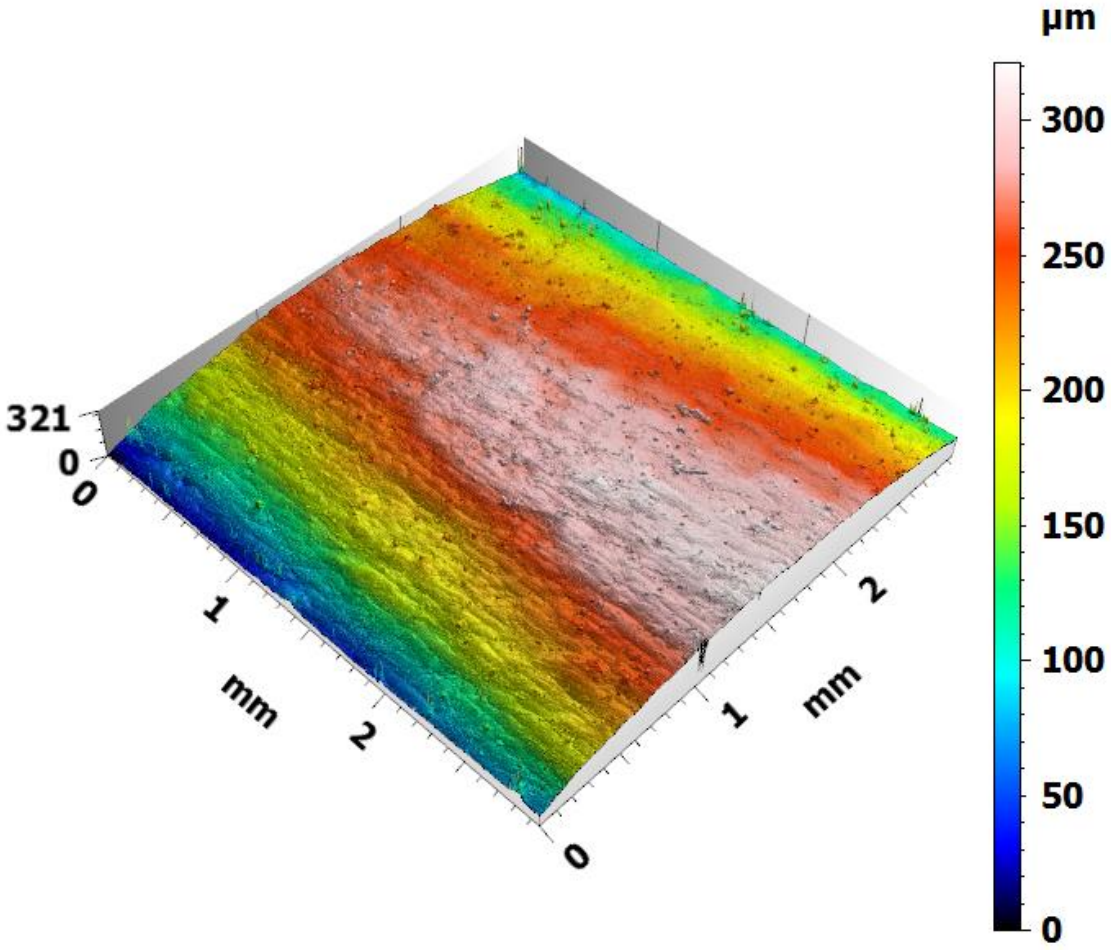

ISO 25178		
Height Parameters		
Sq	66.2	µm
Ssk	-0.717	
Sku	2.69	
Sp	104	µm
Sv	217	µm
Sz	321	µm
Sa	55.2	µm
ASME B46.1		
3D Parameters		
St	321	µm
EUR 15178N		
Hybrid Parameters		
Sdr	2738	%
Sdq	9.90	

Figure 32: Stitched measurement used in the homogeneity crossover analysis

7.2 Homogeneity Crossover Procedure

The following procedure was followed in order to calculate the CoVs of the conventional parameters at each scale during the homogeneity crossover analysis.

1. Import the fully stitched measurement into MountainsMap Premium®.
2. Extract the topography layer of the fully stitched measurement.
3. Use the extract area operator, and position the square region in the upper left corner of the measurement. Adjust the size of the square to match the desired scale. Extract the area.
4. Calculate and export the conventional parameters of the extracted area.
5. Repeat steps 3 and 4 moving the square extraction region down and across the measurement until it have been fully tiled.
6. Import all of the exported conventional parameters into a Microsoft Excel® document.
7. Calculate the mean, standard deviation, and coefficient of variation for each parameter.
8. Repeat steps 1 through 7 for all desired scales.
9. Construct plots of the coefficient of variation as a function of scale.

7.3 Additional Cross Correlation Plots from Homogeneity Crossover Analysis

The following plots show two additional cross correlations that were strong in the hetero-to-homogenous crossover analysis. Skewness and Kurtosis had a strong correlation of 0.893 (Figure 33), and the developed interfacial area and the root-mean-square slope had a strong correlation of 0.859 (Figure 34).

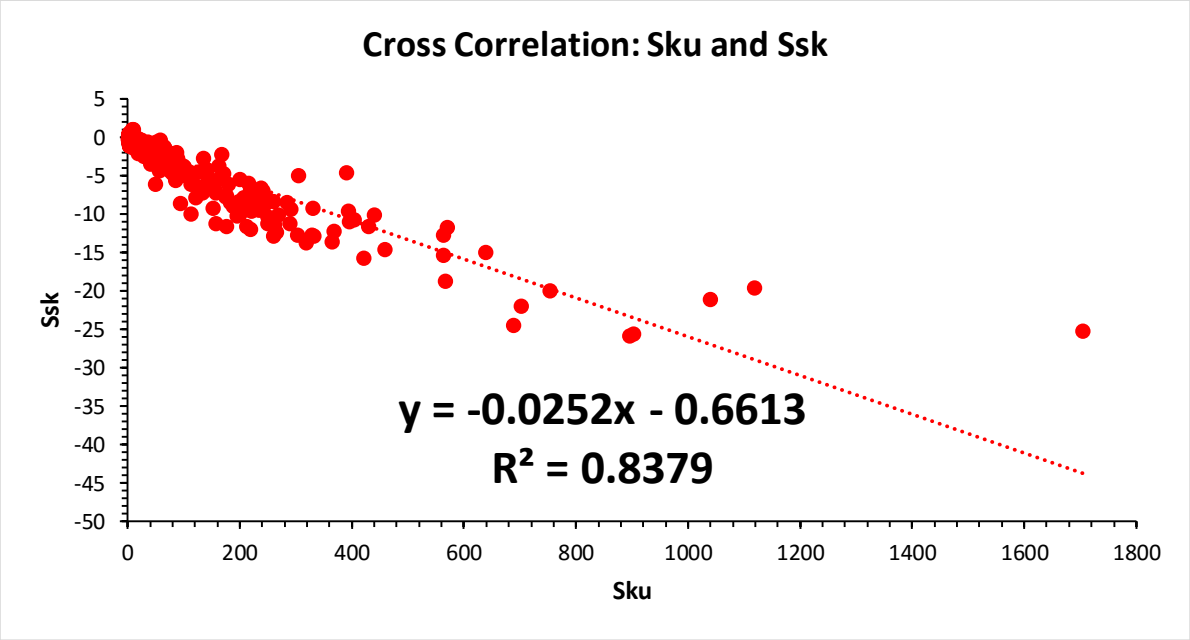

Figure 33: The cross correlation between skewness and kurtosis

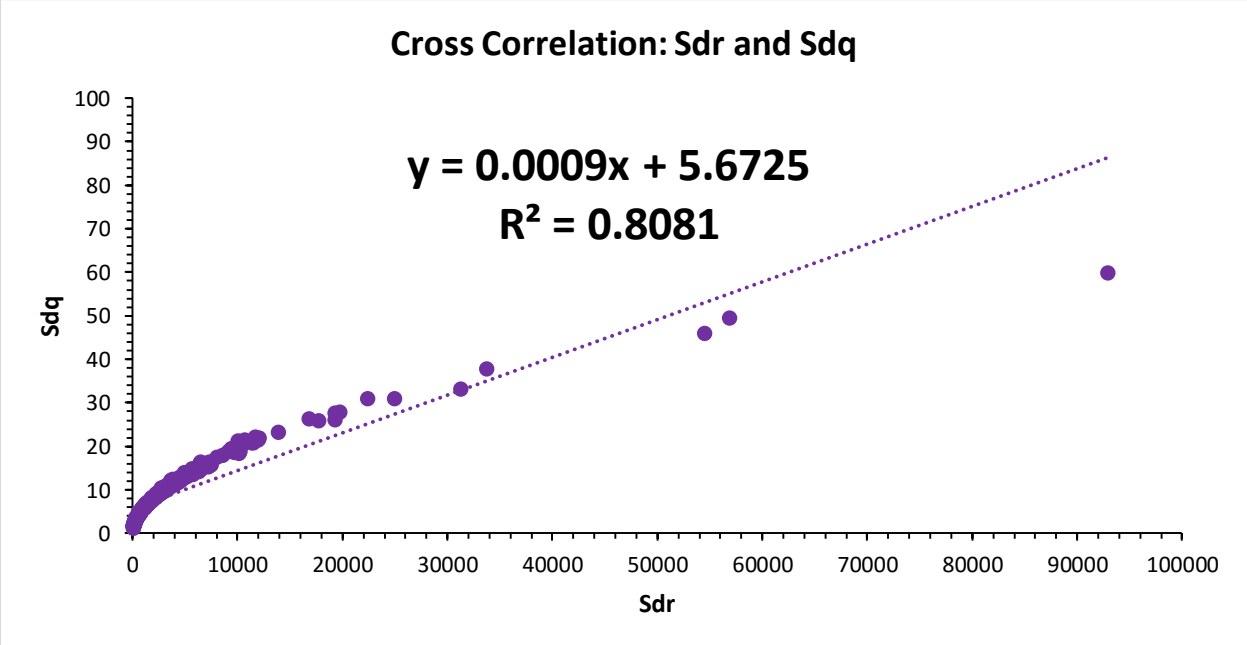

Figure 34: The cross correlation between developed interfacial area and root-mean-square slope

7.4 MATLAB Code Used to Generate Height-to-Height Plots

The following MATLAB script was used to generate the height plots presented in Section 3.1.2.1. The spatial and vertical height data of each surface was exported into a Microsoft Excel® documents, and the MATLAB script was designed to read the vertical height appropriately. The script performed linear regression analyses between the two surfaces, and a height vs. height plot was constructed appropriately.

```
clear all;

clc;

A=xlsread('Surface 1 unfiltered.csv','Surface 1 unfiltered','C:C');
%Reading Unfiltered Surface 1%
B=xlsread('Surface 2 unfiltered.csv','Surface 2 unfiltered','C:C');
%Reading Unfiltered Surface 2%

mdl=fitlm(A,B); %Regression Analysis%

scatter(A,B,'*'); %Plot unfiltered height data%

hold on

C=xlsread('Surface 1 filtered.csv','Surface 1 filtered','C:C');
%Reading Filtered Surface 1%
D=xlsread('Surface 2 filtered.csv','Surface 2 filtered','C:C');
%Reading Filtered Surface 2%

mdl=fitlm(C,D); %Regression Anlysis%

scatter(C,D,'*'); %Plot filtered height data%

xlim([-2,2]);
ylim([-2,2]);
title('Height #1 vs. Height #2');
xlabel('Height 1 [µm]');
ylabel('Height 2 [µm]');
```

Figure 35: The MATLAB script used to construct height vs. height plots

7.5 MATLAB Code Used to Generate Regression Coefficient Matrices

The following MATLAB script was used to generate the matrices of regression coefficients presented in Section 3.1.2.1. The script reads the height data of each surface that had been previously exported into a Microsoft Excel® documents, and linear regression analyses between the surfaces was conducted. The regression coefficient calculated within MATLAB is then written to a specific cell of a second excel document. The code was used repeatedly in order to completely populate the matrices.

```
clear all clc

%C2
A2=xlsread('OutlierFiltered50x.xlsx','Surface 1','C:C');
%Adjust File name and Sheet name%
B2=xlsread('OutlierFiltered50x.xlsx','Surface 2','C:C');
%Adjust File name and Sheet name%
mdl=fitlm(A2,B2);

T=mdl.Rsquared.Ordinary;
xlswrite('Coefficients_filtered.xlsx',T,'Sheet1','C2');
%Adjust cell number%
```

Figure 36: The MATLAB script used to generate regression coefficient matrices

7.6 Measurement-to-Measurement Repeatability Matrices from Section 3.1.2.1

R^2	1	2	3	4	5	6	7	8	9	10
1	1.00	0.85	0.86	0.85	0.85	0.85	0.85	0.84	0.84	0.84
2		1.00	0.86	0.85	0.85	0.85	0.85	0.85	0.85	0.84
3			1.00	0.85	0.85	0.86	0.85	0.85	0.85	0.84
4				1.00	0.85	0.86	0.85	0.85	0.85	0.84
5					1.00	0.86	0.85	0.85	0.85	0.84
6						1.00	0.86	0.86	0.86	0.85
7							1.00	0.86	0.85	0.85
8								1.00	0.86	0.85
9									1.00	0.86
10										1.00

Table 5: The R^2 values for the unfiltered measurements taken from the specimen presented in Figure 14

R^2	1	2	3	4	5	6	7	8	9	10
1	1.00	0.99	0.99	0.99	0.99	0.99	0.99	0.99	0.99	0.99
2		1.00	0.99	0.99	0.99	0.99	0.99	0.99	0.99	0.99
3			1.00	0.99	0.99	0.99	0.99	0.99	0.99	0.99
4				1.00	0.99	0.99	0.99	0.99	0.99	0.99
5					1.00	0.99	0.99	0.99	0.99	0.99
6						1.00	1.00	0.99	0.99	0.99
7							1.00	0.99	0.99	0.99
8								1.00	0.99	0.99
9									1.00	0.99
10										1.00

Table 6: The R^2 values for the filtered measurements taken from the specimen presented in Figure 14

7.7 Surface Measurements of Areal Calibration Surfaces

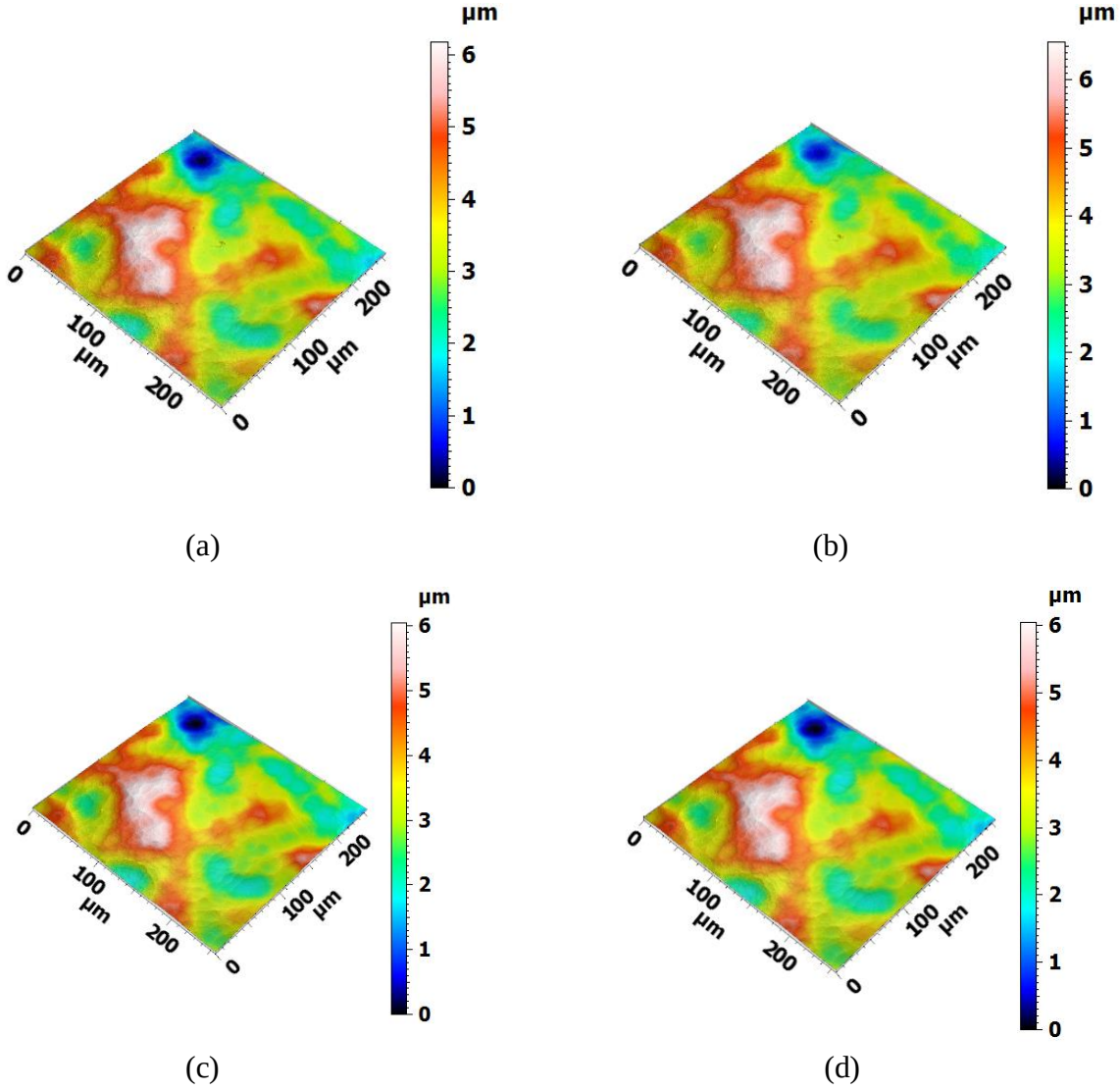

Figure 37: The unfiltered measurements of areal calibration surfaces (a) and (b), and the filtered measurements (c) and (d)

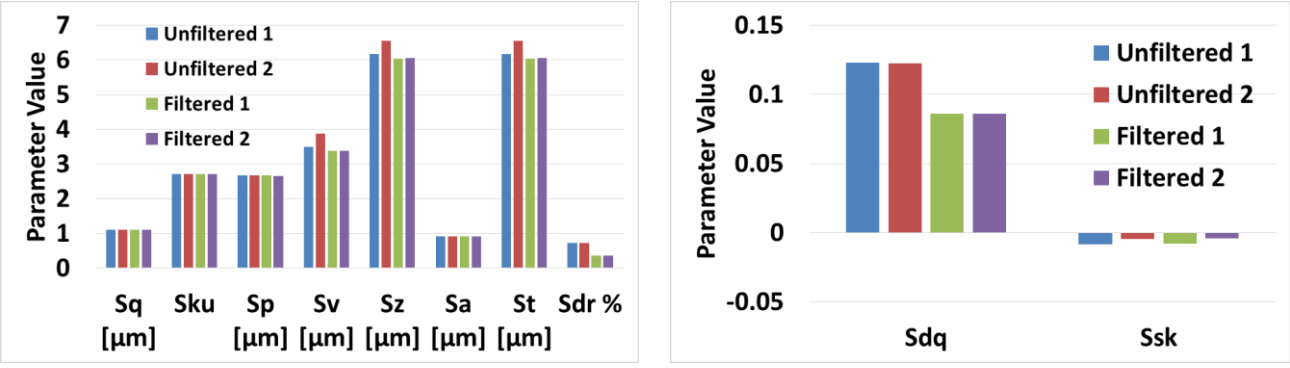

Figure 38: Conventional Parameters for Surfaces Presented in Figure 37

7.8 Surface Measurements: Repeatability between Multiple Locations Experiment

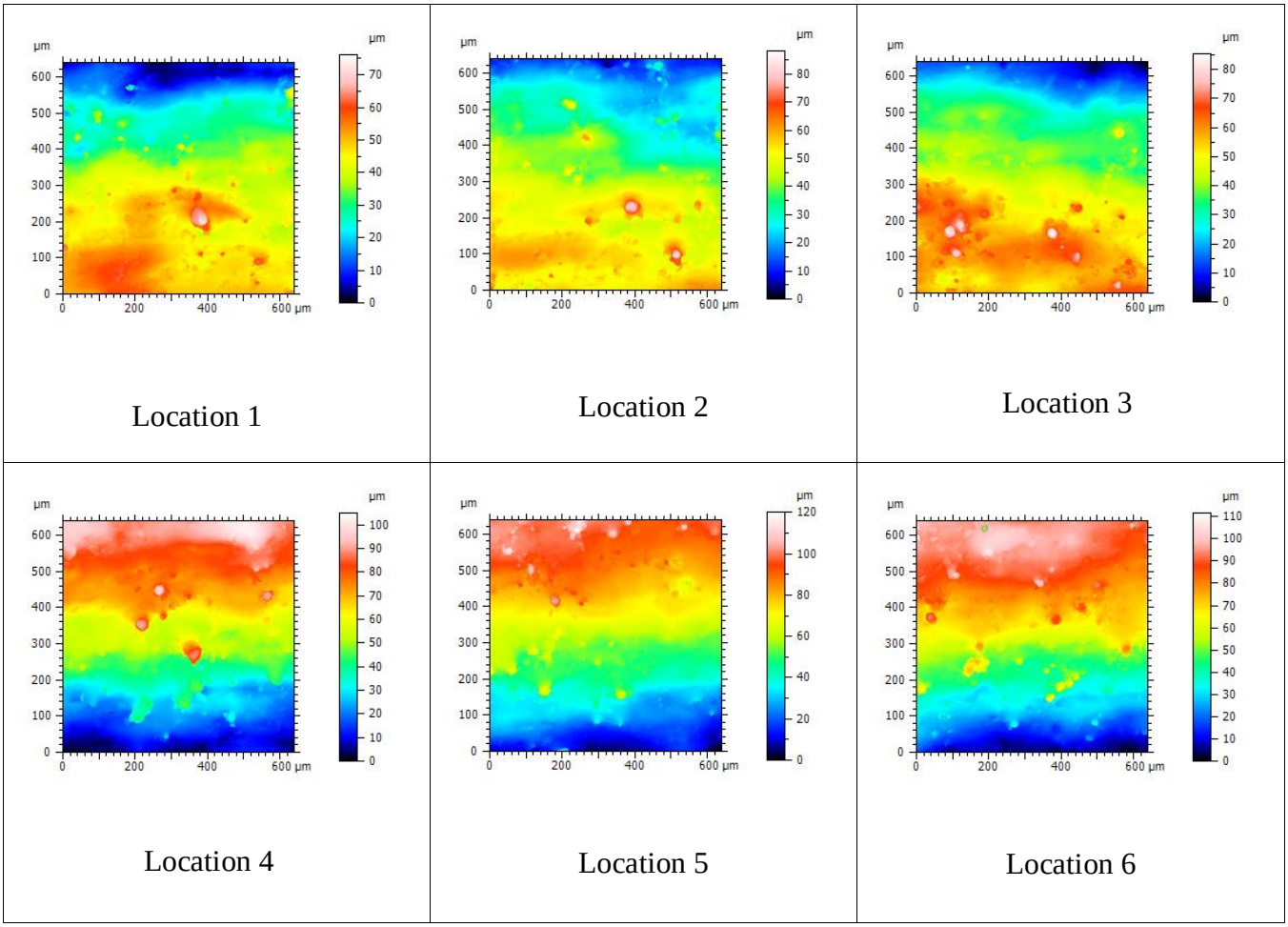

Figure 39: The surface measurements obtained at six different locations

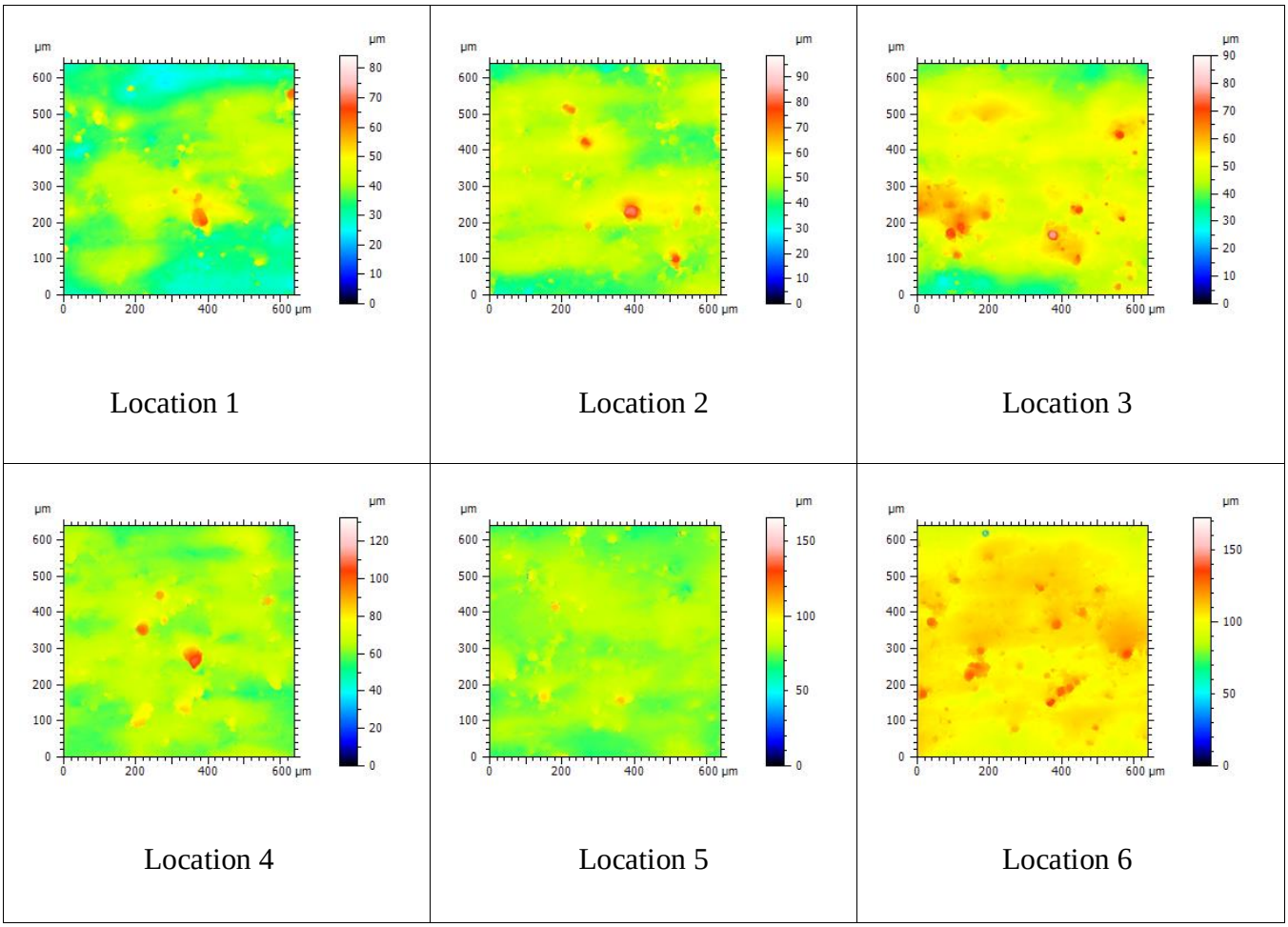

Figure 40: The surface measurements obtained at six different locations leveled

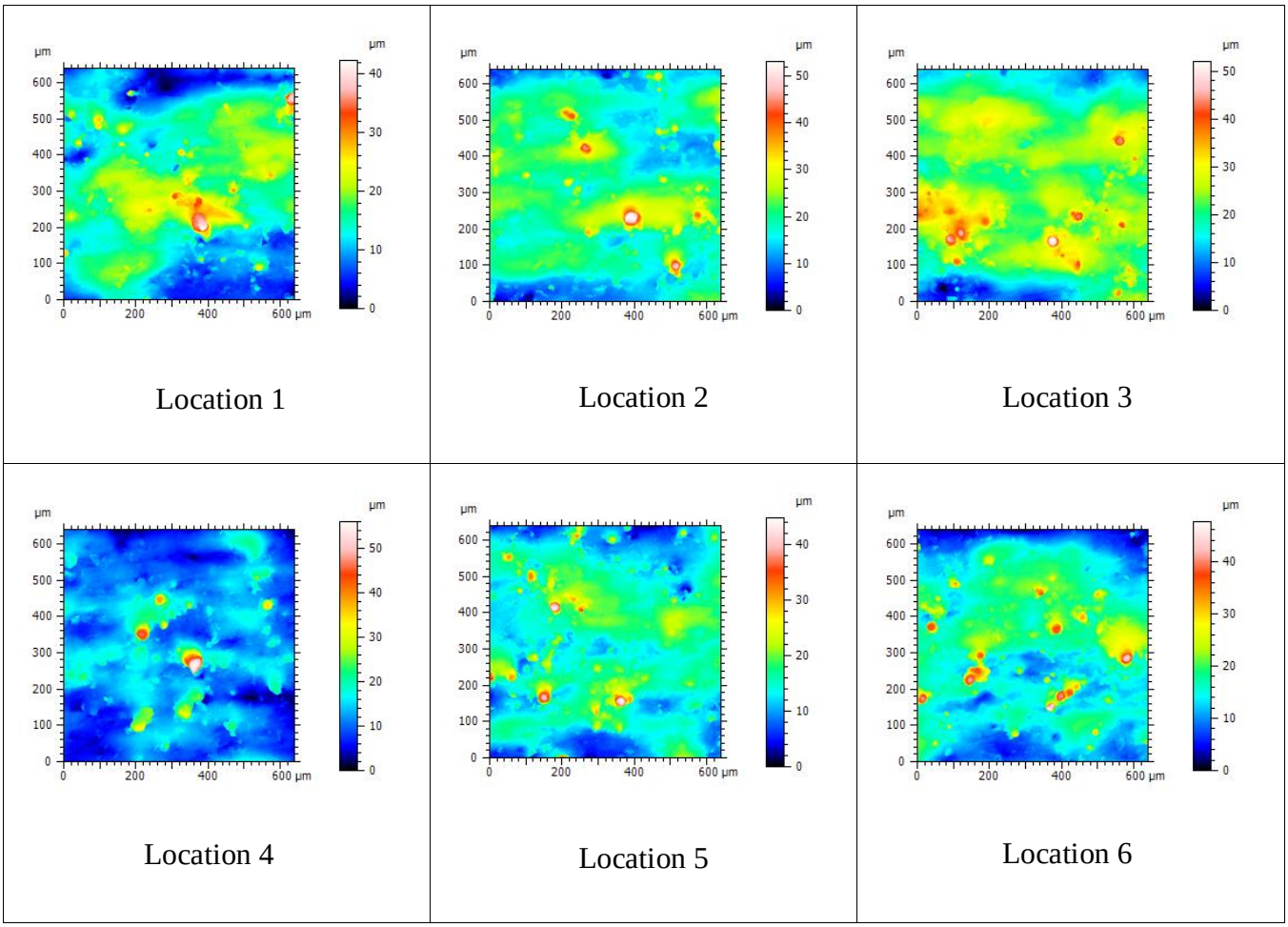

Figure 41: The surface measurements obtained at six different locations outliers removed

7.9 Surface Measurements Used in the Functional Correlation Analysis

	0°	15°	45°	75°	90°
1	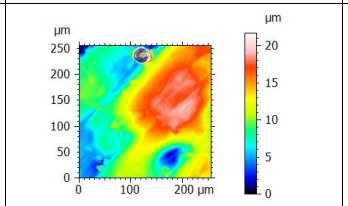	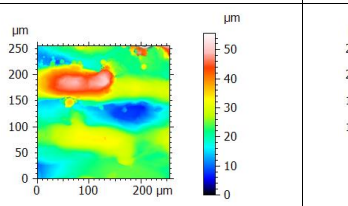	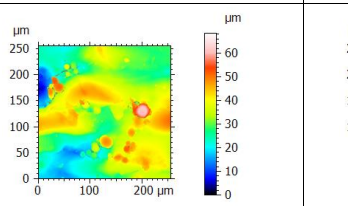	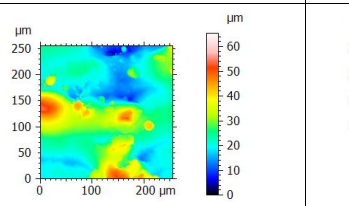	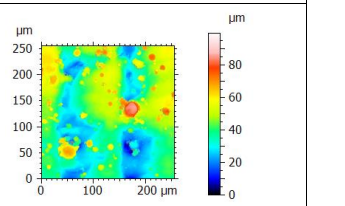
2	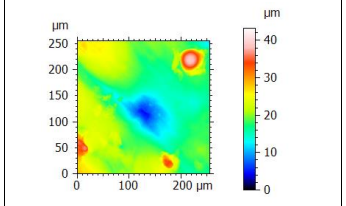	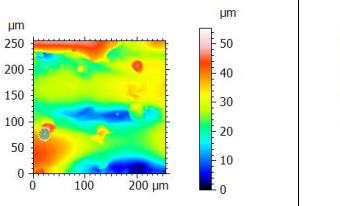	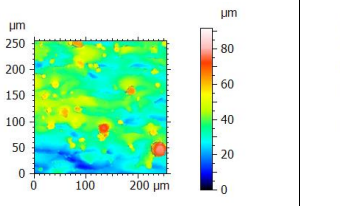	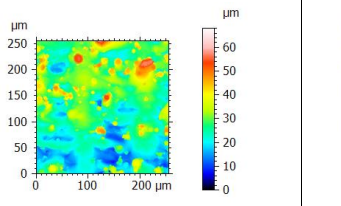	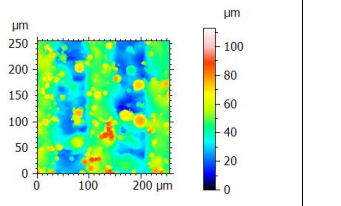
3	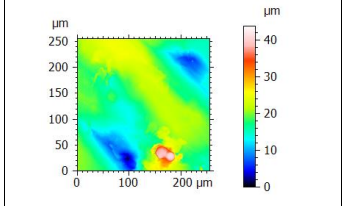	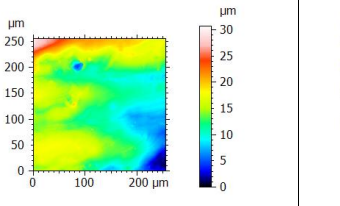	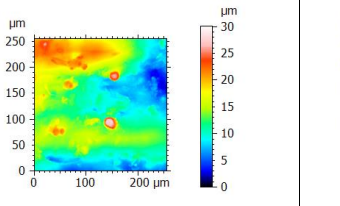	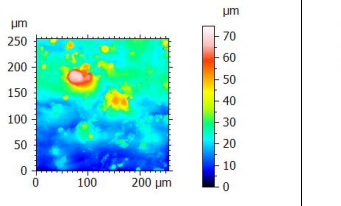	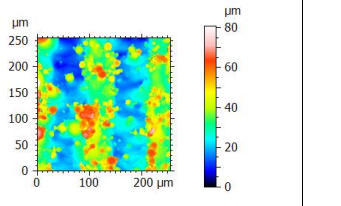
4	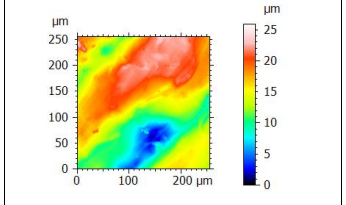	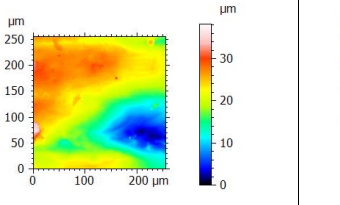	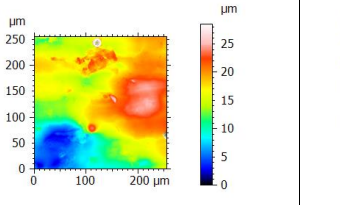	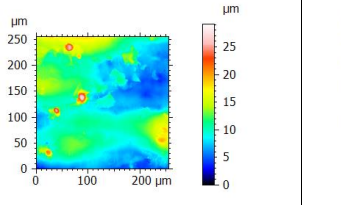	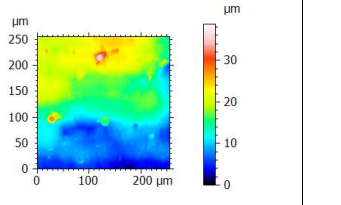

Figure 42: The surface measurements obtained at different inclination angles and energy densities

7.10 Correlation Coefficients between Height Parameters and Linear Energy Density

90 Degrees	Unfiltered	Mountains Outlier Filtered	Modal Filter 125 Modes	Modal Filter 250 Modes	Modal Filter 500 Modes
Sq	0.734	0.723	0.776	0.736	0.726
Ssk	0.405	0.259	0.306	0.435	0.450
Sku	0.996	0.973	0.431	0.593	0.650
Sp	0.871	0.762	0.828	0.819	0.799
Sv	0.958	0.980	0.950	0.857	0.898
Sa	0.707	0.705	0.705	0.683	0.676
St	0.913	0.890	0.888	0.842	0.839
Sdr	0.772	0.418	0.843	0.754	0.813
Sdq	0.799	0.552	0.876	0.807	0.834

(a)

75 Degrees	Unfiltered	Mountains Outlier Filtered	Modal Filter 125 Modes	Modal Filter 250 Modes	Modal Filter 500 Modes
Sq	0.560	0.564	0.709	0.705	0.754
Ssk	0.049	0.059	0.001	0.065	0.126
Sku	0.158	0.183	0.163	0.127	0.229
Sp	0.429	0.152	0.333	0.294	0.210
Sv	0.871	0.808	0.355	0.349	0.521
Sa	0.696	0.698	0.911	0.910	0.921
St	0.614	0.376	0.350	0.317	0.322
Sdr	0.204	0.168	0.086	0.065	0.158
Sdq	0.392	0.269	0.181	0.147	0.282

(b)

45 Degrees	Unfiltered	Mountains Outlier Filtered	Modal Filter 125 Modes	Modal Filter 250 Modes	Modal Filter 500 Modes
Sq	0.631	0.636	0.739	0.762	0.768
Ssk	0.287	0.301	0.370	0.154	0.131
Sku	0.225	0.198	0.337	0.373	0.390
Sp	0.606	0.580	0.546	0.575	0.497
Sv	0.652	0.642	0.706	0.730	0.768
Sa	0.674	0.674	0.764	0.775	0.775
St	0.647	0.656	0.625	0.654	0.633
Sdr	0.354	0.367	0.339	0.371	0.432
Sdq	0.497	0.550	0.516	0.555	0.607

(c)

15 Degrees	Unfiltered	Mountains Outlier Filtered	Modal Filter 125 Modes	Modal Filter 250 Modes	Modal Filter 500 Modes
Sq	0.300	0.298	0.605	0.607	0.612
Ssk	0.772	0.773	0.403	0.483	0.491
Sku	0.199	0.177	0.073	0.004	0.004
Sp	0.725	0.772	0.596	0.594	0.617
Sv	0.300	0.141	0.617	0.653	0.763
Sa	0.218	0.217	0.612	0.612	0.613
St	0.538	0.552	0.627	0.651	0.701
Sdr	0.715	0.755	0.641	0.679	0.700
Sdq	0.732	0.757	0.587	0.636	0.660

(d)

0 Degrees	Unfiltered	Mountains Outlier Filtered	Modal Filter 125 Modes	Modal Filter 250 Modes	Modal Filter 500 Modes
Sq	0.433	0.433	0.003	0.006	0.003
Ssk	0.498	0.508	0.013	0.006	0.015
Sku	0.015	0.014	0.455	0.568	0.451
Sp	0.043	0.068	0.048	0.048	0.045
Sv	0.019	0.106	0.026	0.077	0.031
Sa	0.542	0.620	0.126	0.118	0.113
St	0.011	0.010	0.043	0.054	0.042
Sdr	0.502	0.835	0.086	0.075	0.051
Sdq	0.645	0.826	0.110	0.125	0.075

(e)

Table 7: The regression coefficients for correlations between conventional parameters and LED

7.11 Additional Relative Area Plots at Different Inclination Angles

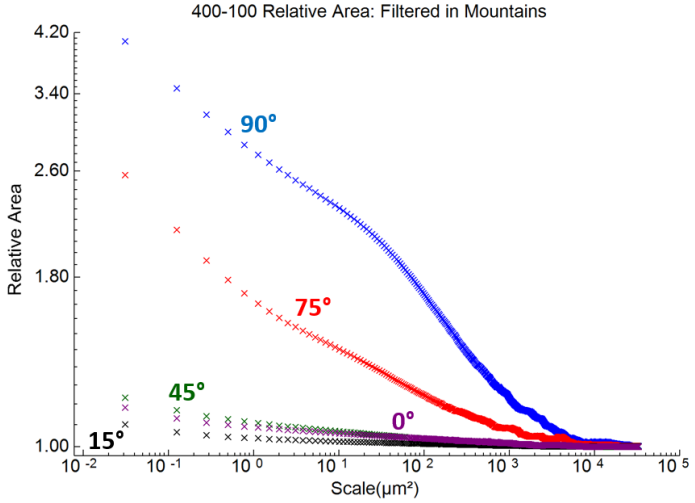

(a)

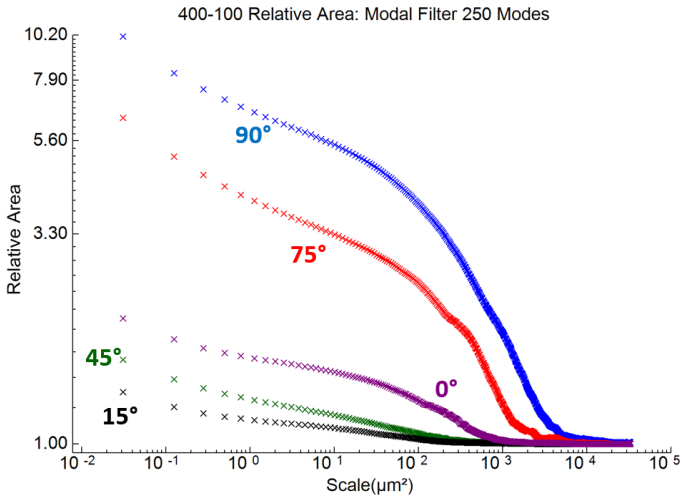

(c)

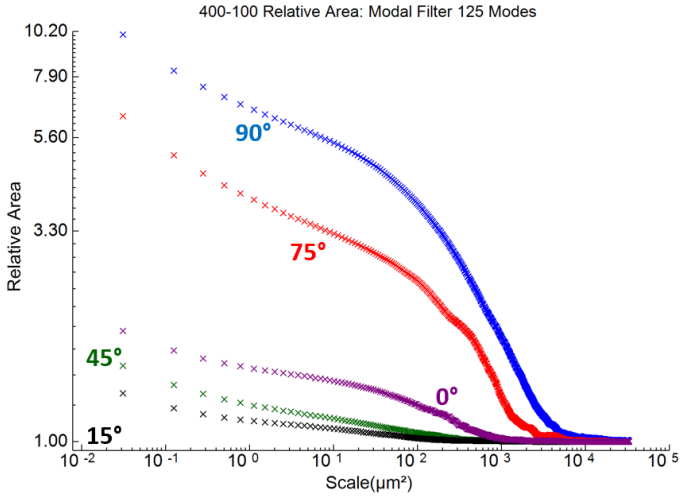

(b)

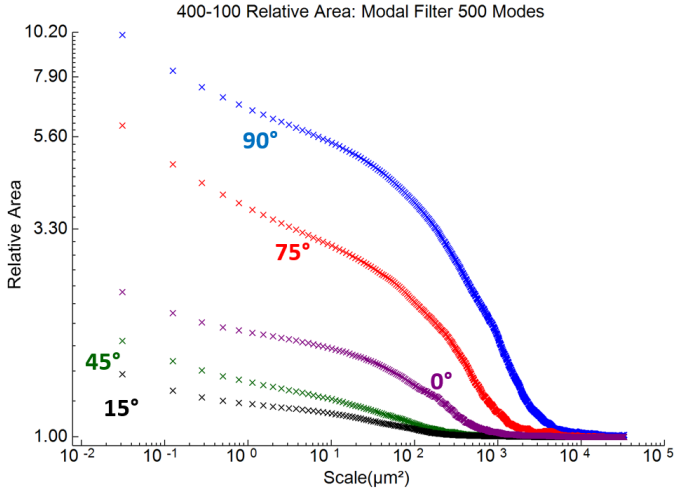

(d)

Figure 43: Relative area plots of the part laser melted using a contour speed of 400 mm/s and a contour power of 100 watts

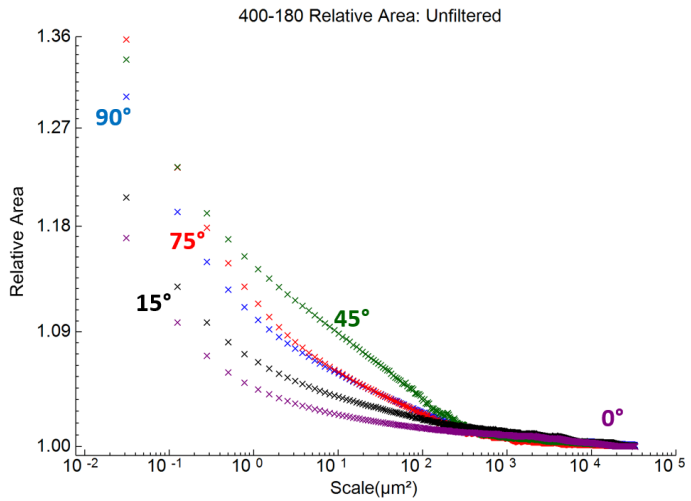
400-180 Relative Area: Unfiltered
Relative Area
Scale(μm²)
90°
75°
15°
45°
0°

(a)

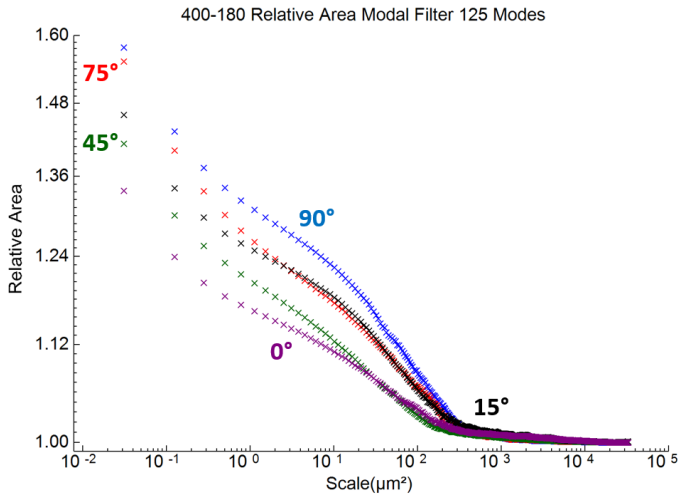
400-180 Relative Area Modal Filter 125 Modes
Relative Area
Scale(μm²)
75°
45°
90°
0°
15°

(c)

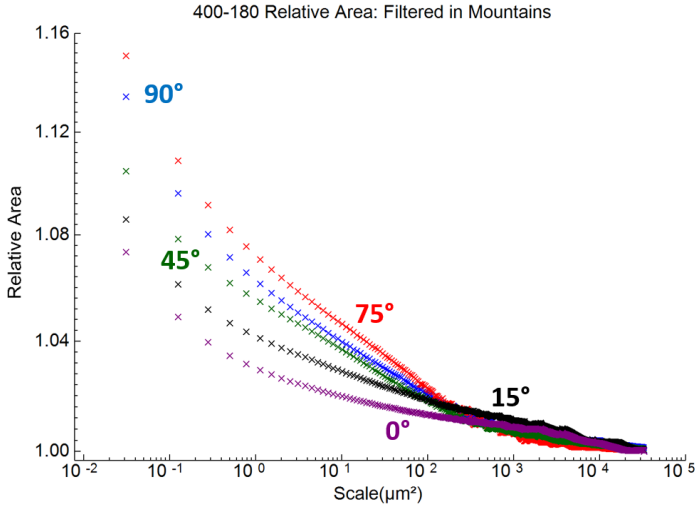
400-180 Relative Area: Filtered in Mountains
Relative Area
Scale(μm²)
90°
45°
75°
15°
0°

(b)

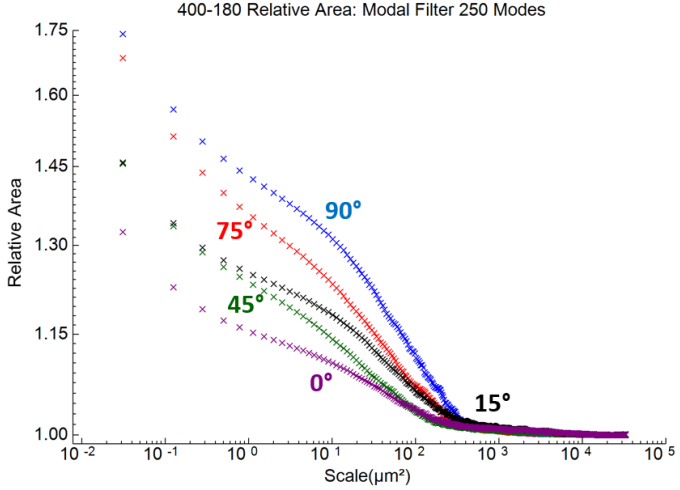
400-180 Relative Area: Modal Filter 250 Modes
Relative Area
Scale(μm²)
90°
75°
45°
0°
15°

(d)

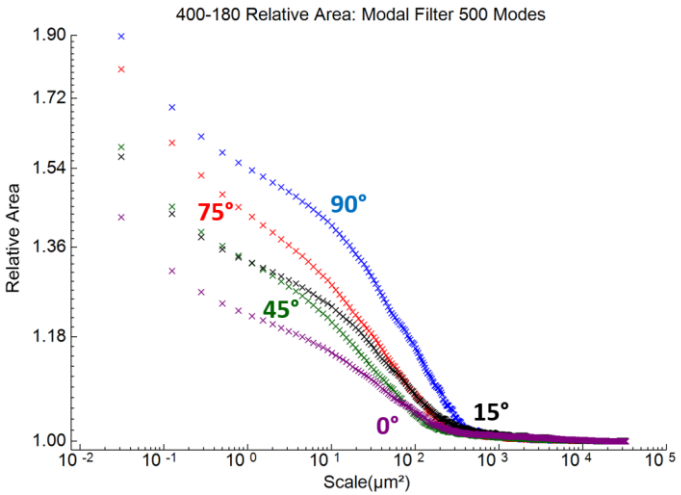

(e)

Figure 44: Relative area plots of the part laser melted using a contour speed of 400 mm/s and a contour power of 180 watts

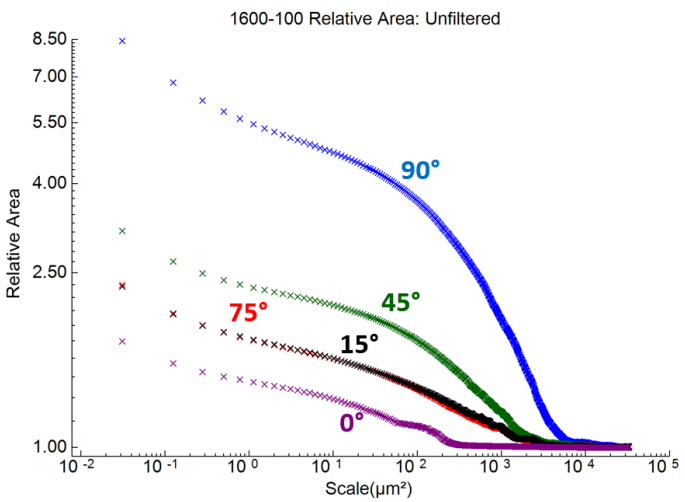
1600-100 Relative Area: Unfiltered
Relative Area
8.50
7.00
5.50
4.00
2.50
1.00
90°
45°
75°
15°
0°
10 -2
10 -1
10 0
10 1
10 2
10 3
10 4
10 5
Scale(µm²)

(a)

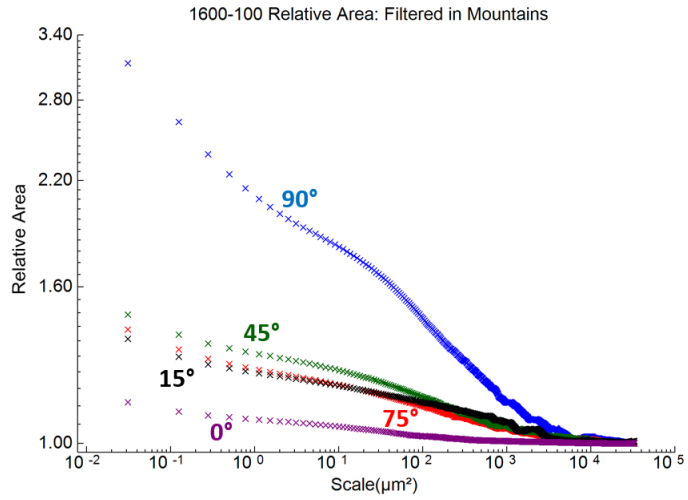
1600-100 Relative Area: Filtered in Mountains
Relative Area
3.40
2.80
2.20
1.60
1.00
90°
45°
15°
0°
75°
10 -2
10 -1
10 0
10 1
10 2
10 3
10 4
10 5
Scale(µm²)

(b)

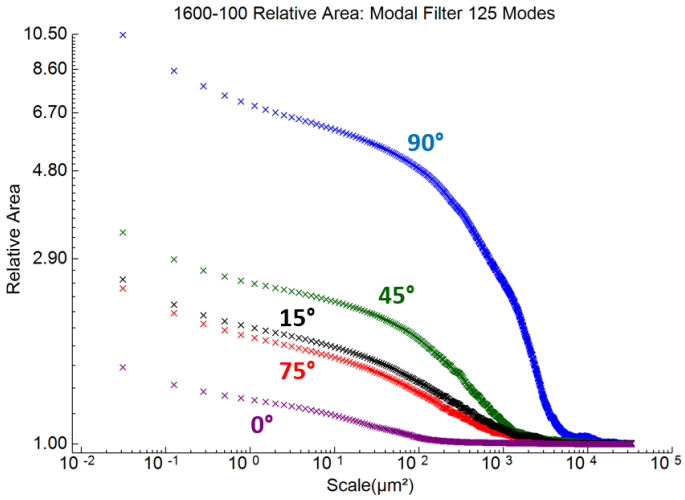
1600-100 Relative Area: Modal Filter 125 Modes
Relative Area
10.50
8.60
6.70
4.80
2.90
1.00
90°
45°
15°
75°
0°
10 -2
10 -1
10 0
10 1
10 2
10 3
10 4
10 5
Scale(µm²)

(c)

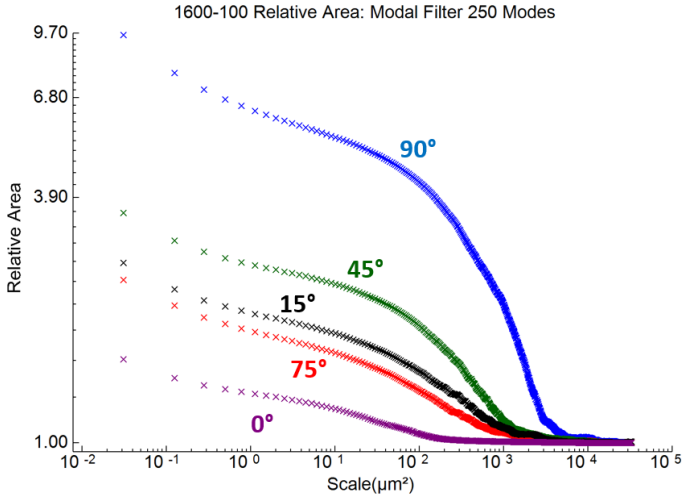
1600-100 Relative Area: Modal Filter 250 Modes
Relative Area
9.70
6.80
3.90
1.00
90°
45°
15°
75°
0°
10 -2
10 -1
10 0
10 1
10 2
10 3
10 4
10 5
Scale(µm²)

(d)

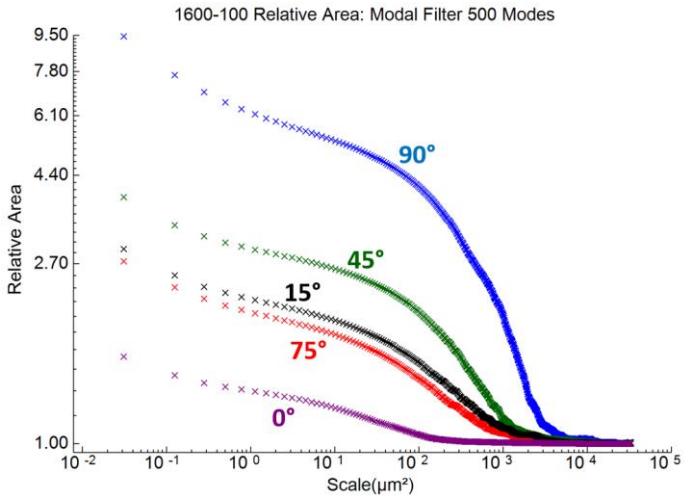

(e)

Figure 45: Relative area plots of the part laser melted using a contour speed of 1600 mm/s and a contour power of 100 watts

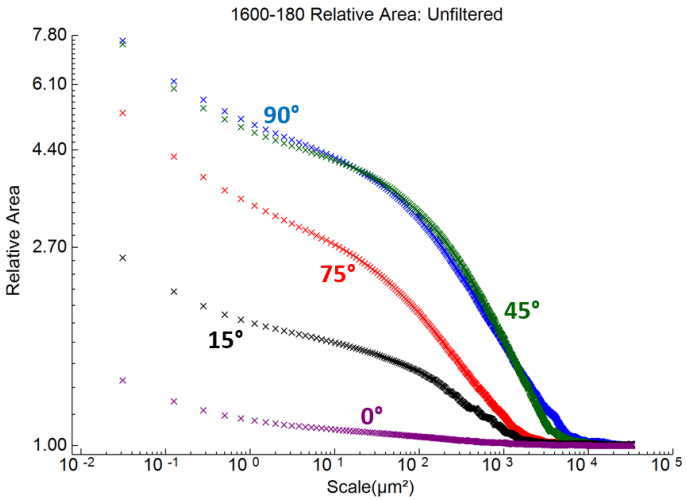
1600-180 Relative Area: Unfiltered
Relative Area
Scale(µm²)
90°
75°
45°
15°
0°

(a)

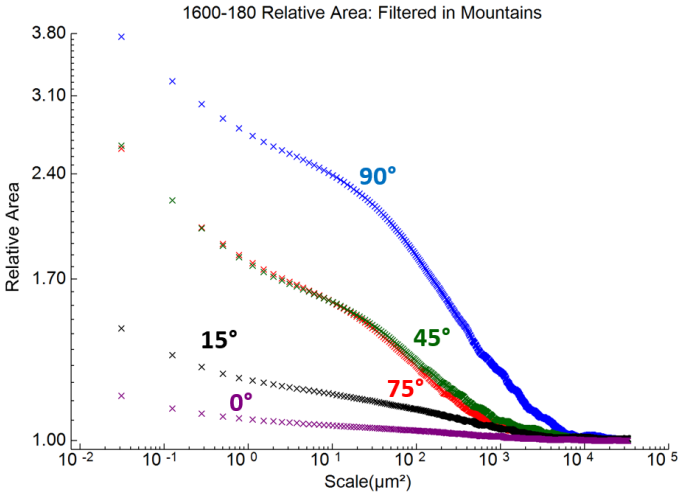
1600-180 Relative Area: Filtered in Mountains
Relative Area
Scale(µm²)
90°
15°
45°
75°
0°

(b)

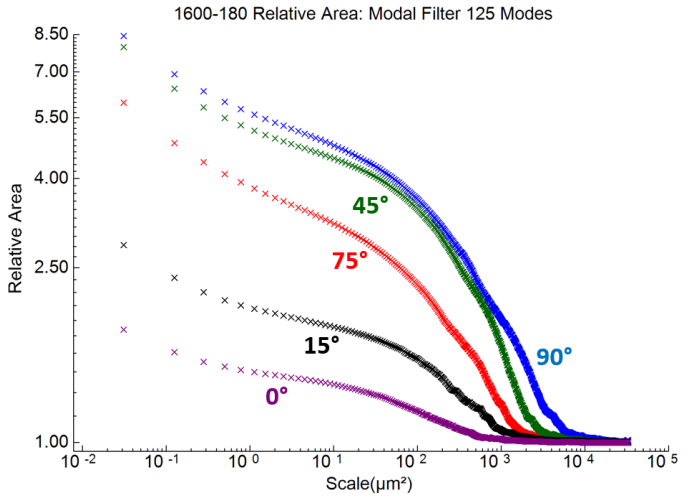
1600-180 Relative Area: Modal Filter 125 Modes
Relative Area
Scale(µm²)
45°
75°
15°
90°
0°

(c)

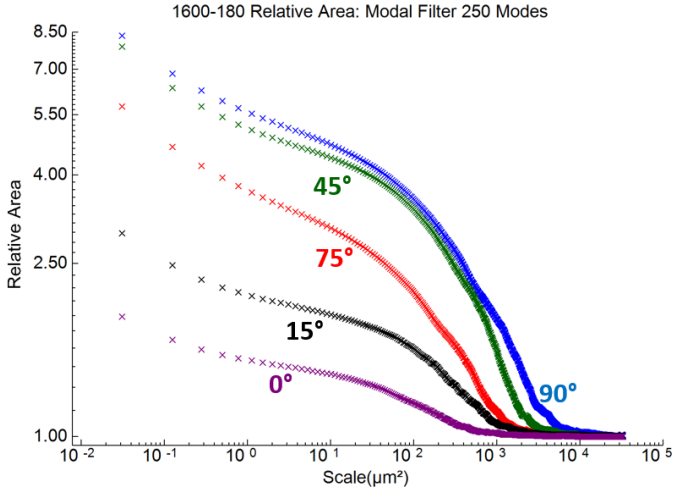
1600-180 Relative Area: Modal Filter 250 Modes
Relative Area
Scale(µm²)
45°
75°
15°
0°
90°

(d)

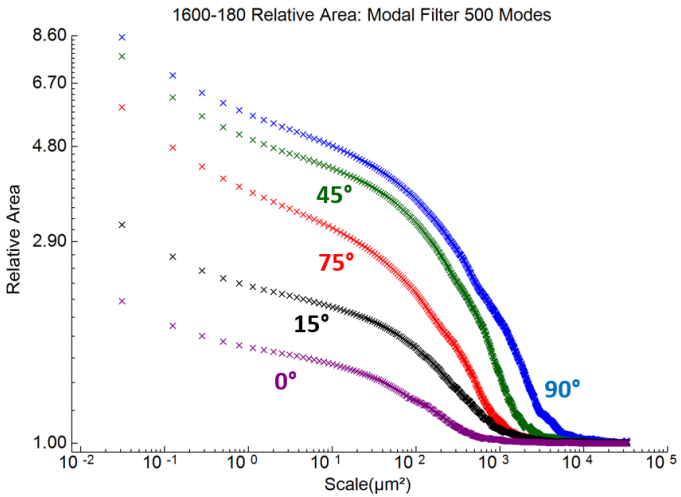

(e)

Figure 46: Relative area plots of the part laser melted using a contour speed of 1600 mm/s and a contour power of 180 watts

7.12 Additional Regression Coefficients of Relative Area and LED as a Function of Scale

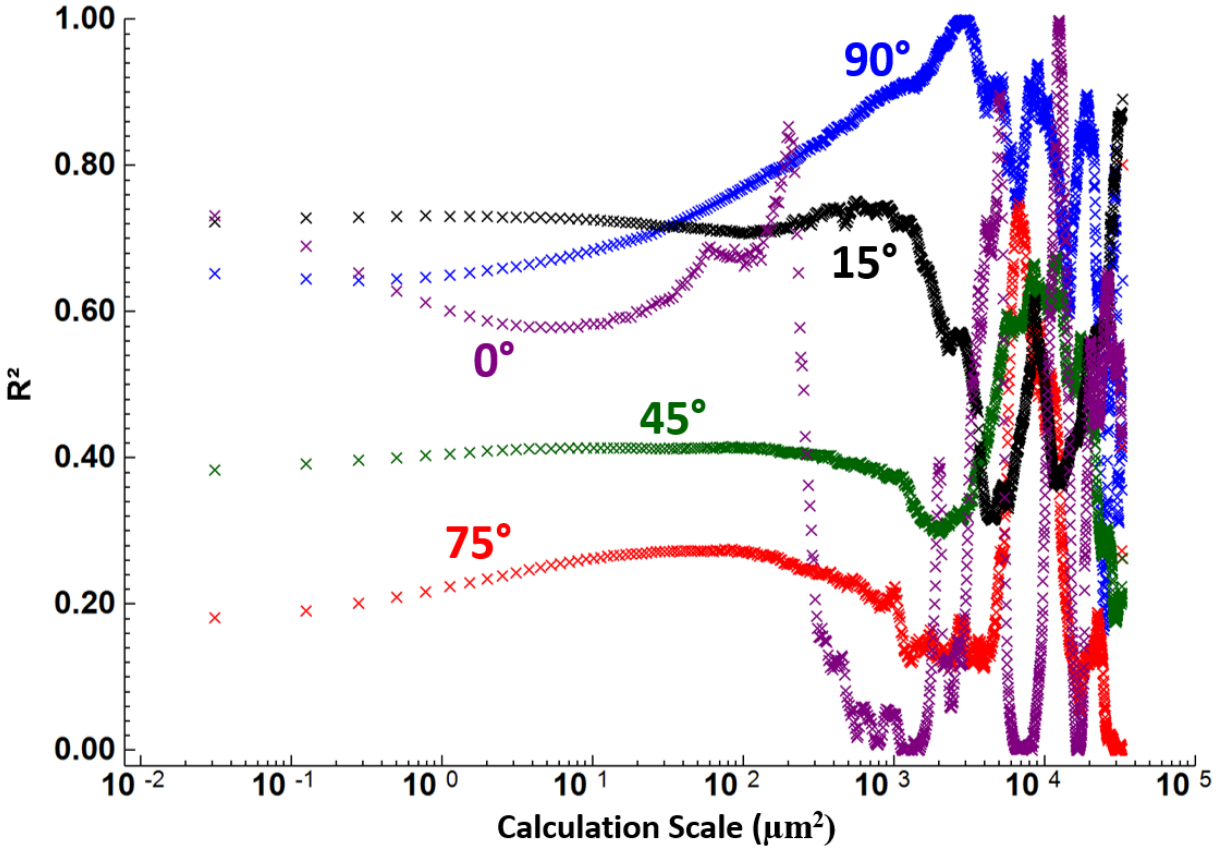

Figure 47: Correlation coefficients, R^2, for correlations between relative area and LED: unfiltered surfaces

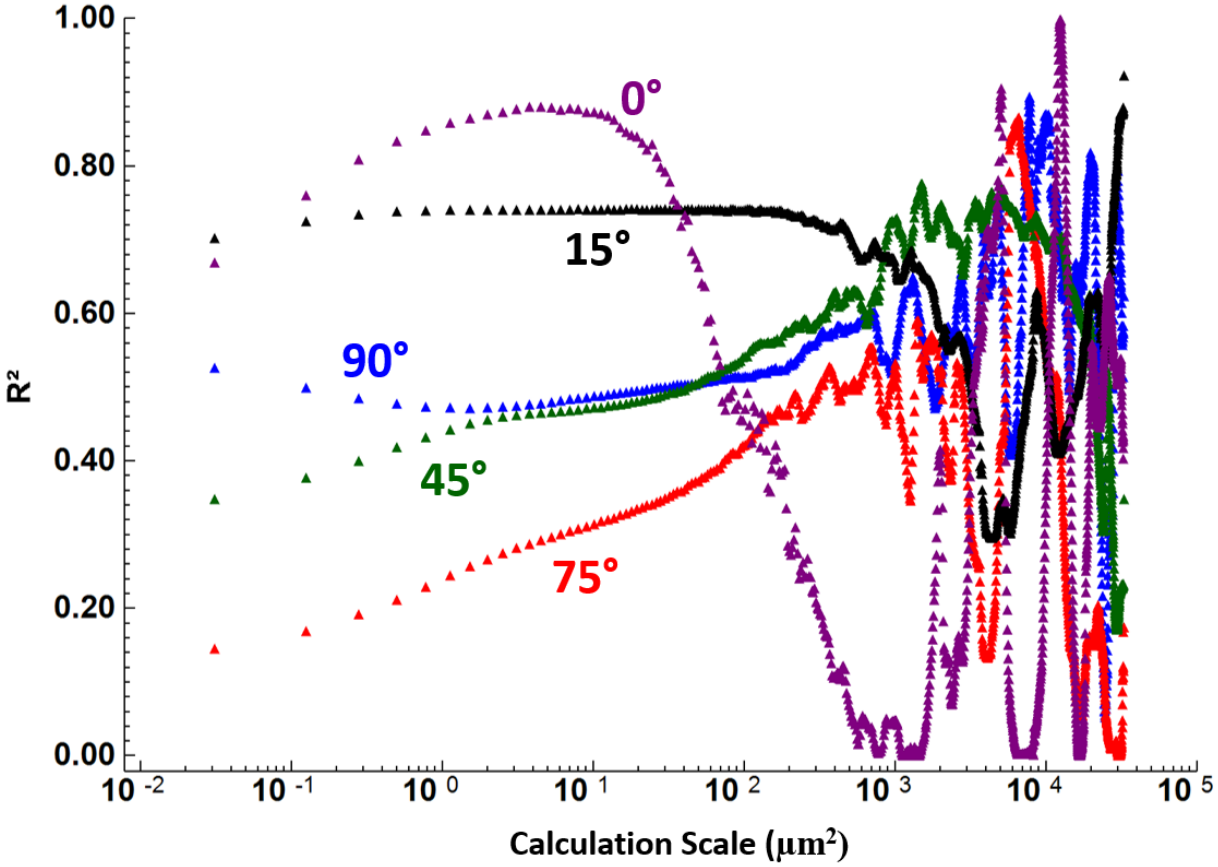

Figure 48: Correlation coefficients, R^2, for correlations between relative area and LED: filtered within mountains

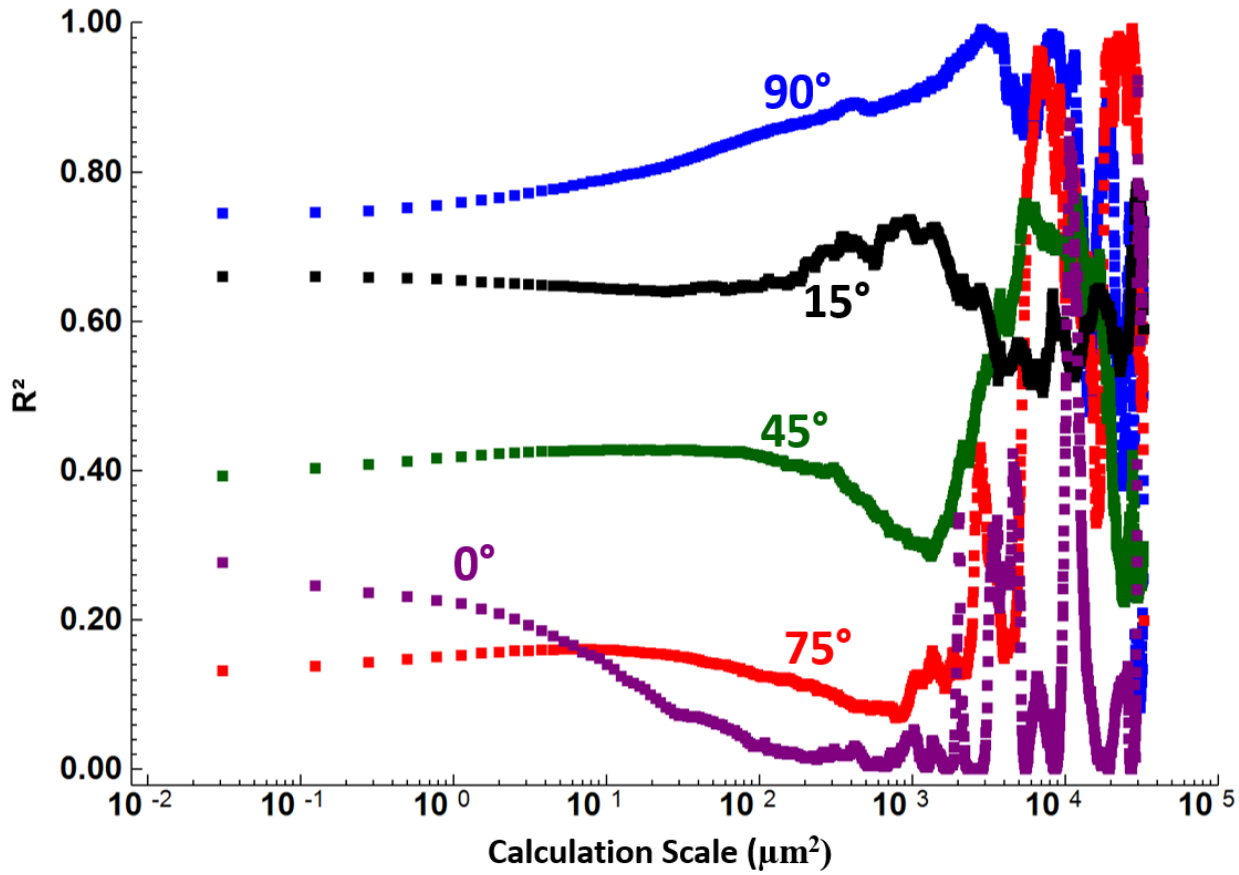

Figure 49: Correlation coefficients, R^2, for correlations between relative area and LED: modal filtered using 125 modes

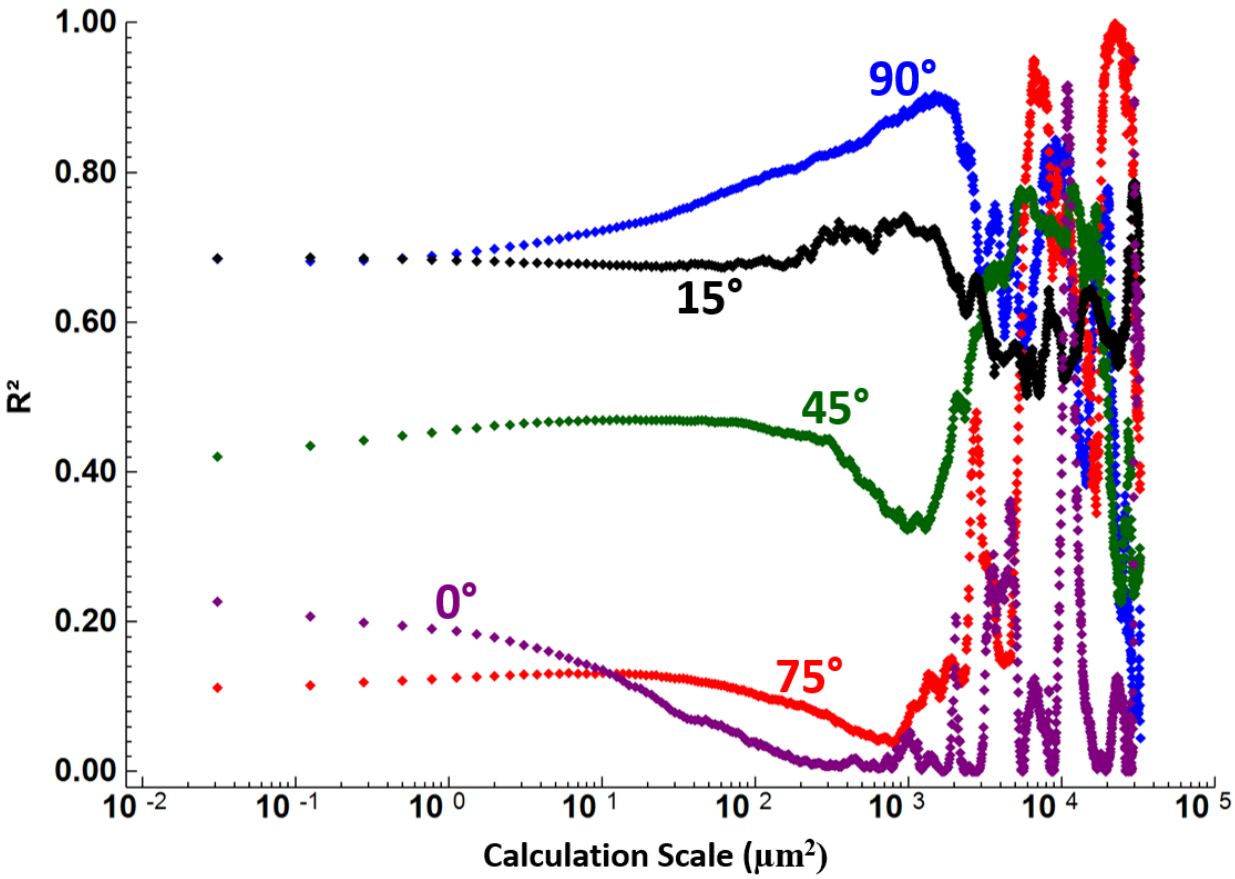

Figure 50: Correlation coefficients, R^2, for correlations between relative area and LED: modal filtered using 250 modes

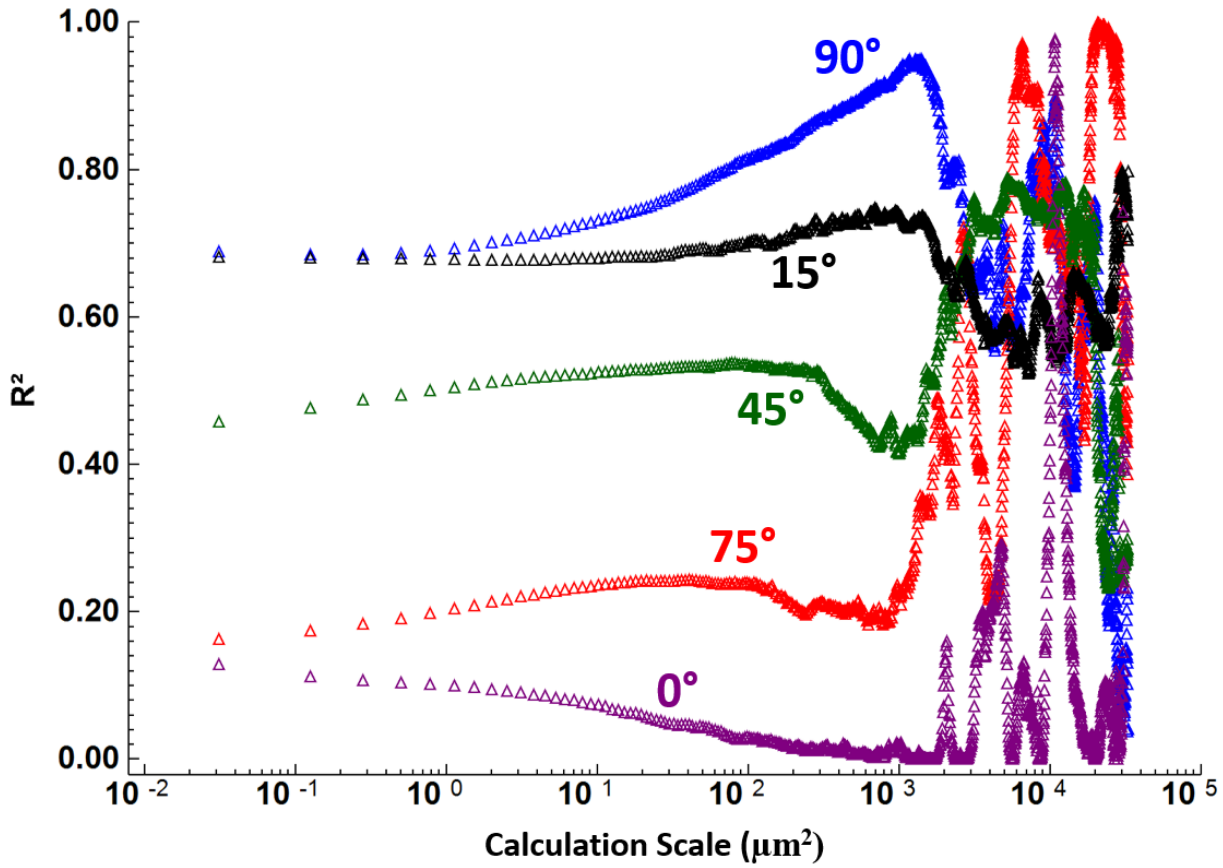

Figure 51: Correlation coefficients, R^2, for correlations between relative area and LED: modal filtered using 500 modes

7.13 Additional Complexity Plots at Different Inclination Angles

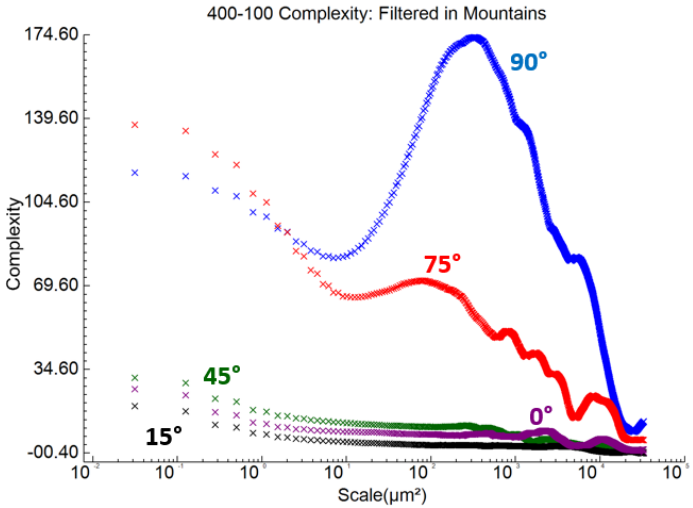

(a)

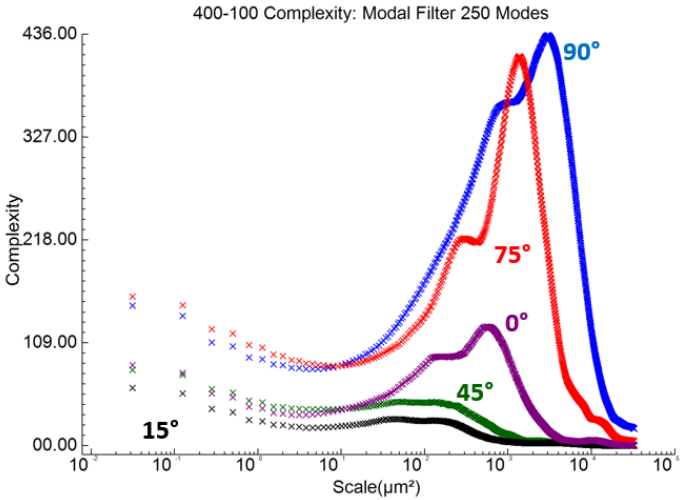

(c)

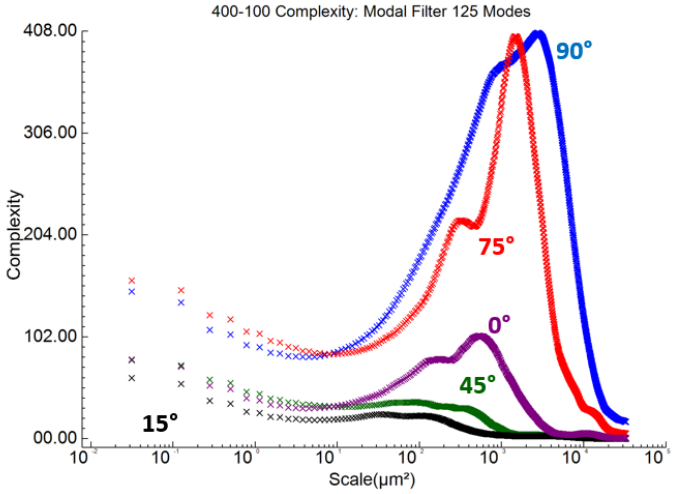

(b)

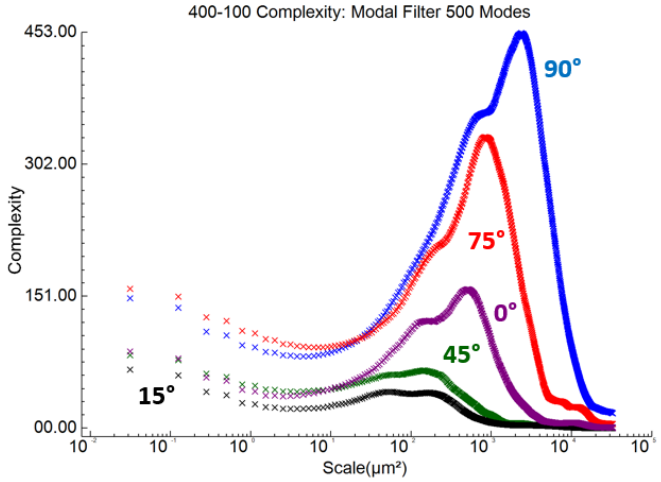

(d)

Figure 52: Complexity plots of the part laser melted using a contour speed of 400 mm/s and a contour power of 100 watts

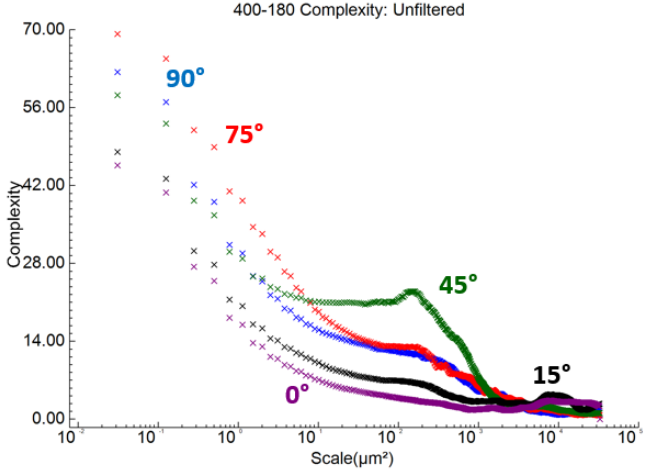
400-180 Complexity: Unfiltered
Complexity
Scale(μm²)
90°
75°
45°
15°
0°

(a)

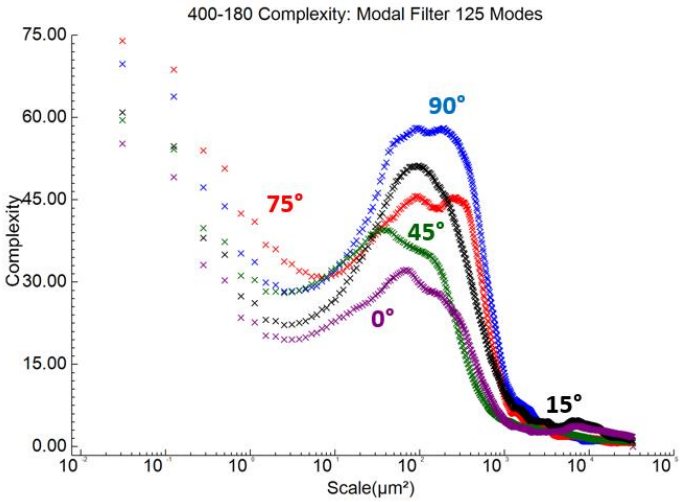
400-180 Complexity: Modal Filter 125 Modes
Complexity
Scale(μm²)
90°
75°
45°
0°
15°

(c)

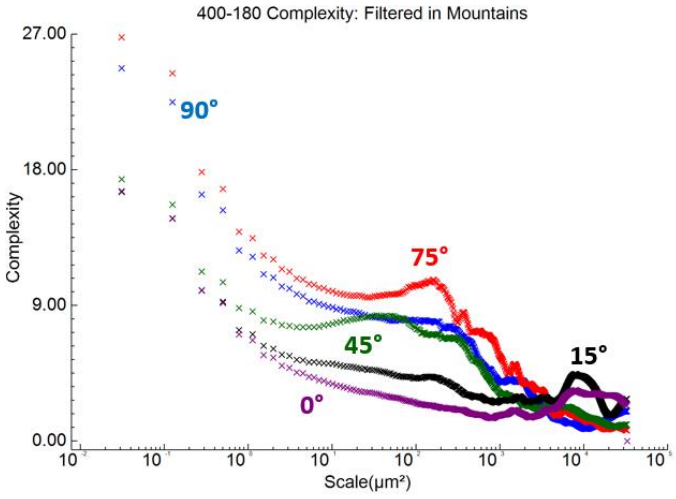
400-180 Complexity: Filtered in Mountains
Complexity
Scale(μm²)
90°
75°
45°
15°
0°

(b)

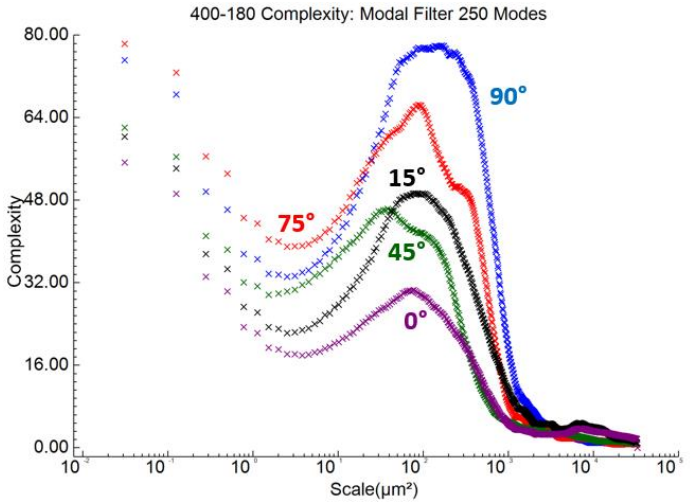
400-180 Complexity: Modal Filter 250 Modes
Complexity
Scale(μm²)
90°
15°
75°
45°
0°

(d)

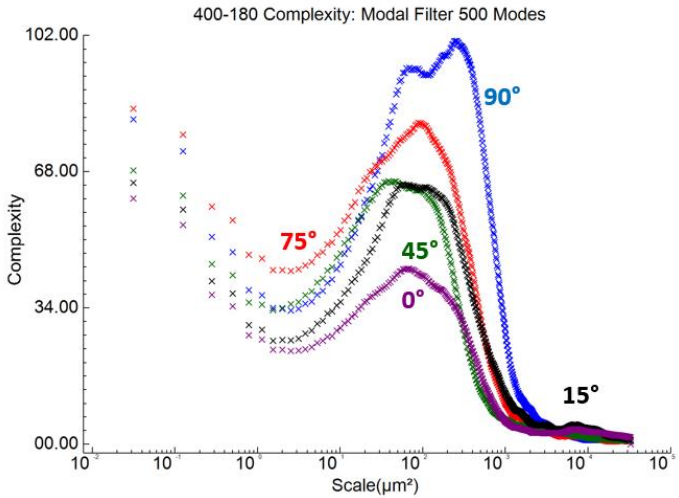

(e)

Figure 53: Complexity plots of the part laser melted using a contour speed of 400 mm/s and a contour power of 180 watts

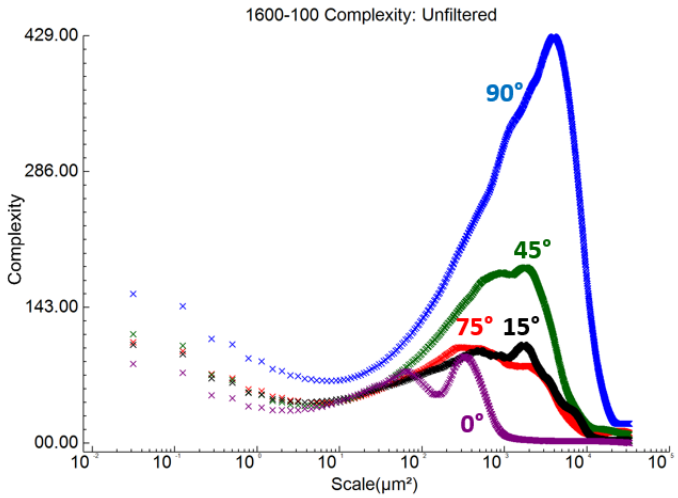
1600-100 Complexity: Unfiltered
429.00
286.00
143.00
00.00
Complexity
90°
45°
75°
15°
0°
Scale(µm²)

(a)

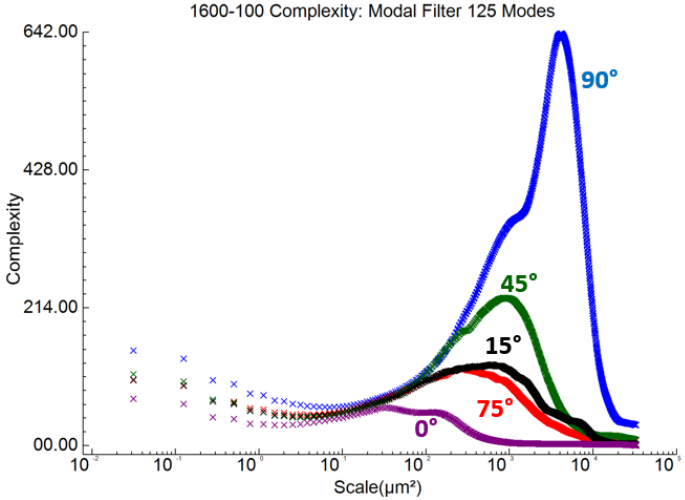
1600-100 Complexity: Modal Filter 125 Modes
642.00
428.00
214.00
00.00
Complexity
90°
45°
15°
75°
0°
Scale(µm²)

(c)

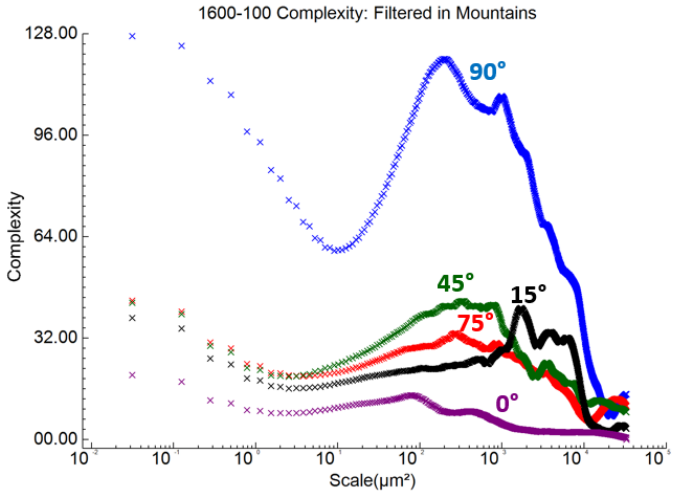
1600-100 Complexity: Filtered in Mountains
128.00
96.00
64.00
32.00
00.00
Complexity
90°
45°
75°
15°
0°
Scale(µm²)

(b)

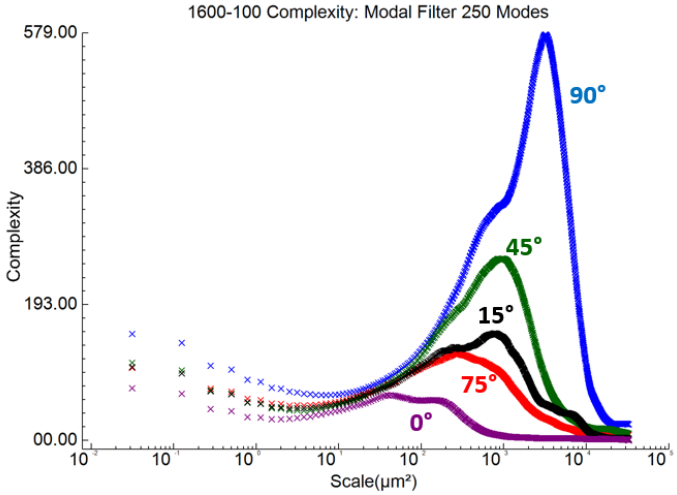
1600-100 Complexity: Modal Filter 250 Modes
579.00
386.00
193.00
00.00
Complexity
90°
45°
15°
75°
0°
Scale(µm²)

(d)

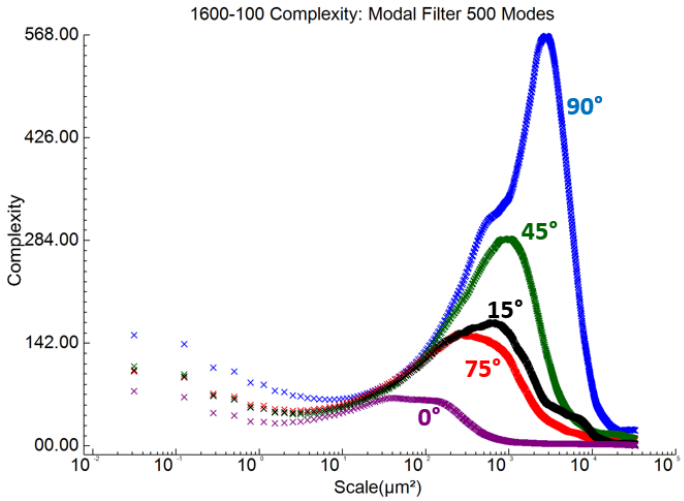

(e)

Figure 54: Complexity plots of the part laser melted using a contour speed of 1600 mm/s and a contour power of 100 watts

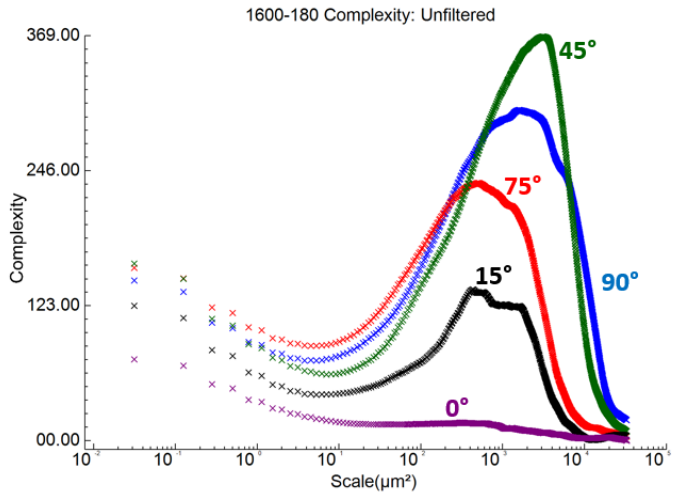
1600-180 Complexity: Unfiltered
369.00
246.00
123.00
00.00
Complexity
Scale(µm²)
45°
75°
15°
90°
0°

(a)

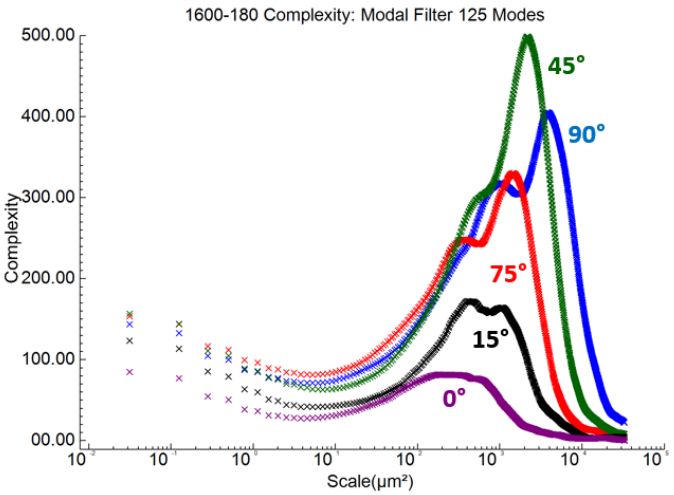
1600-180 Complexity: Modal Filter 125 Modes
500.00
400.00
300.00
200.00
100.00
00.00
Complexity
Scale(µm²)
45°
90°
75°
15°
0°

(c)

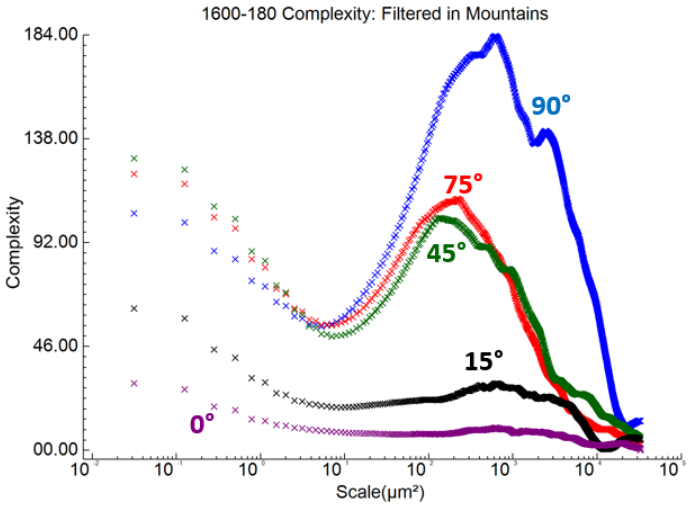
1600-180 Complexity: Filtered in Mountains
184.00
138.00
92.00
46.00
00.00
Complexity
Scale(µm²)
90°
75°
45°
15°
0°

(b)

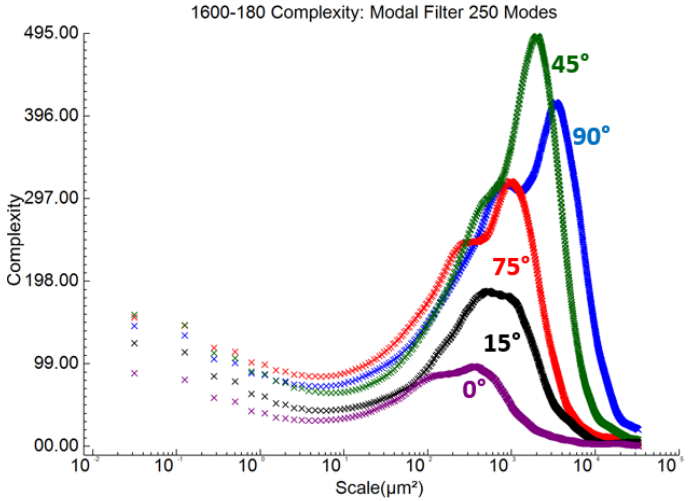
1600-180 Complexity: Modal Filter 250 Modes
495.00
396.00
297.00
198.00
99.00
00.00
Complexity
Scale(µm²)
45°
90°
75°
15°
0°

(d)

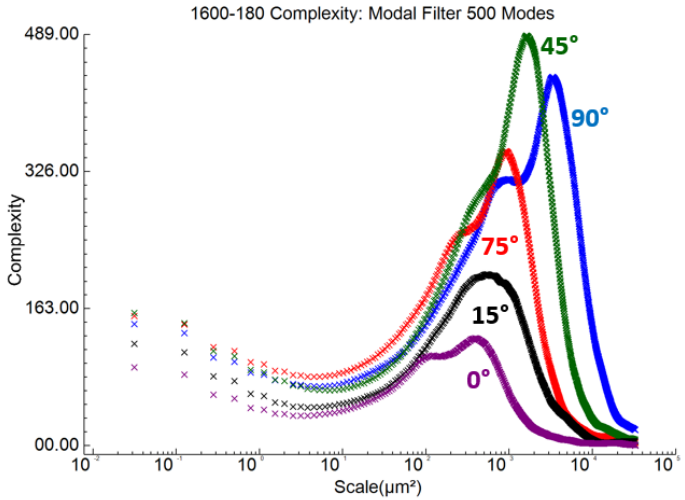

(e)

Figure 55: Complexity plots of the part laser melted using a contour speed of 1600 mm/s and a contour power of 180 watts

7.14 Additional Regression Coefficients of Complexity and LED as a Function of Scale

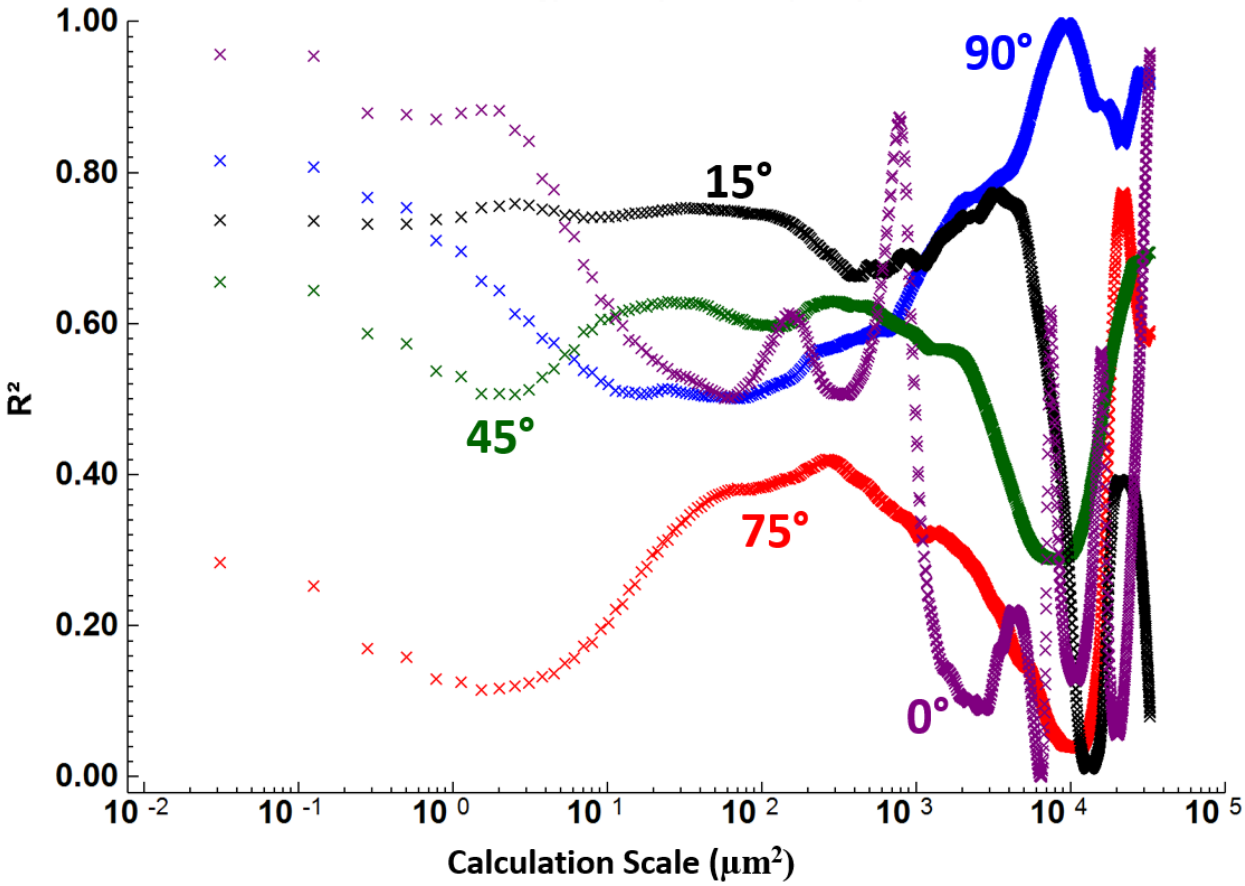

Figure 56: Correlation coefficients, R^2, for correlations between complexity and LED: unfiltered

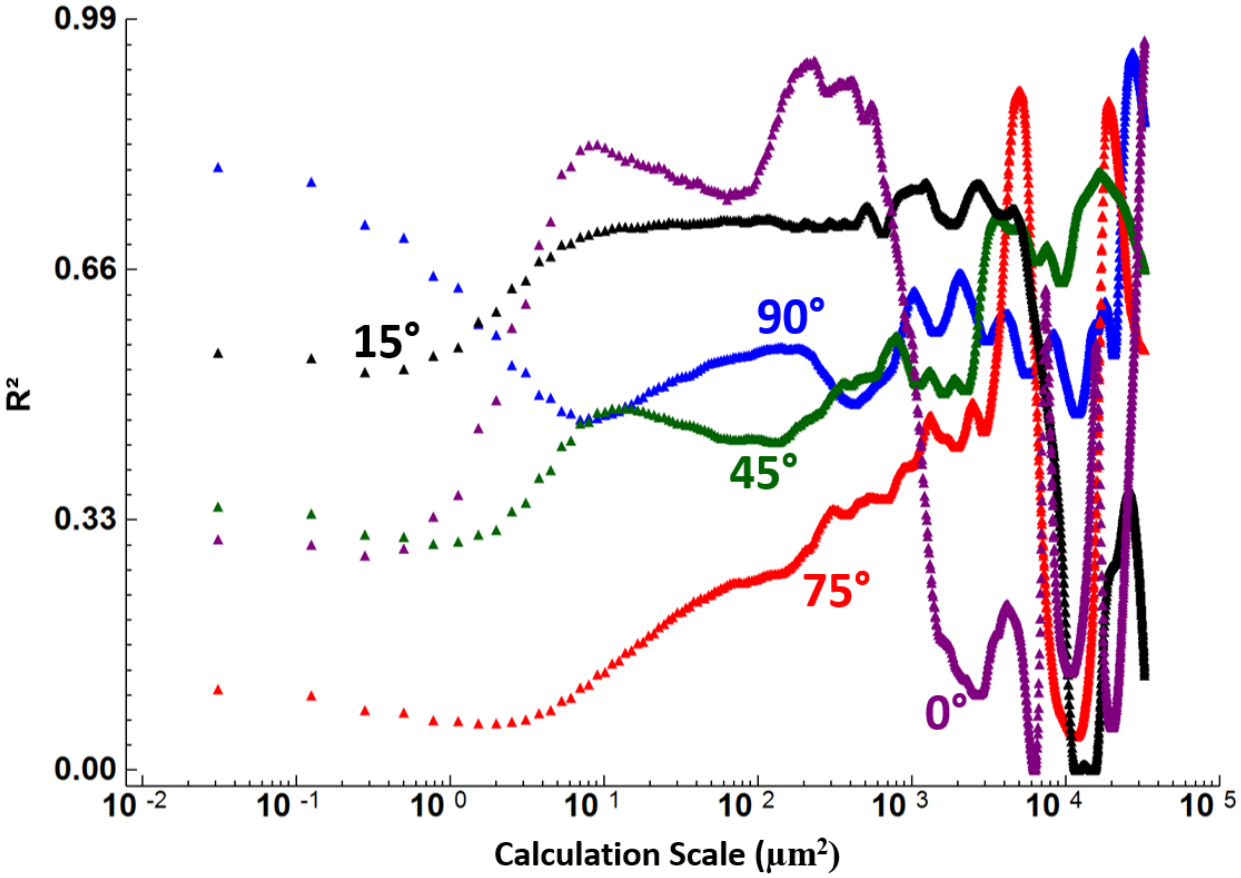

Figure 57: Correlation coefficients, R^2, for correlations between complexity and led: filtered within mountains

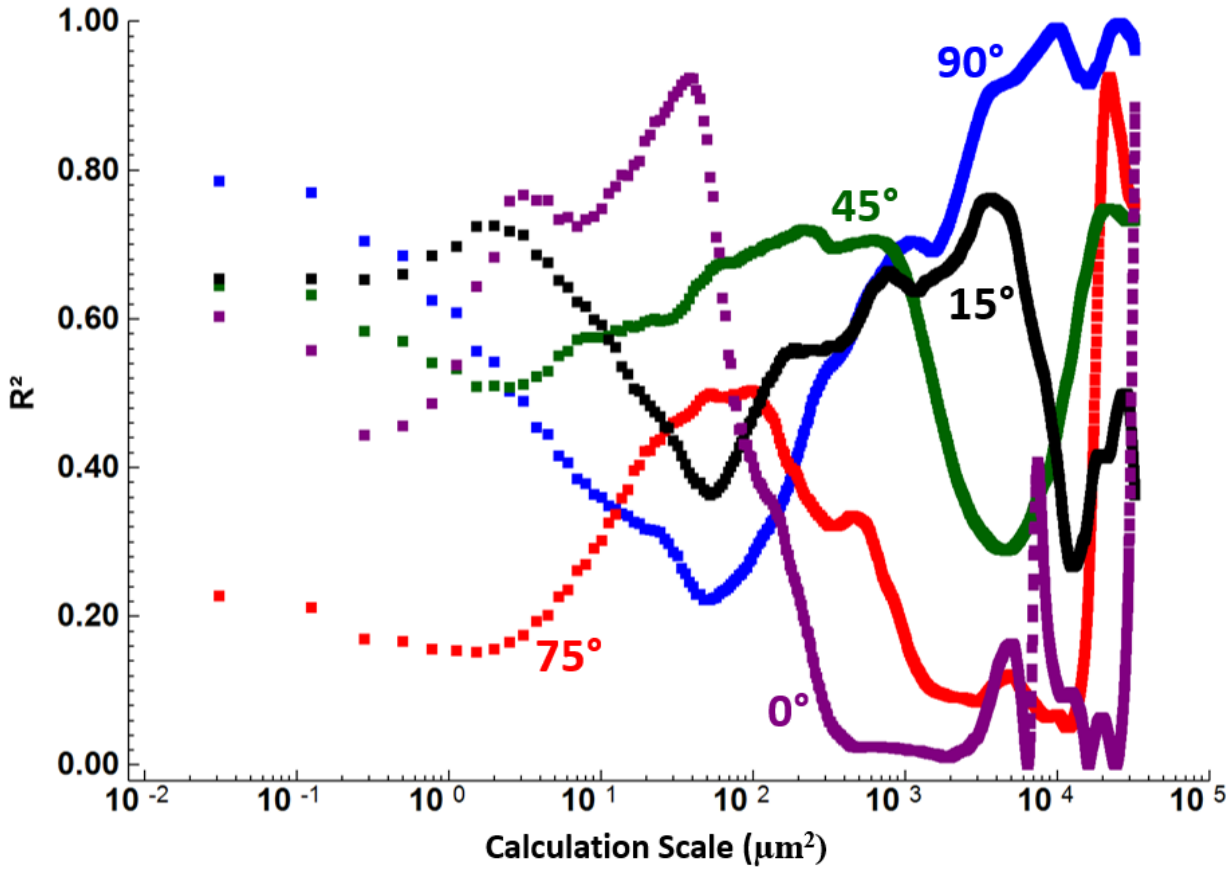

Figure 58: Correlation coefficients, R^2, for correlations between relative area and LED: modal filtered using 125 modes

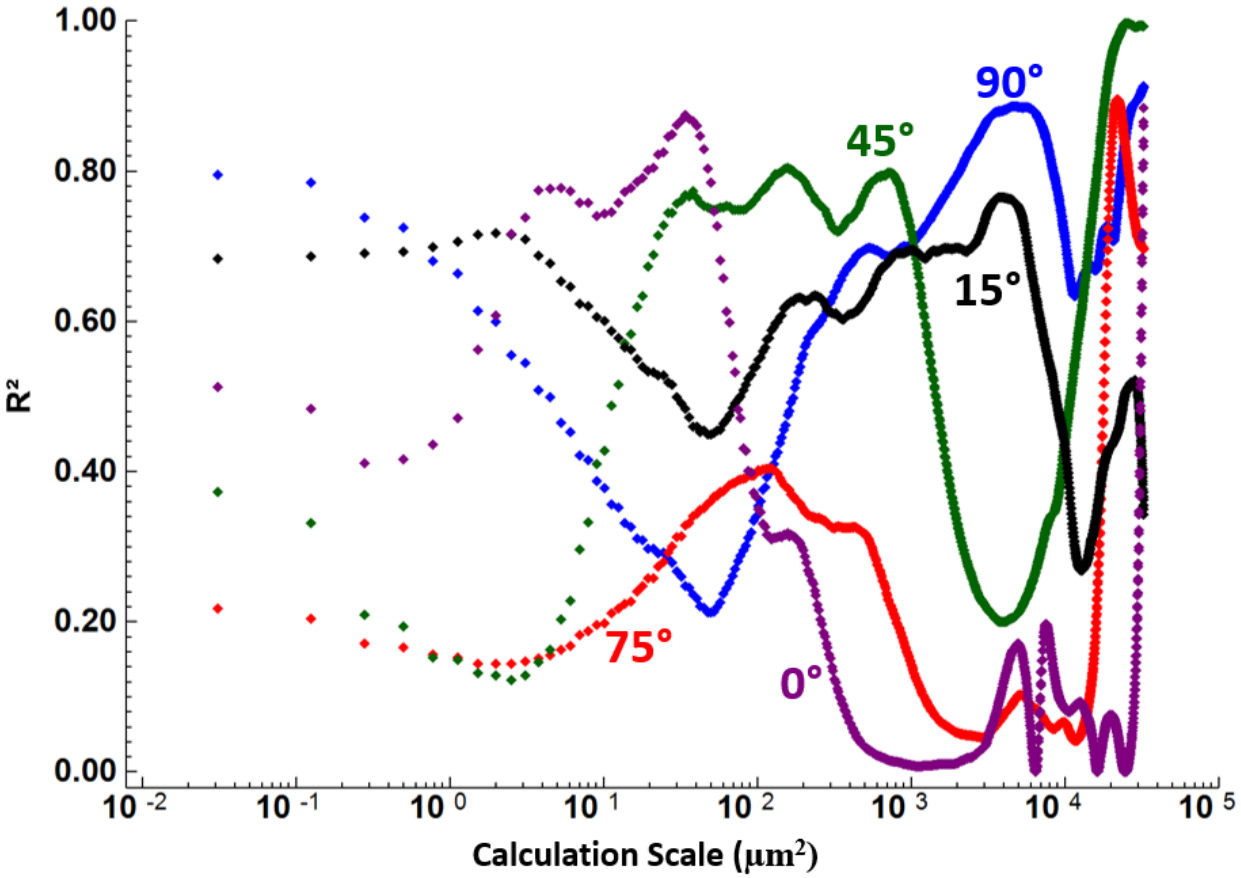

Figure 59: Correlation coefficients, R^2, for correlations between complexity and LED: modal filtered using 250 modes

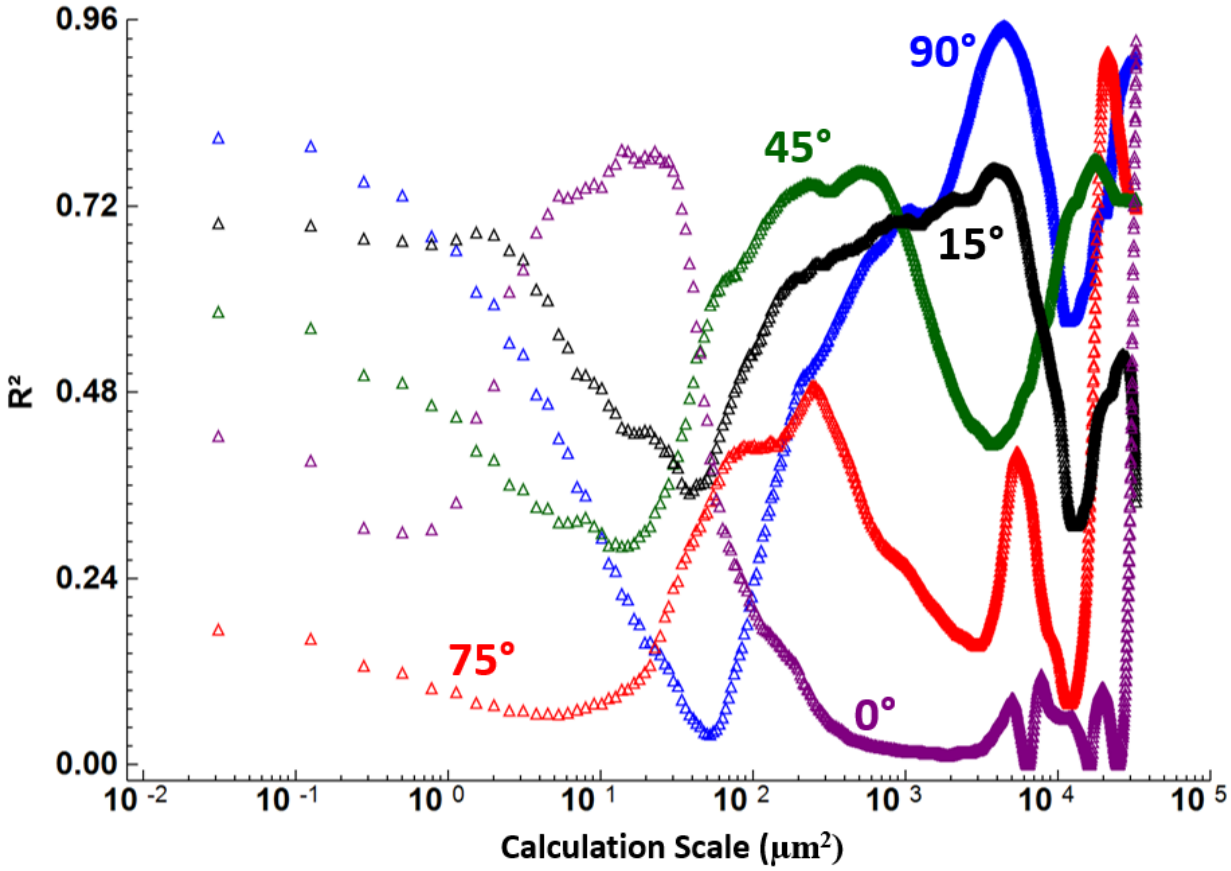

Figure 60: Correlation coefficients, R^2, for correlations between complexity and LED: modal filtered using 500 modes

7.15 Axiomatic Design Decomposition

An initial objective of this work was to decompose laser melted surfaces using the principles of axiomatic design in order to relate the surface topography with functional performance and manufacturing processes. Axiomatic design theory utilizes two axioms, the independence axiom and the information axiom (Suh, 1990). The independence axiom states that the best design will maintain the independence of the function requirements, and the information axiom states that the best design will contain the minimal amount of information (Suh, 1990).

Influential surface characteristics of laser melted surfaces were identified and decomposed into a set of functional requirements (FRs) and corresponding design parameters (DPs) (Figure 61). The decomposition was constructed using a "Zig Zag" process between the functional requirements and the design parameters, starting with FR0. A design matrix was constructed from the decomposition (Figure 62) in order to visualize the satisfaction of the independence axiom. It was determined that the design was a decoupled design, because there is a clear order of adjustment in the FRs. This is seen in the triangular design matrix (Figure 62). Therefore, the independence axiom will be satisfied if this order of adjustment is maintained. The decomposition shown in Figure 61 shows the various citations from the literature where each DP was obtained, and these citations can be found in the references section.

#	[FR] Functional Requirements	[DP] Design Parameters
0	FR Design comparable surface roughness	DP Additive manufacturing process characteristics
1	FR Control the formation of the staircase effect (Grimm et al., 2015)	DP Process characteristics that influence the formation of stepping
1.1	FR Control the step length	DP Inclination angle of part build (Grimm et al., 2015)
1.2	FR Control the vertical height of each sintered layer	DP Layer thickness (Ghanekar, 2003)
1.3	FR Control the distance between each hatch line	DP Hatch distance (Grimm et al., 2015)
1.4	FR Control the thermal variation of the layer during sintering	DP Volumetric energy density of the laser (Gu, 2015)
1.4.1	FR Control the frequency of laser pulses on a given volume of powder per scan	DP Laser repetition rate (Mumtaz et al., 2009)
1.4.2	FR Control the temperature of the powder per unit volume per scan	DP Laser beam power (Mumtaz et al, 2009)
1.4.3	FR Control the amount of time a given volume of powder is exposed to the laser	DP Scan speed of the laser (Mumtaz, 2009)
2	FR Control the formation of the balling effect (Grimm et al., 2015)	DP Process characteristics that only influence balling
2.1	FR Control the remelting of previously sintered layers	DP Repetition of scan lines (Hashmi, 2014)
2.2	FR Control the spreading and flattening of the melt on the previously sintered layer	DP Addition of deoxidants to the powder (Gu et al., 2009)
3	FR Control the formation of the orange peel effect (Grimm et al., 2015)	DP Process characteristics that only influence the formation of the Orange peel effect
3.1	FR Control the overall particle size of the powder	DP Powder screening characteristics (Kalpakjian et al., 2014)
3.2	FR Control the empirical melting temperature of the powder	DP Powder refreshing rate (Kruth et al., 2008)

Figure 61: The axiomatic design decomposition

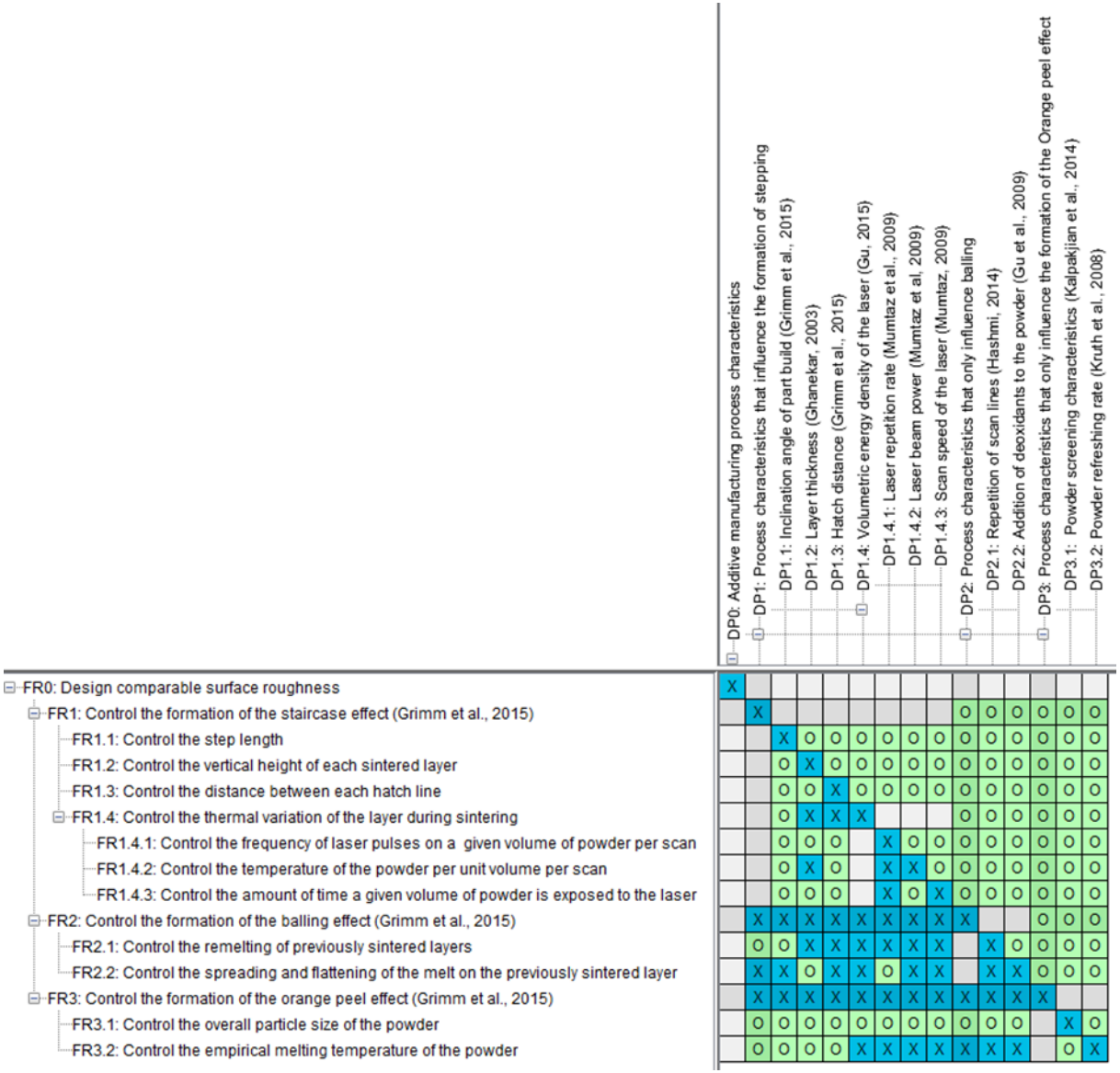

Figure 62: The design matrix

7.16 Measurement-to-Measurement Repeatability Using Additional Measurements

The procedure presented in Section 2.1.2.1 was repeated using 20 measurements obtained at a single location and on a single specimen. A 50x objective was used (numerical aperture of 0.95 and a sampling interval of 0.25 μm). The measurements were taken on the same specimen presented in Section 2.1.2.1. Linear regression analyses between the vertical heights of the measurements was performed, and two matrices showing the regression coefficients were constructed. The first matrix shows the regression coefficients calculated using the unfiltered surface measurements, and the second matrix shows the regression coefficients calculated using the filtered measurements.

R^2	1	2	3	4	5	6	7	8	9	10	11	12	13	14	15	16	17	18	19	20
1	**1.00**	0.65	0.66	0.58	0.65	0.57	0.65	0.66	0.67	0.58	0.57	0.57	0.67	0.60	0.70	0.65	0.68	0.70	0.70	0.71
2		1.00	0.75	0.71	0.73	0.69	0.72	0.72	0.75	0.74	0.73	0.72	0.72	0.62	0.71	0.65	0.65	0.62	0.59	0.67
3			1.00	0.75	0.92	0.73	0.88	0.84	0.85	0.67	0.67	0.65	0.82	0.60	0.79	0.61	0.63	0.60	0.57	0.76
4				1.00	0.76	0.79	0.72	0.69	0.70	0.69	0.70	0.66	0.67	0.57	0.65	0.57	0.57	0.55	0.53	0.61
5					1.00	0.75	0.90	0.85	0.85	0.67	0.67	0.66	0.82	0.60	0.78	0.60	0.62	0.59	0.56	0.75
6						1.00	0.75	0.72	0.72	0.76	0.78	0.73	0.69	0.60	0.66	0.59	0.58	0.56	0.54	0.62
7							1.00	0.91	0.89	0.69	0.69	0.67	0.86	0.62	0.81	0.62	0.63	0.59	0.57	0.76
8								1.00	0.91	0.69	0.68	0.68	0.89	0.64	0.83	0.63	0.64	0.60	0.58	0.77
9									1.00	0.71	0.70	0.70	0.92	0.65	0.85	0.65	0.66	0.62	0.60	0.78
10										1.00	0.91	0.89	0.68	0.65	0.65	0.63	0.62	0.58	0.56	0.60
11											1.00	0.88	0.68	0.64	0.64	0.62	0.61	0.57	0.55	0.59
12												1.00	0.68	0.67	0.65	0.64	0.63	0.59	0.56	0.60
13													1.00	0.67	0.88	0.66	0.67	0.63	0.61	0.79
14														1.00	0.69	0.71	0.69	0.64	0.62	0.63
15															1.00	0.71	0.72	0.67	0.64	0.83
16																1.00	0.88	0.77	0.72	0.67
17																	1.00	0.83	0.75	0.69
18																		1.00	0.84	0.69
19																			1.00	0.68
20																				1.00

Figure 63: The regression coefficient matrix using 20 unfiltered surfaces taken with a 50x objective

R^2	1	2	3	4	5	6	7	8	9	10	11	12	13	14	15	16	17	18	19	20
1	**1.00**	0.68	0.60	0.63	0.59	0.63	0.60	0.60	0.63	0.62	0.61	0.61	0.62	0.66	0.64	0.69	0.70	0.72	0.71	0.67
2		1.00	0.65	0.74	0.64	0.73	0.64	0.63	0.68	0.76	0.75	0.73	0.64	0.68	0.65	0.71	0.71	0.69	0.66	0.63
3			1.00	0.64	0.90	0.62	0.85	0.82	0.83	0.56	0.56	0.55	0.82	0.56	0.79	0.56	0.57	0.55	0.53	0.77
4				1.00	0.64	0.83	0.62	0.61	0.64	0.74	0.75	0.72	0.61	0.68	0.61	0.69	0.68	0.67	0.64	0.59
5					1.00	0.64	0.88	0.83	0.82	0.57	0.57	0.56	0.82	0.56	0.79	0.55	0.57	0.55	0.52	0.76
6						1.00	0.64	0.63	0.65	0.78	0.80	0.77	0.62	0.70	0.62	0.70	0.69	0.68	0.65	0.60
7							1.00	0.90	0.86	0.58	0.58	0.57	0.86	0.57	0.81	0.56	0.58	0.55	0.53	0.77
8								1.00	0.89	0.58	0.57	0.57	0.89	0.58	0.83	0.57	0.58	0.56	0.53	0.77
9									1.00	0.61	0.61	0.60	0.90	0.62	0.86	0.61	0.62	0.59	0.57	0.80
10										1.00	0.91	0.89	0.58	0.72	0.59	0.72	0.70	0.69	0.67	0.56
11											1.00	0.89	0.58	0.72	0.58	0.72	0.70	0.68	0.67	0.55
12												1.00	0.57	0.74	0.58	0.73	0.70	0.68	0.67	0.55
13													1.00	0.61	0.88	0.59	0.60	0.58	0.55	0.80
14														1.00	0.64	0.78	0.76	0.73	0.70	0.60
15															1.00	0.63	0.65	0.61	0.59	0.83
16																1.00	0.89	0.83	0.77	0.61
17																	1.00	0.85	0.79	0.64
18																		1.00	0.85	0.62
19																			1.00	0.61
20																				1.00

Figure 64: The regression coefficient matrix using 20 filtered surfaces taken with a 50x objective

7.17 The Three Developing Principles of Surface Metrology

The following slides were extracted from a tutorial presented at the 5th International Conference on Surface Metrology. They illustrate the three developing principles of surface metrology.

Discrete Interaction Model

Interactions that are considered continuous at a macroscopic scale are made up of a

- finite number of ***discrete interactions*** where
- each requires a certain amount of space on the surface, the ***fundamental scale of interaction***
- each has a certain strength, ***fundamental strength of an interaction***

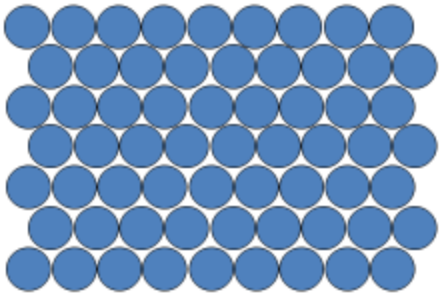

Atomism for surface interactions

Atomism from Greek ἄτομον, *atomon*, i.e. "uncuttable", "indivisible"

- On some, sufficiently fine scale interactions with surfaces are not continuous, instead they are discrete, i.e., distinct and individual
- Each distinct interaction takes place over a certain region on a surface and excludes other similar interactions from that region at that same moment.

Suppositions

- Large number of **discrete interactions** distributed over the surface
- Each has a **fundamental strength**

  Macroscopic = ∑ (discrete micro&nanoscopic)
- The scale of the discrete interaction is its **fundamental scale**

Theoretical Interaction Strength

Macroscopic Strength: $S_t = N \frac{S_s}{A_p}$

Number of Interactions (blue circles): $N = m \frac{A_{ts}}{A_s}$

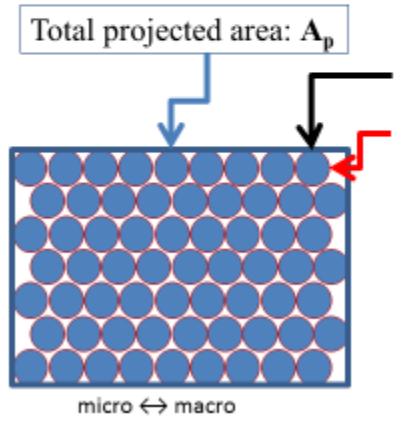

S_s Strength of a single interaction

A_s Area for one discrete interaction

A_{ts} Total area at the scale of a single interaction

m fraction of total possible interaction sites that are active.

Which must be: $0 \leq m \leq 1$

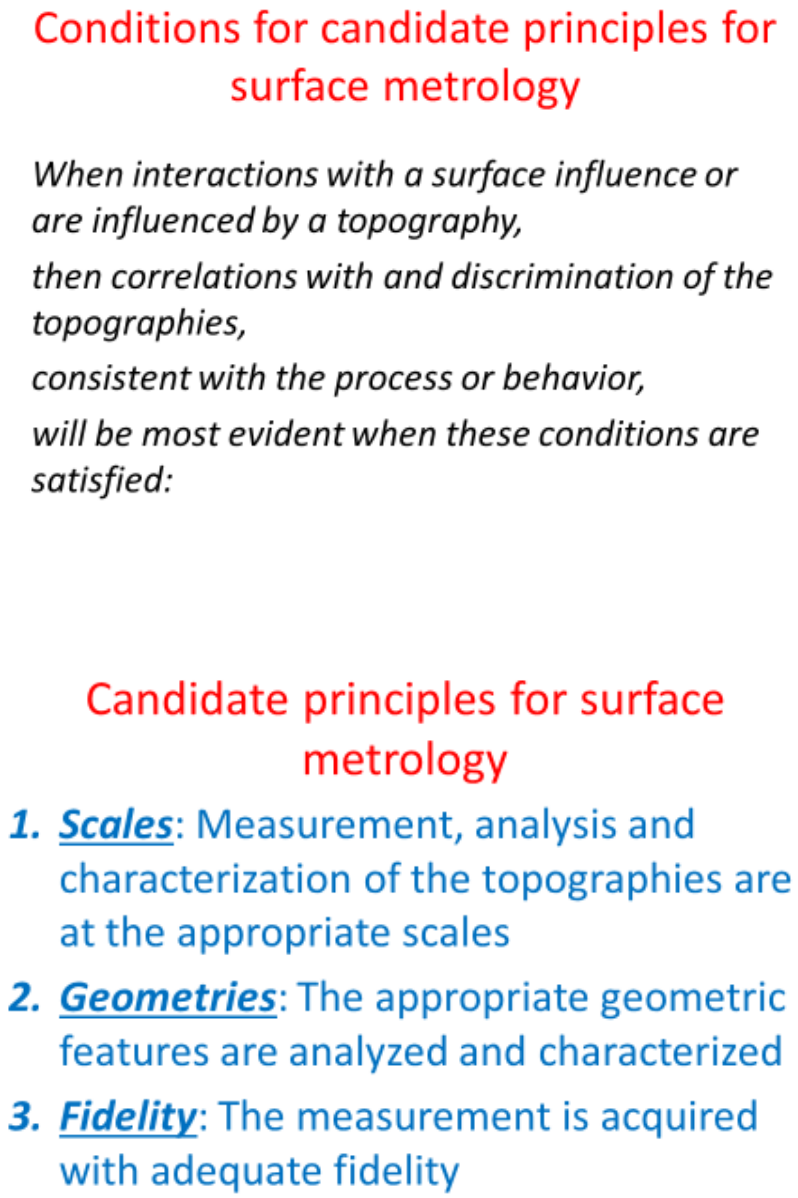

Figure 65: Slides extracted from the tutorial presented at the 5th International Conference on Surface Metrology, presented in Poznan, Poland